ABSTRACT

Title of dissertation: AN INTERNAL tRNA-LIKE STRUCTURE REGULATES THE LIFE CYCLE OF A PLUS-SENSE RNA VIRUS

John Crisler McCormack, III, Doctor of Philosophy, 2007

Dissertation directed by: Professor Anne E. Simon
Department of Cell Biology and Molecular Genetics

Turnip crinkle virus (TCV) is a 4054 b plus-sense RNA virus that belongs to the genus Carmovirus in the Family *Tombusviridae*. The 3' terminal 200 b of TCV are predicted to fold into 5 hairpins labeled in the 3' to 5' direction as the promoter (Pr), hairpin 5 (H5), hairpin 4b (H4b), hairpin 4a (H4a), and hairpin 4 (H4), using 3' UTR phylogenetic comparisons with other carmoviruses and the RNA structural prediction program, *mfold*. H5 was found to be a highly-conserved structure containing a large symmetrical loop (LSL) that formed a tertiary interaction between the 3' side of the LSL and the 3' terminal nucleotides using compensatory mutational analysis *in vivo*. In plants, LSL mutations resulted in a mutation frequency that was increased by as much as 12-fold without inducing error catastrophe. The original mutations frequently reverted and led to second site alterations biased for uridylate to cytidylate and adenylate to guanylate changes. These results suggest that H5 may function as a chaperone to properly fold the RdRp.

The TCV 5' UTR, which binds 40S ribosomal subunits, contains two short segments exhibiting IRES activity that function synergistically with the 3' terminal region to enhance cap-independent translation *in vivo*. In the TCV 3' UTR, H4a, H4b, H5, and flanking sequences, form an internal tRNA-like structure (iTLS) that binds 60S ribosomal subunits and the P-site of salt washed 80S ribosomes. The iTLS may therefore mediate assembly of 80S ribosomes, which are then transported to the 5' end for translation of virally-encoded proteins.

Phylogenetic comparisons of carmovirus 3' UTRs revealed that *Cardamine chlorotic fleck virus* (CCFV) and *Japanese iris necrotic ring virus* (JINRV) are capable of forming the 5 elemental features comprising the iTLS. Ribosome binding and plant cell culture assays showed that only the CCFV iTLS bound 80S ribosomes and could functionally replace the TCV iTLS. These results suggest that closely-related members of the same viral genus may utilize different strategies for cap-independent translation.

AN INTERNAL tRNA-LIKE STRUCTURE REGULATES THE LIFE CYCLE OF A PLUS-SENSE RNA VIRUS

by

John Crisler McCormack, III

Thesis submitted to the Faculty of the Graduate School of the
University of Maryland, College Park in partial fulfillment
of the requirements for the degree of
Doctor of Philosophy
2007

Advisory Committee:

Professor Anne E. Simon, Chair
Professor Barbara L. Thorne
Associate Professor Jonathan D. Dinman
Associate Professor James N. Culver
Assistant Professor Daniel R. Perez

In memory of my father,
John Crisler McCormack, II
(June 24, 1943-September 30, 2007)

ACKNOWLEDGEMENTS

I would like to acknowledge my advisor, Dr. Anne E. Simon, for giving me a project that allowed me to develop an interest in RNA structure and function and for her collaborative efforts, which led to the discovery and characterization of the internal tRNA-like structure (iTLS). To my core committee members, Dr. Jonathan D. Dinman, Dr. James N. Culver, and Daniel R. Perez, I thank them for their support and constructive criticism of my project for the past six and a half years. I express my gratitude to Dr. Barbara L. Thorne, for agreeing to serve as Dean's Representative on short notice. To my collaborators, Dr. Arturas Meskauskas and Dr. Jonathan D. Dinman, I thank them for their interest in the iTLS project for the past year and a half and their analysis of the iTLS using in vitro ribosome binding assays. To Dr. Vera A. Stupina, I am grateful for her development of an in vivo assay to study TCV translation. I acknowledge Dr. Yaroslava G. Yingling and Dr. Bruce A. Shapiro for RNA structural prediction analysis of TCV using MPGAfold and RNA2D3D. I would like to express my gratitude to former lab member, Dr. Sohrab Bodaghi, for his friendship, advice, and technical assistance during my first semester of graduate school. To my past and present colleagues, Dr. Fengli Zhang, Dr. Xiaoping Sun, Dr. Jiuchun Zhang, Dr. Guohua Zhang, Dr. Vera A. Stupina, Rong Guo, Dr. Alicia J. Manfre, and Dr. Xuefeng Yuan, I thank them for their discussions, friendship, and reagents. To Megan Young, Omar Memon, Chaohong Liu, and Yanan Lou, I wish them the best of luck in their graduate studies.

TABLE OF CONTENTS

LIST OF TABLES

LIST OF FIGURES

ABBREVIATIONS

%:	Percent
°C:	Degrees in Celsius
2,4-D:	2,4-dichlorophenoxyacetic acid
3'CCS:	3' carmoviral consensus sequence
3'PE:	3' proximal element
5'PE:	5' proximal element
AcPhe-tRNA:	Acetylated Phe-tRNA
ADAR:	Adenosine deaminase that acts on RNA
AFM:	Atomic force microscopy
AlMV:	*Alfalfa mosaic virus*
ATP:	Adenosine triphosphate
b:	Base(s)
BMV:	*Brome mosaic virus*
bp:	Basepair(s)
BTE:	Barley yellow dwarf luteovirus-like translational enhancer
BYDV:	*Barley yellow dwarf luteovirus*
CarMV:	*Carnation mottle virus*
CCFV:	*Cardamine chlorotic fleck virus*
CITE:	Cap-independent translational enhancer
CM:	Callus maintenance agar
cm:	Centimeter

CNV:	*Cucumber necrosis virus*
CP:	Coat protein
CPMoV:	*Cowpea mottle virus*
CrPV:	*Cricket paralysis virus*
CryoEM:	Cryo-electron microscopy
CSE:	Conserved sequence elements in SIN
CTP:	Cytidine triphosphate
DI RNA:	Defective-interfering RNA
DNA:	Deoxyribonucleic acid
dNTP:	Deoxynucleotide triphosphate
dpi:	Days post-inoculation
DR:	Derepressor element in satC
DTT:	Dithiothreitol
DV:	*Dengue virus*
EDTA:	Ethylenediaminetetraacetate, disodium, dihydrate
eEF1A:	Eukaryotic elongation factor 1A
eIF(iso)4E:	Plant isoform of eIF4E
eIF(iso)4F:	Plant isoform of eIF4F
eIF(iso)4G	Plant isoform of eIF4G
eIF:	Eukaryotic initiation factor
eIF1:	Eukaryotic initiation factor 1
eIF1A:	Eukaryotic initiation factor 1A
eIF2:	Eukaryotic initiation factor 2

eIF3:	Eukaryotic initiation factor 3
eIF4A:	Eukaryotic initiation factor 4A
eIF4E:	Eukaryotic initiation factor 4E
eIF4F:	Eukaryotic initiation factor 4F
eIF4G:	Eukaryotic initiation factor 4G
eIF5B:	Eukaryotic initiation factor 5B
EMCV:	*Encephalomyocarditis virus*
EMSA:	Electrophoretic mobility shift assay
FLuc:	Firefly luciferase
g:	Gram
GaMV:	*Galinsoga mosaic virus*
gRNA:	Genomic RNA
GTP:	Guanosine triphosphate
H4:	Hairpin 4
H4a:	Hairpin 4a
H4b:	Hairpin 4b
H5:	Hairpin 5
HCRSV:	*Hibiscus chlorotic ringspot virus*
HCV:	*Hepatitis C virus*
hpi:	Hours post-inoculation
hr:	Hour(s)
HRV-14	*Human rhinovirus 14*
IGR:	Intergenic region

IRES: Internal ribosomal entry site

iTLS: Internal tRNA-like structure

JINRV: *Japanese iris necrotic ring virus*

K_d: Dissociation constant

KU: Kilounit

L: Liter

LB: Lysogeny broth

Link1: Region between H5 and Pr

Link2: Region between H4b and H5

LSL: Large symmetrical loop

M: Molarity

M1H: Motif 1 hairpin

M3H: Motif 3 hairpin

mCi: Millicurie

MES: 2[N-Morphalino]ethanesulfonic acid

Met-$tRNA_{i:}$ Initiator methionine tRNA

mg: Milligram

min: Minute(s)

ml: Milliliter

mM: Millimolarity

MMLV: *Moloney murine leukemia virus*

MNSV: *Melon necrotic spot virus*

MP: Movement protein

mRNA:	Messenger RNA
MS salts:	Murashige and Skoog basal salt mixture
N:	Normality
ng:	Nanogram
NMR:	Nuclear magnetic resonance
nsP1:	non-structural protein 1 of SIN
nt:	Nucleotide(s)
OD:	Optical density
ODC:	Ornithine decarboxylase
ORF:	Open reading frame
PABP:	Poly(A) binding protein
PCM:	Protoplast culture medium
PCR:	Polymerase chain reaction
PEG:	Polyethylene glycol
PFBV:	*Pelargonium flower break virus*
pH:	Measure of acidity or alkalinity of a solution
Phe-tRNA:	Phenylalanine tRNA (charged)
PIM:	Protoplast inoculation medium
PK:	Pseudoknot
pmol:	Picomole
PNK:	Polynucleotide kinase
Pr:	Promoter
PSNV:	*Pea stem necrosis virus*

RCNMV: *Red clover necrotic mosaic virus*

RdRp: RNA-dependent RNA polymerase

RNA: Ribonucleic acid

RPM: Revolutions per minute

RRL: Rabbit reticulocyte lysate

rRNA: Ribosomal RNA

RT: Reverse transcription

SARS: Severe acute respiratory syndrome

SatC: Satellite RNA C

SCV: *Saguaro cactus virus*

SDS: Sodium dodecyl sulfate

sec: Second(s)

sgRNA: Subgenomic RNA

SIN: *Sindbis virus*

SL: Stemloop

SSL: Small symmetrical loop

STNV: Tobacco necrosis virus satellite RNA

STNV-1: Tobacco necrosis virus satellite RNA, strain 1

Tail: Bases downstream of Pr

TBSV: *Tomato bushy stunt virus*

TCV: *Turnip crinkle virus*

TE: Translational enhancer

TED: Translational enhancer domain in sTNV

TEV: *Tobacco etch virus*

TLS: tRNA-like structure

TMV: *Tobacco mosaic virus*

Tris: Tris[hydroxymethyl]aminomethane

$tRNA_{Phe}$: Phenylalanine tRNA (uncharged)

$tRNA^{Val}$: Valine tRNA

TYMV: *Turnip yellow mosaic virus*

U: Unit

$UP\Psi_3$: Upstream partner sequence of Ψ_3

UTP: Uridine triphosphate

UTR: Untranslated region

v: Volume

VEGF: Vascular endothelial growth factor

w: Weight

Wt: Wild-type

Δ: Deletion

Ψ_1: Pseudoknot 1

Ψ_2: Pseudoknot 2

$\Psi_{2'}$: Pseudoknot 2'

Ψ_3: Pseudoknot 3

Ψ_4: Pseudoknot 4

α-^{32}P: Alpha phosphorus-32

α-^{35}S: Alpha sulfur-35

γ-^{32}P:	Gamma phosphorus-32
μg:	Microgram
μl:	Microliter
μM:	Micromolarity
μmol:	Micromole

CHAPTER I

CIS-ACTING ELEMENTS INVOLVED IN TRANSLATION AND REPLICATION OF PLUS-STRANDED RNA VIRUSES: AN OVERVIEW

Introduction

Viruses that contain plus-sense single-stranded ribonucleic acid (RNA) as genetic material can directly act as templates for synthesis of viral proteins. The discovery of the first plus-stranded RNA virus, *Tobacco mosaic virus* (TMV), is often attributed to Dimitri Ivanovski for his work in 1892 on a pathogenic agent that remained infectious after passage through a bacterial filter. In the past 100 years, plus-stranded RNA viruses have been shown to infect all types of organisms and result in diseases such as hepatitis C, polio, and severe acute respiratory syndrome (SARS), in humans and in tremendous economic losses in crops.

As shown in Fig. 1.1, viruses initiate infections by entry into cells. Animal viruses bind membrane receptors resulting in endocytosis and introduction of their encapsidated genomes into the cytoplasm (not shown), whereas plant viruses must be mechanically inoculated by insects or farm machinery. Disassembly of the capsid and release of the genetic material can occur due to conformational changes induced by membrane receptor binding, a change in pH, or by protease activity (Flint *et al.*, 2004). Most plus-stranded RNA viruses remain in the cytoplasm where their genomic RNA can

function as templates during early stages of infection for translation of the RNA-dependent RNA polymerase (RdRp) open reading frame (ORF) using cellular translational proteins. The RdRp is recruited by virally-encoded proteins or domains within the RdRp to specific membranes of cellular compartments where replication occurs (Kopek *et al.*, 2007). Since translation progresses in a 5' to 3' direction and replication in the opposite direction, minus-strand synthesis of viral RNAs is mediated by a putative RNA conformational change of the template plus-strands, which represses translation and allows for recognition of *cis*-acting elements by the RdRp for transcription initiation at the 3' end. To switch from synthesis of minus-strands to plus-strands, proteolytic processing of the RdRp or a second plus-stranded RNA conformational switch is proposed to exist that prevents further minus-strand synthesis (Flint *et al.*, 2004, Pogany *et al.*, 2003). Minus-strands then act as templates for the asymmetrical production of plus-strands, which is believed to occur due to more efficient synthesis of RNA on minus-strand templates (Panavas *et al.*, 2002). Some RNA viruses are associated with the production of 3' coterminal subgenomic RNAs, which are produced by either premature termination of the RdRp during minus-strand synthesis (not shown), or internal initiation on minus-strands during plus-strand synthesis, to facilitate expression of the 3' proximal ORFs (White, 2002). Virally-encoded coat protein recognizes *cis*-acting packaging signals on viral plus-stranded RNA, which then interacts with other coat protein molecules to nucleate the formation of a capsid. Non-enveloped and enveloped animal viruses exit the cell by destroying or pinching off from the cellular membrane respectively (not shown), whereas plant viral RNA and virus particles move

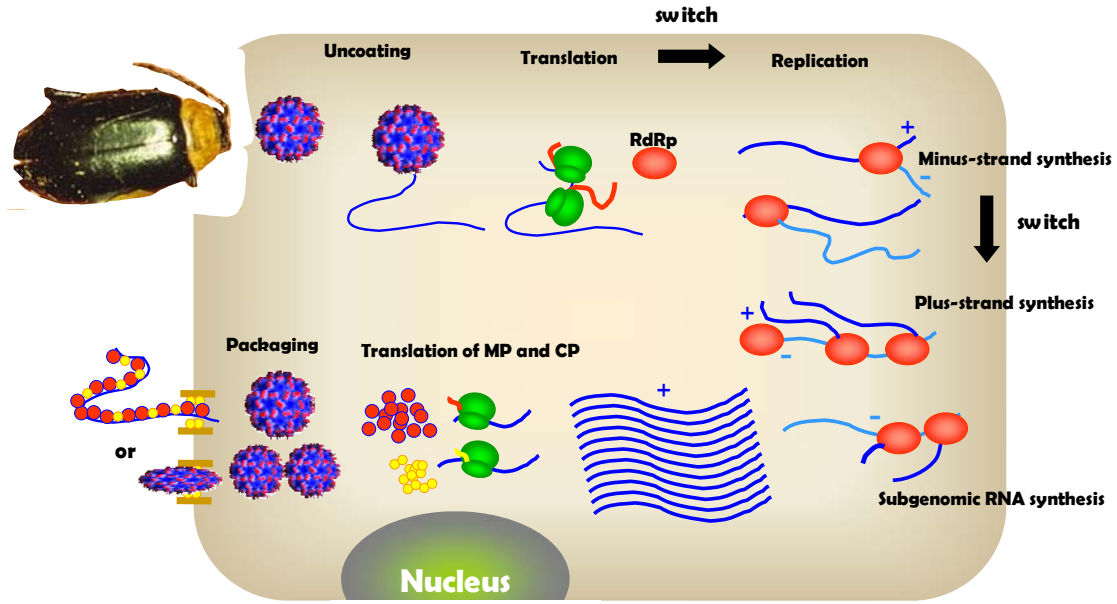

Figure 1.1. Viral Life Cycle of a Plus-Stranded RNA Plant Virus. Infection initiates with viral entry into the cell and disassembly of the virus particle to release the viral RNA into the cytoplasm. Ribosomes are recruited to the viral RNA template for translation of RNA-dependent RNA polymerase (RdRp). A putative RNA conformational switch occurs, which represses translation and promotes the recruitment of the RdRp to the 3' terminus of viral plus-strands to produce minus-strands. A second predicted plus-stranded RNA conformational switch is proposed to occur to inactivate minus-strand synthesis, which then allows for minus-strands to act as templates for the excess production of plus-strands. Translation of 3' proximal open reading frames (ORFs) occurs by synthesis of subgenomic RNAs produced by either internal initiation of RdRp during plus-strand synthesis (shown) or premature termination of RdRp during minus-strand synthesis. Exit of viral RNA and virus particles from the cell occurs through plasmodesmata with the assistance of virally-encoded movement proteins (MP) and unencapsidated coat protein (CP).

intercellularly through channels (plasmodesmata) with the assistance of virally-encoded movement proteins and unpackaged coat protein (Flint *et al*., 2004).

Since viral *cis*-acting elements are known to be important in regulating steps in the life cycle of plus-stranded RNA viruses, the purpose of this chapter will be to present the current body of knowledge for viral *cis*-acting elements involved in translation and replication.

Translation of Cellular mRNAs

Cap-dependent translation of about 95-97% of cellular mRNAs commences with binding of eIF4F containing eIF4A, eIF4E, and eIF4G, to the 5' cap structure and association of the poly(A) binding protein (PABP) with the 3' poly(A) tail (Merrick, 2004). Interaction between PABP and eIF4G has been proposed to circularize the mRNA and allow for recruitment of the 43S ribosomal complex containing the 40S ribosomal subunit, eIF2-GTP-Met-tRNA$_i$, eIF3, and eIF1A to the mRNA template (Wells *et al*., 1998). The 48S ribosomal complex then scans from the 5' terminus using an ATP-dependent mechanism until an AUG in a favorable context is identified. The 60S ribosomal subunit joins once eIF5B promotes release of eIF2-GTP by GTP hydrolysis and displacement of the remaining translation initiation factors. 80S ribosomes then initiate the elongation phase of translation upon dissociation of eIF5B (Fig. 1.2; Merrick, 2004).

During adverse conditions resulting in growth factor depletion, heat shock, and hypoxia, cap-dependent translation is compromised and a small percentage of cellular

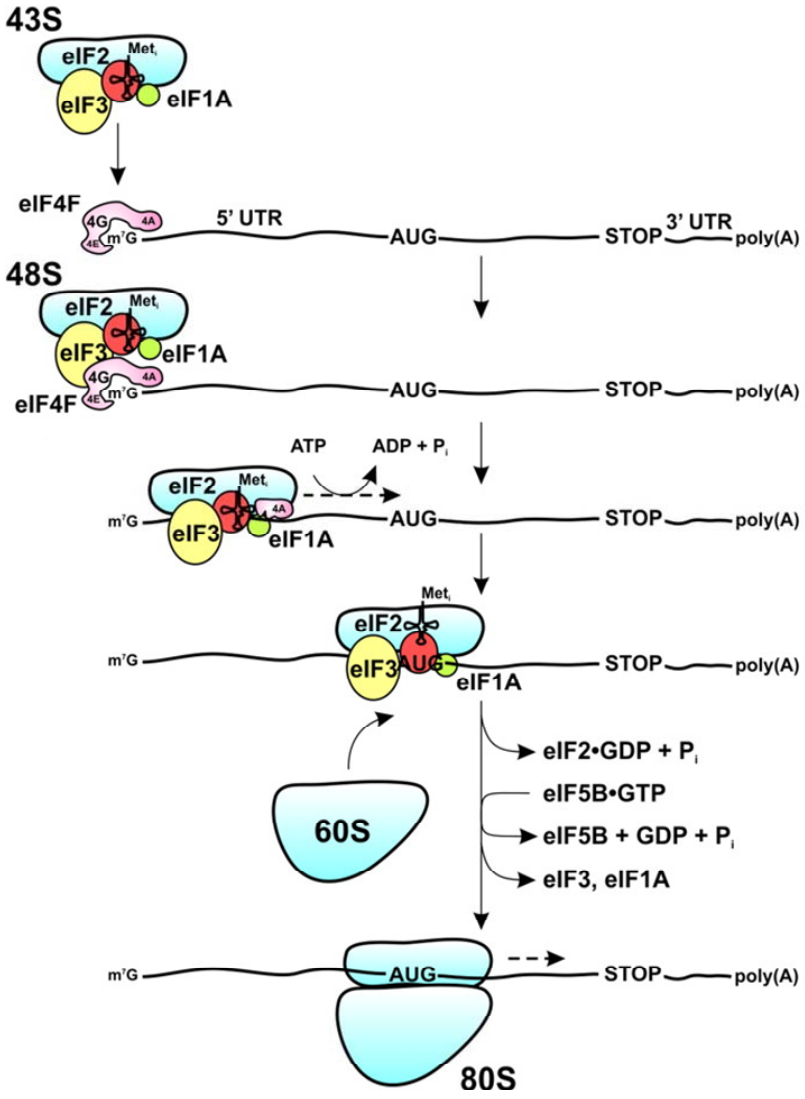

Figure 1.2. Cap-Dependent Translation of Cellular mRNAs. The 43S ribosomal complex containing the 40S ribosomal subunit, eIF2-GTP-Met-tRNA$_i$, eIF2, and eIF1A, is recruited to eIF4F bound to the 5' cap structure of cellular mRNAs. The 48S ribosomal complex then scans from the 5' end until an AUG initiation codon in an optimum context is identified. eIF5B promotes dissociation of eIF2 by GTP hydrolysis and displaces eIF3 and eIF1A, which allows for recruitment of 60S ribosomal subunits to form 80S ribosomes that commence the elongation phase of translation from the AUG initiation codon.

mRNAs involved in cell growth, proliferation, differentiation, and regulation of apoptosis are translated by a cap-independent mechanism (Sonenberg and Dever, 2003; Morrish and Rumsby, 2002; Stoneley *et al*., 2000; Qin and Sarnow, 2004; Holcik *et al*., 2000). The most common mechanism for cap-independent translation involves internal ribosomal entry sites (IRESes), which are *cis*-acting elements located in untranslated regions of RNA that directly recruit 40S ribosomal subunits for translation of downstream ORFs. To date, at least 85 putative cellular IRESes have been identified (Baird *et al*., 2006).

Viral Cis-acting Elements Involved in Translation

Internal Ribosomal Entry Sites (IRESes)

As with cap-independently translated cellular mRNAs, some RNA viruses that do not contain 5' cap structures utilize IRESes. Translation of *Hepatitis C virus* (HCV) is driven by a 5' UTR IRES comprising a highly structured region with 3 domains (II, III, and IV) (Rijnbrand and Lemon, 2000; Hellen and Pestova, 1999; Honda *et al*., 1996; Wang *et al*., 1993; Brown *et al*., 1992; Tsukiyama-Kohara *et al*., 1992). The base of domain III binds 40S ribosomal subunits at a high affinity *in vitro* (Kieft *et al*., 2001; Lukavsky *et al*., 2000; Kolupaeva *et al*., 2000), showing that recruitment of the small subunit to the viral template occurs in the absence of translation initiation factors. eIF2-GTP-Met-tRNA$_i$ and eIF3, which binds to the distal portion of domain III, interacts with the surface of the 40S ribosomal subunit, suggesting that these initiation factors join after binding of the small subunit to the viral template to form an intermediate 48S ribosomal

complex (Ji *et al*., 2004; Otto and Puglisi, 2004; Pestova *et al*., 1998;). In the absence of scanning, the 60S ribosomal subunit is proposed to join to form the functional 80S ribosome, which then utilizes the Met-tRNA$_i$ to translate beginning with the AUG initiation codon located in the terminal portion of domain IV (Pestova *et al*., 1998; Boehringer *et al*., 2005).

Encephalomyocarditis virus (EMCV) has a multi-domained (H, I, J-K, and L) ~450 b IRES sequence upstream of its initiation codon (Jackson and Kaminski, 1995). Domains I and J-K are essential for IRES activity with specific binding of eIF4G occurring at the J-K domain (Kolupaeva *et al*., 1998; Lomakin *et al*., 2000; Marcotrigiano *et al*., 2001; Pestova *et al*., 1996b; Pilipenko *et al*., 2000). Interaction of eIF4A with eIF4G enhances the ability of this complex to bind the IRES in an ATP-dependent manner and causes a conformational rearrangement downstream of the initiation codon, suggesting that eIF4G and eIF4A induce the formation of a ribosome binding site (Kolupaeva *et al*., 2003; Lomakin *et al*., 2000; Marcotrigiano *et al*., 2001). Reconstitution of the 48S complex using the EMCV IRES revealed that the 43S initiation complex was able to bind the mRNA in the absence of eIF1, eIF1A, and eIF4F, indicating that cap-independent translation requires fewer initiation factors than cap-dependent translation (Pestova *et al*., 1998; Pestova *et al*., 1996a; Pestova *et al*., 1996b). Like HCV, assembly of the 80S ribosome occurs in close proximity to the AUG initiation codon, thereby obviating the need for ribosomal scanning (Kaminski *et al*., 1990; Pestova *et al*., 1996a).

The ~190 b intercistronic IRES of *Cricket paralysis virus* (CrPV) contains 3 pseudoknots (PKI, PKII, and PKIII) that direct translation of a downstream ORF that

lacks an AUG initiation codon (Wilson *et al*., 2000a). Using systematic omission experiments, the 40S ribosomal subunit bound the CrPV in the absence of translation initiation factors, a finding that is similar to the HCV IRES. Toe printing assays of the translation initiation complex on the CrPV IRES revealed that a basepaired CCU in PKIII occupies the P-site, suggesting that PKIII is mimicking the interaction between Met-$tRNA_i$ and the AUG initiation codon used during cap-dependent translation. A GCU codon, which is downstream of the basepaired CCU, is proposed to be in the A-site and is the first codon translated by the 80S ribosome in a factor-independent manner (Wilson *et al*., 2000b). The CrPV IRES also binds to preassembled 80S ribosomes, but not 60S ribosomal subunits, suggesting that CrPV may facilitate rapid translation of its genome by using 80S monosomes that transiently accumulate after shut-off of host translation (Pestova *et al*., 2004; Nishiyama *et al*., 2003).

In the plant virus *Tobacco etch virus* (TEV), cap-independent translation is directed by an IRES contained in the 143 b 5' leader sequence (Carrington and Freed, 1990; Gallie *et al*., 1995). RNA structural prediction analysis and chemical probing showed the existence of 3 pseudoknots (PK1, PKII, and PKIII) with mutational analysis indicating that the core translational element comprised PK1 and upstream flanking sequences using an in vivo luciferase assay. Sequence in the loop of PK1 has been proposed to recruit 40S ribosomal subunits by basepairing with the 18S rRNA (Zeenko and Gallie, 2005). eIF4G, which is required for translation of TEV, binds with high affinity to the TEV 5' UTR in the absence of other initiation factors or *trans*-acting factors, suggesting that eIF4G recruitment to the viral RNA template may be the first step in translation initiation (Ray *et al.*, 2006).

Translational Enhancers (TEs)

Cis-acting elements known as translational enhancers may recruit protein factors that stimulate translation. In HCV, the 3' UTR is divided into three elements (variable region [VR], poly[U/C] tract, and 3'X region), which contribute equally to enhancement of translation mediated by the 5' UTR IRES *in vivo* (Song *et al.*, 2006). Deletion of the 3' UTR reduced translation efficiency by 10-fold, which was restored to a level 2-fold higher than wt when a 50 b poly(A) tail was substituted *in vivo*, suggesting that the HCV 3' UTR can be functionally replaced by a poly(A) tail. Deletion of the 3' UTR did not affect assembly of ribosomes using density gradient fractionation *in vitro*, showing that the defect in translation may occur after translation initiation. To test for ribosome disassembly, the efficiency of polypeptide release was analyzed *in vitro* by measuring the amount of accumulated free Luciferase polypeptide versus ribosome-bound Luciferase using fractionation. The levels of unbound Luciferase were equivalent for wt and the poly(A) replacement, but at low levels for the 3' UTR deletion, showing that the HCV 3' UTR enhances translation by regulating termination (Bradrick *et al.*, 2006).

Turnip yellow mosaic virus (TYMV) is a capped non-polyadenylated plant virus containing a 109 b tRNA-like structure (TLS) and upstream pseudoknot (UPSK) in its 3' UTR. TYMV TLS is able to be modified or bound by CCA nucleotidyltransferase, valyl-tRNA synthetase, and translation elongation factor eEF1A, indicating that this element mimics $tRNA^{Val}$ (Dreher and Goodwin, 1998; Florentz and Giegé, 1995; Mans *et al.*, 1991). An aminoacylated TYMV TLS and UPSK were found to enhance luciferase expression of a capped reporter RNA by 25-fold *in vivo*, indicating that this element is

functioning as a translational enhancer (Matsuda and Dreher, 2004). Using a cell-free wheat germ translation system, an aminoacylated TYMV TLS was found to functionally replace initiator tRNA by donation of a valine to the N-terminus of the polyprotein (PP) polypeptide (Barends *et al*., 2003); however, these results were not able to be duplicated by Matsuda and Dreher (2007), bringing into question their validity.

The uncapped non-polyadenylated RNA of satellite Tobacco necrosis virus (STNV) contains one ORF preceded by a 29 b 5' UTR and followed by a 622 b 3' UTR harboring a translational enhancer domain (TED) predicted to fold into a hairpin structure (Horst *et al*., 1971; Ysebaert *et al*., 1980). Deletion of the TED in strain 1 of sTNV (STNV-1) reduced translational efficiency, which was restored when a 5' cap was added *in vitro*, suggesting that the TED is mimicking the function of a 5' cap (Timmer *et al*., 1993). TED specifically bound eIF4F and the plant isoform eIF(iso)4F, showing that this element may enhance translation by recruiting translational proteins to the viral template. eIF4E and eIF(iso)4E were able to independently bind the TED, but the presence of eIF4G or eIF(iso)4G enhanced binding by 10-fold. These results suggest translation initiation may occur when the eIF4E/eIF4G complex binds the TED and the 40S ribosomal subunit with eIF2 and eIF3 recognizes the 5'end. A putative interaction between eIF4G and eIF3 is proposed to circularize the RNA, which may facilitate translation (Gazo *et al*., 2004).

Some viral members in genera Tombusvirus and Necrovirus (Family *Tombusviridae* and *Luteoviridae*, respectively) have been shown to or are predicted to contain translational enhancers (TEs) in their 3' UTRs. The *Barley yellow dwarf luteovirus* (BYDV; tombusvirus) TE was unable to promote translation of a downstream

ORF when positioned in an intercistronic region, indicating that it is not an IRES. The BYDV TE was able to bind to eIF4F and eIF(iso)4F, suggesting that it may be enhancing translation using a similar mechanism as STNV TED (Kneller *et al*., 2006). The structure of BYDV TE contains three stemloops (SL-I, SL-II, and SL-III) presented at the apex of a helical region (Stem-IV), whereas necrovirus TEs contain all BYDV structural elements except for SL-II. These enhancers have been designated as Barley yellow dwarf virus-like translational enhancers (BTEs) and are known to function *in vivo* and *in vitro*, have similar hairpin structures containing the signature motif 5'-GGAUCCUGGGAAA CAGG presented in SL-I, can function when ectopically positioned in the 5' UTR, and may form a 4 to 5 bp long-range interaction between SL-III and the 5' UTR when located at the 3' end (Shen and Miller, 2004; Guo *et al*., 2001).

Tomato bushy stunt virus (TBSV), regulates translation using an element designated as the 3' cap-independent translational enhancer (3'CITE), which has been predicted to exist in some members of all 8 genera composing the Family *Tombusviridae*. The core 3'CITE adopts a Y-shaped conformation containing elements SL-B, SL-C, and S-A with deletion of either SL-B or SL-C causing a 90% reduction in translation *in vivo* (Fabian and White, 2004). RNA-RNA electrophoretic mobility shift assays (EMSAs) and compensatory mutational analysis between the SL-B terminal loop and a 5' UTR structure (SL3) containing complementary loop sequence revealed the existence of a long-range interaction between these regions *in vitro* and *in vivo*. Circularization of the TBSV template by the SL-B/SL3 interaction has been proposed to deliver hypothetical translational proteins that bind the 3'CITE to the 5' UTR, where scanning from the 5' terminus takes place (Fabian and White, 2006; Fabian and White, 2004).

Cis-acting Elements That Function in Viral Replication

Core Promoters for Minus-Strand Synthesis

RdRps initiate transcription of minus-strands at the 3' termini of plus-strands. While cellular mRNAs contain poly(A) tails at their 3' ends, the 3' UTRs of plus-sense RNA viruses terminate with a variety of structures that may function as core promoters, which are defined as the minimal *cis*-acting sequences required to independently direct transcription. These structures include tRNA-like structures (TLSes), poly(A) tails, and non-TLS heteropolymeric sequences. TLSes have been identified in at least 7 genera of plant viruses, including bromoviruses, cucumoviruses, furo-like viruses, hordeiviruses, tobamoviruses, tobraviruses, and tymoviruses, and may be uncharged or aminoacylated with valine, histidine, or tyrosine, in a similar manner as canonical tRNAs. Viral poly(A) tails have a length between 20 to 100 bases and are found in plant viruses, such as comoviruses, capilloviruses, carlaviruses, potexviruses, and potyviruses. Viruses with non-TLS heteropolymeric 3' ends have no commonalities with each other, cannot be grouped in the above two categories, and are present in sobemoviruses, luteoviruses, tombusviruses, dianthoviruses, and closteroviruses (Dreher, 1999; Duggal *et al*., 1994; Zaccomer *et al*., 1995).

Brome mosaic virus (BMV) comprises 3 RNAs (RNA1, RNA2, and RNA3) with highly-conserved 200 b sequences at their 3' ends, which are able to independently direct minus-strand synthesis *in vitro* (Dreher *et al.*, 1984). These regions have been found to interact with tRNA-synthetase and nucleotidyl transferase, suggesting that the 3' ends

form a TLS (Dreher and Hall, 1988b; Haenni *et al*., 1982). Characterization of the BMV TLS identified 6 elements designated as A, B1, B2, B3, C and D. Alterations in A, B1, B2, and C were shown to reduce minus-strand synthesis with the single-stranded regions of stem-loop C (SLC) being involved directly in binding the RdRp, even in the absence of the rest of the TLS *in vitro* (Dreher and Hall, 1988a; Chapman and Kao, 1999). High resolution NMR analysis of a minimal SLC RNA revealed that a clamped adenine motif existed in its AUA triloop and is presumably the primary structural determinant for RdRp binding (Kim *et al*., 2000).

The TLS of *Tobacco mosaic virus* (TMV) contains an acceptor stem mimic and a 3' end terminating with a single-stranded CCA sequence (Felden *et al*., 1996; van Belkum *et al*., 1985). This TLS specifically binds CTP, ATP, nucleotidyltransferase, tRNA-synthetase, and eEF1A (Litvak *et al*., 1973a; Litvak *et al*., 1973b; Mans *et al*., 1991). Located upstream is a domain containing three pseudoknots with the most 3' proximal pseudoknot being critical for accumulation in plants and protoplasts and required for directing minus-strand synthesis in the presence of the TLS *in vitro* (Takamatsu *et al*., 1990; Osman *et al*., 2000).

The *Turnip yellow mosaic virus* (TYMV) TLS mimics the structure and function of a $tRNA^{Val}$ (Dreher and Goodwin, 1998; Rietveld *et al*., 1982; Dreher *et al*., 1992; de Smit *et al*., 2002). With the exception of the terminal CCA bases, all of the tRNA-like structure is dispensable for minus-strand synthesis *in vitro*. These results suggest that the TLS may function to negatively regulate replication (Deiman *et al*., 1998). Binding of eIF1A-GTP to the TLS abolished minus-strand synthesis *in vitro*, possibly by interfering

with the ability of the RdRp to recognize the 3'-terminal nucleotides (Matsuda *et al*., 2004)

A 10 bp hairpin (hpE) is located 100 bases upstream of the transcription start site in all genomic RNAs of the tripartite virus, *Alfalfa mosaic virus* (AlMV). Deletion of the terminal loop or one side of the hairpin eliminated minus-strand synthesis using an in vitro transcription assay, showing that hpE is part of a core promoter (van Rossum *et al*., 1997). The TLS downstream of hpE did not independently have template activity and was unable to bind RdRp by itself *in vitro*; however, mutagenesis of the TLS resulted in minus-strand synthesis at internally-located cryptic initiation sites *in vitro*, suggesting that the TLS directs the RdRp to properly initiate replication at the 3' terminus (Olsthoorn and Bol, 2002).

Sindbis virus (SIN) contains a highly-conserved 19 b element (3'CSE) at its 3' end followed by a poly(A) tail (Pfeffer *et al*., 1998; Strauss *et al*., 1984). Deletion of the poly(A) tail revealed that minus-strand synthesis was reduced to 4% of wt levels, whereas deletions in the 3'CSE resulted in nearly undetectable levels, *in vitro*. These results show that the 3'CSE may function as the core promoter for minus-strand synthesis. Insertion of 3 cytidylates between the 3'CSE and poly(A) tail eliminated minus-strands *in vitro*, suggesting that spacing between the two elements is important (Hardy and Rice, 2005).

Dengue virus (DV) employs a unique strategy for minus-strand synthesis involving a hairpin core promoter (SLA) in its 5' UTR. Disruption of the hairpin structure or mutagenesis of the terminal loop reduced to levels below detection or delayed replication *in vivo*, respectively. Binding assays revealed that the RdRp specifically recognized the 5' UTR, but not the 3' UTR *in vitro* (Filomatori *et al*., 2006).

Two sets of complementary sequences found in the 5' UTR (5' CS and 5' UAR) and 3' UTR (3' CS and 3' UAR) were shown to circularize the RNA for replication (Alvarez *et al*., 2005) and RdRp was found to bind the viral RNA in the presence of these interactions using atomic force microscopy (AFM). These results suggest that SLA recruits the RdRp to the viral template followed by transfer to the 3' end by circularization of the genome (Filomatori *et al*., 2006).

Tomato bushy stunt virus (TBSV) and associated defective-interfering RNAs (DI RNAs) terminate at their 3' ends with hairpins containing 5 bp stems and GNRA terminal tetraloops (SL1). DI RNAs contain sequences that are mostly to completely derived from the progenitor virus and utilize the virally-encoded RdRp for amplification. In vitro transcription assays revealed that this stemloop along with 2 upstream and 3 downstream bases comprise the core promoter for minus-strand synthesis (Panavas *et al*., 2002). Mutagenesis of this hairpin in DI RNA (DI-72) showed that altering bases in the tetraloop reduced accumulation, whereas disruption of 2 bp in the lower stem resulted in undetectable levels of accumulation, which was partially restored in the presence of mutations that reformed the stem (Fabian *et al*., 2003)

Two RNAs (RNA1 and RNA2) compose the genome of *Red clover necrotic mosaic virus* (RCNMV). The 72 terminal bases of RNA1, which contains two hairpins (SLDE and SLF) and an intervening sequence, were required for minus-strand synthesis using an in vitro translation-coupled replication system (Iwakawa *et al*., 2007). The loop sequences of SLDE and SLF were found to be critical elements, whereas maintenance of the stem was important, but not essential, for minus-strand synthesis *in vitro*. These

results for RNA1 are consistent with elements known to be important in RNA2 for accumulation *in vivo* (Turner and Buck, 1999).

Core Promoters for Plus-Strand Synthesis

Initiation of plus-strand synthesis occurs at the 3' ends of viral minus-strands and has not been investigated as extensively as minus-strand synthesis. For BMV, genomic plus-strand synthesis requires a core promoter containing 26 unstructured terminal bases from the 3' ends of minus-strands and 1 downstream non-templated base (-1 position) *in vitro*, which is added by the replicase complex during minus-strand synthesis (Sivakumaran *et al*., 1999; Sivakumaran and Kao, 1999; Siegel *et al*., 1997). The identity of nucleotides at positions -1, +1, and +2 on minus-strands are recognized by the replicase for initiation of plus-strand synthesis. Mutations that introduced guanylates at positions +8 or +10 resulted in plus-strand synthesis above wt levels *in vitro*, showing that increased stability between the template and nascent strands may enhance transcription by allowing for tighter binding by the replicase complex during elongation (Sivakumaran *et al*., 1999). The observation that guanylates and cytidylates are naturally more prevalent between positions +6 to +10 suggests that this region is involved in the transition of the replicase from initiation to elongation (Sun and Kao, 1997a; Sun and Kao, 1997b; Adkins *et al*., 1998).

For DI-72 of TBSV, plus-strand synthesis can be independently directed by an unstructured 11 base sequence at the 3' terminus of minus-strands *in vitro*. Individual mutations in the core promoter did not eliminate transcription; however, replacement of 9 of the bases with a G/C or A/U-rich sequence resulted in undetectable levels of plus-

strands. Deletion of most of the element resulted in initiation of transcription at a adjacent sequence, suggesting that DI-72 harbors two sequences at its 3' end that exhibit promoter activity *in vitro* (Panavas *et al*., 2002).

Replication Enhancers

Replication enhancers are defined as *cis*-acting elements that are not critical for replication, but enhance transcription directed by the core promoter. Enhancers are able to function in a position-independent manner on either plus- or minus-strands. For example, RNA3 of BMV contains a 240 b intergenic region (IGR) downstream of the movement protein 3a ORF and upstream of the coat protein (CP) (Sullivan and Ahlquist, 1999). Partial or complete deletion of the IGR resulted in low levels of minus-strand synthesis *in vivo* using yeast RdRp and *in vitro* (Quadt *et al*., 1995; French and Ahlquist, 1987), suggesting that the IGR functions as a replication enhancer. BMV protein 1a, which is expressed from RNA1 and is a component of the replicase, increased RNA stability when bound to a 150 to 190 b fragment of the IGR, showing that this region is able to recruit proteins involved in replication to the viral RNA to promote minus-strand synthesis (Sullivan and Ahlquist, 1999).

Five bases upstream of the hpE core promoter hairpin in AlMV is a 4 bp hairpin capped by a GNRA tetraloop that is found in RNA3, but not in the other two genomic RNAs. Deletion of this hairpin resulted in reduced levels of minus-strand synthesis using a transcription assay and reduced accumulation in inoculated plants. These results suggest that the element enhances transcription of minus-strands *in vitro* and *in vivo*.

RNA1, RNA2, and RNA3 may therefore contain unique sequences that enhance the activity of their core promoters for minus-strand synthesis (van Rossum *et al*., 1997).

The 51 b CSE is a highly conserved *cis*-acting element in SIN that is located in the 5'-proximal non-structural protein 1 (nsP1) ORF and near the 5' ends of all naturally occurring DI RNAs (Frolov *et al*., 2001). This region is predicted to fold into two small hairpins (SL3 and SL4) on the plus-strand using *mfold* structural prediction analysis and comparative analysis with other alphaviruses (Frolov *et al*. , 2001; Niesters and Strauss, 1990). Silent mutations or deletions in the CSE of SIN reduced replication *in vivo* (Frolov *et al*., 2001; Niesters and Strauss, 1990), whereas the CSEs in DI RNAs were found to be dispensable in vertebrate cells (Levis *et al*., 1986). These findings suggest that the CSE only enhances replication in the virus.

Human rhinovirus 14 (HRV-14) is a picornavirus containing a single large ORF that encodes a polyprotein cleaved by proteases to produce functionally active viral proteins. The P1 segment of the polyprotein ORF is near the 5' end of the viral genome and is dispensable for replication of poliovirus, another picornavirus member. However, replacement of all but 21 nucleotides in the P1 segment of HRV-14 with a β–galactosidase or luciferase ORF resulted in replication levels that were reduced *in vivo*. Stepwise in-frame deletions from the 3' end of the P1 segment revealed that a 602 b region was involved in this decrease. Introduction of this sequence into HRV-14 containing lucerifase in place of the P1 ORF was able to restore replication to near wt levels, indicating the existence of a replication enhancer in the P1 segment of the polyprotein ORF (McKnight and Lemon, 1996).

Prototypical TBSV DI RNAs, such as DI-70F, contain 4 regions (I, II, III, and IV) derived from the helper virus. Region III, which is 70 b long, contains a 35 nucleotide element known as segment A. Replacement of Region III with segment A in either forward or reverse orientations resulted in DI RNA accumulation that was 40% of wt levels for both mutants, suggesting that this element can function independently in the absence of flanking region III sequence on either plus- or minus-strands. Structural prediction analysis of segment A revealed that it could potentially adopt a hairpin conformation, which was designated as stem-loop 1 (SL1). Mutations that disrupted the stem of SL1 on minus-strands but maintained basepairing on plus-strands reduced accumulation by about 80% in comparison to wt, whereas alterations testing the opposite possibility accumulated to near wt levels, suggesting that SL1 functioned primarily in its minus-sense orientation (Ray and White, 2003). Since SL1 can be deleted without reducing accumulation to undetectable levels *in vivo*, these results suggest that SL1 functions as a replication enhancer on the minus-strand to promote plus-strand synthesis (Ray and White, 1999; Ray and White, 2003).

Upstream of the core promoter for minus-strand synthesis in RCNMV is a series of small hairpins labeled SLDa, SLDb, and SLDc. SLDa was not detrimental when its terminal loop was altered or when the entire hairpin was deleted *in vitro*, indicating that this element was dispensable for replication. However, mutagenesis or deletion of SLDb or SLDc resulted in a modest reduction in replication, suggesting that these hairpins may enhance minus-strand synthesis directed by the core promoter (Iwakawa *et al*, 2007).

RdRp Chaperones

RdRp chaperones are viral *cis*-acting elements that are involved in properly folding and assembling proteins forming the replicase. In BMV, proteins 1a and 2a are translated from RNA1 and RNA2 respectively, and compose the RdRp. Expression of 1a and 2a from genes devoid of UTRs (B12) in yeast and isolation of RdRp, resulted in a lack of activity when subsequently used in an in vitro transcription assay. However, addition of a replication-competent RNA3 was able to rescue the activity of RdRp. Transformation of B12 with RNA3 mutant cDNAs revealed that sequences in the 3' UTR and intercistronic region resulted in active RdRp, suggesting that these regions may interact with the replicase proteins to properly assemble them into complexes capable of transcription (Quadt *et al*., 1995).

In AlMV, RNA1 and RNA2 are templates for the synthesis of proteins P1 and P2 that interact to form the RdRp. Agroinfiltration of *Nicotiana benthamiana* with T-DNA vectors transiently expressing RNA1 and RNA2 with deleted 3' UTRs revealed that P1 and P2 were able to assemble into replication complexes, but were unable to direct transcription *in vitro*. Addition of either the RNA1 or RNA2 3' UTR resulted in active RdRp, suggesting that the 3' UTR is important for RdRp stability or for properly assembling an active RdRp complex (Vlot *et al*., 2001).

Expression in yeast of TBSV DI-72 and the replication proteins (p33 and p92) of *Cucumber necrosis virus* (CNV), a closely related tombusvirus, resulted in a 40-fold enhancement in RdRp activity in comparison to p33 and p92 alone, *in vitro* (Panaviene *et al*., 2004). To determine specific elements involved in RdRp assembly, deletions of DI-72 were constructed and co-expressed in yeast with CNV replication proteins. Short stretches of sequences in the 3'-terminal core promoter for minus-strand synthesis (gPr),

a nearby upstream hairpin (SL3), and an internally located hairpin (RII(+)-SL) that binds p33 *in vitro*, were identified (Panaviene *et al*., 2005; Pogany *et al*., 2005). The proposed model for replicase assembly commences with recruitment of p33 to RII(+)-SL, binding of p92, which may interact with p33, and transfer of the RdRp complex to the gPr and SL3 for proper initiation of minus-strand synethesis at the 3'terminus (Panaviene *et al*., 2005).

Turnip Crinkle Virus (TCV): A Model RNA Virus for Studying Translation and Replication

TCV, a member of the genus Carmovirus in the Family *Tombusviridae,* has been used as a model system for identifying and characterizing *cis*-acting elements important for replication. The TCV genomic RNA is 4054 bases and consists of a plus-sense single-stranded RNA with five overlapping open reading frames that encode for proteins functioning in replication, movement, and packaging (Fig. 1.3; Carrington *et al*., 1989; Oh *et al*., 1995; Hacker *et al*., 1992). The two TCV-encoded products that are required for replication *in vivo* are p28 and its readthrough product p88. p88 contains the RdRp active site and can by itself promote complementary strand synthesis from cognate templates *in vitro* (Rajendran *et al*., 2002). Additionally, TCV is naturally associated with several non-coding satellite (sat) RNAs with satC, a 356 base molecule sharing its 3' terminal 166 bases with TCV, being the best-characterized (Fig. 1.3; Fig. 1.4; Simon and Howell, 1986).

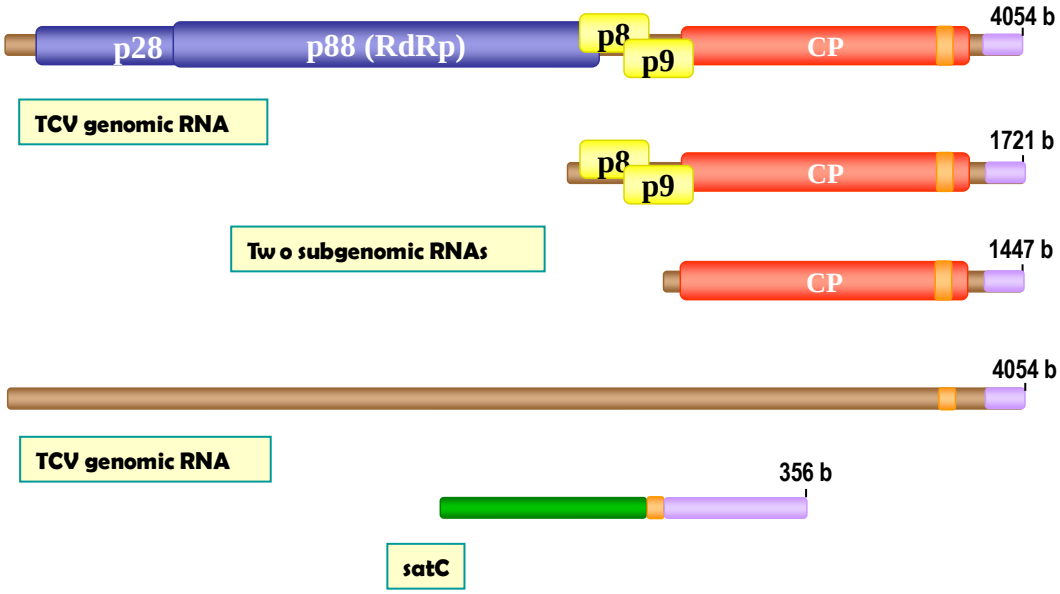

Figure 1.3. Genomic Organization of TCV and SatC. In TCV, p28 and p88 are replication proteins, p8 and p9 are proteins involved in virus movement, and the coat protein (CP) encapsidates the viral and satC RNA. satC comprises a sequence not related to TCV fused to two regions derived from the 3' end of TCV. Similar sequences between TCV and satC are colored alike.

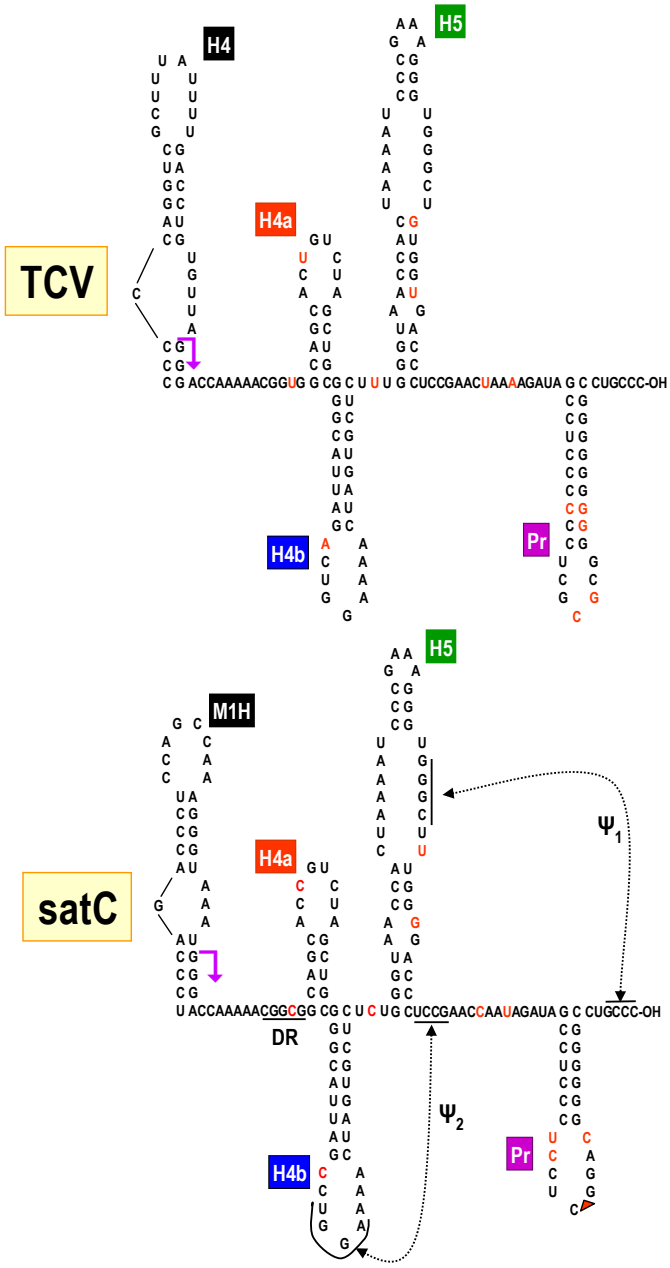

Figure 1.4. Sequence and Structure of the TCV and SatC 3' Ends. Names of predicted hairpins (M1H, H4, H4a, H4b, H5, and Pr) are designated by boxes. Tertiary interactions (Ψ) in satC are shown by double-headed arrows. Nucleotides comprising the derepressor (DR) element in satC are underlined. Base variations between the 3' terminal homologous regions of TCV and satC are denoted in red and the red triangle in satC represents the absence of four bases. Purple arrows delineate the end of sequence similarity between TCV and satC.

Identification of several *cis*-acting elements that may be important for TCV helper virus replication have been identified in satC. The 29 bases at the 3' terminus of plus-strands, which contains the core promoter hairpin (Pr) and a six-base (5'-CUGCCC) tail, can direct transcription of an inactive RNA template unrelated to TCV using partially purified RdRp *in vitro* (Fig. 1.4; Song and Simon, 1995). Mutagenesis of the Pr showed that the size and sequence of the loop region were flexible and maintenance of the lower stem was of high importance *in vitro* and *in vivo* (Stupina and Simon, 1997; Song and Simon, 1995). Computer modeling revealed that the ability of these mutants to accumulate *in vivo* was directly associated with the stability of the Pr hairpin; however, stability was not the only contributing factor (Stupina and Simon, 1997).

In vivo systematic evolution of ligands by exponential enrichment (SELEX) is a technique that can be used to overcome the limitations of site-directed mutagenesis by allowing for side-by-side evolution of large numbers of randomized bases. To analyze the sequence requirements for satC Pr that result in an increased level of fitness, nearly the entire predicted hairpin was randomized, inoculated onto turnip plants, and incubated until 14 days post-inoculation (dpi). Isolated total RNA from round 1 was then pooled from all the plants and re-inoculated two more times to initiate rounds 2 and 3, respectively. Analysis of the cloned progeny from all three rounds revealed that helical stability and fitness increased with each successive round and paralleled results observed with site-directed mutagenesis (Stupina and Simon, 1997). However, sequencing of viral progeny RNA at the end of round 3 revealed a preference for 6 base tails downstream of the Pr, CG basepairs at the base of the stem, and a UG or UA basepair at the fourth position from the base (Carpenter and Simon, 1998).

Deletion of the three terminal cytidylates in the six-base tail resulted in a 3.5-fold increase in transcription of full-length satC and the appearance of aberrant internal initiation products *in vitro* (Guan and Simon, 2000, Zhang *et al*., 2004a). In vitro chemical and enzymatic probing of satC RNA lacking the terminal cytidylates revealed that three consecutive guanylates 55 b upstream of the 3' terminus became single-stranded in comparison to wild-type (wt). To determine if the three guanylates basepaired with the three terminal cytidylates to regulate minus-strand synthesis, mutations were made to disrupt or maintain this predicted interaction. Disruption of this interaction substantially enhanced synthesis of full-length products *in vitro*, whereas alterations that maintained basepairing resulted in transcription near baseline levels (Zhang *et al*., 2004a). These results indicated that the 3'-terminal cytidylates basepair with internally-located guanylates (Ψ_1) for repression of minus-strand synthesis and promotion of correct initiation at the 3' end (Fig. 1.4).

To alleviate repression of minus-strand synthesis, a *cis*-acting element that basepairs with sequences comprising Ψ_1 presumably exists. A possible candidate for such a derepressor element (DR) has been identified as a sequence located 76 b upstream from the consecutive guanylates involved in repression. Alteration of the DR, which was initially predicted to basepair with the 3' end tail, resulted in barely detectable levels of transcription *in vitro*. However, the mutated DR in conjunction with deletion of the 3' terminal cytidylates *in vitro* resulted in transcription that was considerably above wild-type levels (Zhang *et al*, 2004a). These results show that removal of the terminal cytidylates obviates the need for a properly functioning DR element, suggesting that the DR is antagonistic to sequences involved in repression of minus-strand synthesis.

Using *mfold*, a program used to determine the free energies of optimal and suboptimal RNA structures (Zuker, 2003), full-length satC was folded and the most stable conformation analyzed. In addition to the Pr, the 3' terminal 140 b were predicted to form a series of hairpins that have been designated as Hairpin 4a (H4a), Hairpin 4b (H4b), and Hairpin 5 (H5) (Fig. 1.4; Zhang *et al*., 2004a). The three consecutive guanylates involved in repression of minus-strand synthesis were predicted to form the 3' side of a large symmetrical loop (LSL) within H5. Phylogenetic comparisons, which are a type of analysis used to determine biologically functional RNA conformations by analyzing the predicted structures of closely related viruses, identified equivalent H5 structures in nearly all carmoviruses (Zhang *et al.*, 2004a). Sequence analysis between the carmoviruses revealed that covariation existed in the lower and upper stems, the terminal loops were mostly stable tetraloops or pentaloops, and the 3' sides of the LSL contained highly-conserved consecutive guanylates that were predicted to basepair with the 3' termini (Zhang *et al*., 2004a).

Mutagenesis of the satC LSL revealed that sequence conservation in the middle of the loop was stringent and substitutions in the lower part of the loop were well-tolerated. Some mutations were associated with second-site alterations in the LSL or nearby upstream sequences in viral progeny RNA extracted from inoculated plants. The most notable second-site mutations were found in three clones derived from two constructs in an identical position within the terminal loop of satC H4a. However, mutations in the H4a loop that either disrupted or maintained potential basepairing with the 3' side of the H5 LSL did not support the existence of an interaction (Zhang *et al*., 2004b). Replacements of H4a, neighboring H4b, or both, with analogous predicted structures

from a closely-related carmovirus showed that the double replacement construct accumulated higher than either of the single exchanges *in vivo*, suggesting the existence of a structural domain comprising H4a and H4b. The terminal loop of H4b containing a 5'-UGGA sequence was found to interact with bases adjacent to H5 (Ψ_2) using compensatory mutational analysis, which was suggested to be a part of a structural switch regulating minus-strand synthesis (Fig. 1.4; Zhang *et al*., 2006a).

On satC minus-strands, several unstructured *cis*-acting elements exhibiting promoter activity have been identified as being involved in plus-strand synthesis. Six bases located at the 3' end constitute the 3' terminal carmovirus consensus sequence (3' CCS). This sequence, which is well-conserved at the 3' ends of minus-strands for all carmoviral genomic, subgenomic, and subviral RNAs, contains a combination of three to seven adenylates and uridylates followed by two to three cytidylates (3'-$C_{2-3}A/U_{3-7}$; Guan *et al*., 1997), and is required for plus-strand synthesis *in vivo* (Guan *et al*., 2000a), but is dispensable for transcription using minus-strand templates and partially purified RdRp *in vitro* (Guan *et al.,* 1997). Non-viral bases added to the 3' ends of satC minus-strands resulted in exclusive internal initiation 12 bases from the 3' terminus *in vitro*. Analysis of the internal initiation site, which also contained a CCS (3'-CCCAAA), uncovered a second element named the 3' proximal element (3' PE; Guan *et al*., 1997). However, mutations introduced into this region were not detrimental *in vivo* (Guan *et al*, 2000a), suggesting that this element is not essential, but was found to be important in transcription *in vitro*. Surprisingly, deletion of all of the satC minus-strand except for the 5' terminal 100 b resulted in the synthesis of a product smaller than the input RNA *in vitro* (Song and Simon, 1994). This result pointed to internal initiation near the 5' end at

a third minus-strand *cis*-acting element displaying promoter activity. Mapping of this internal initiation site, which is labeled the 5' proximal element (5' PE), uncovered a sequence located 41 bases from the 5' end with characteristics similar to the 3' PE. Both the 5' and 3' PE lack predicted secondary structures, contain consecutive purines that are followed by multiple cytidylates, and promote internal initiation *in vitro* (Guan *et al*, 1997). Mutagenesis of the cytidylates within the 5' PE showed sequence specificity and a disproportionate negative effect on plus-strand accumulation in comparison to minus-strand synthesis *in vivo* (Guan *et al*., 2000b). Interestingly, the 5' PE sequence coincides partially with the 3' side of the satC H5 lower stem on the plus-strand.

Another minus-stranded *cis*-acting element that functions as a replication enhancer is a 28-base hairpin named the motif 1 hairpin (M1H). M1H is required for the efficient replication of satC monomers *in vivo* and was found to stimulate plus-strand synthesis 10-fold in its minus-sense orientation *in vitro* (Nagy *et al*., 2001, Nagy *et al*., 1999). Like the 3' and 5' PE, the M1H has been proposed to recruit the RdRp to the minus-strand satC template RNA *in vitro*, as evidenced by the composition of the minus-stranded M1H containing sequence elements found in the satC 5' PE and TCV 3' CCS (Nagy *et al*., 1998). However, minus-sense M1H cannot initiate transcription *de novo* unless two to three consecutive cytidylates that can function as transcription initiators are placed immediately downstream of the hairpin (Nagy *et al.*, 1999). Mutagenesis of upstream and downstream sequences flanking the M1H significantly reduced viral accumulation in vivo, supporting the possibility that these sequences are important for full enhancer activity of M1H (Nagy *et al*., 2001). In addition to its role as a replication enhancer, M1H also functions as a hotspot for RNA recombination in its minus-sense

orientation (Cascone *et al*., 1993; Nagy *et al*., 1999) and as an inhibitor of virion accumulation in its plus-sense orientation by bridging important flanking sequences (Zhang and Simon, 2003, Sun and Simon, 2003).

Thesis Plan

This thesis investigates *cis*-acting elements involved in translation and replication of TCV. The roles of H5 in properly folding the TCV RdRp and regulating minus-strand synthesis are described in Chapter II. In Chapter III, identification and characterization of the internal tRNA-like structure (iTLS), a translation *cis*-acting element that binds 60S ribosomal subunits, is presented. Chapter IV discusses the possible similarities and differences in translational strategies between TCV and two closely-related carmoviruses, *Cardamine chlorotic fleck virus* (CCFV) and *Japanese iris necrotic ring virus* (JINRV).

CHAPTER II

BIASED HYPERMUTAGENESIS ASSOCIATED WITH MUTATIONS IN AN UNTRANSLATED HAIRPIN OF AN RNA VIRUS

Introduction

Replicases of plus-strand RNA viruses comprise the viral-encoded RNA-dependent RNA polymerase, other virally-encoded proteins, and possibly host factors (Lai, 1998). Replication of viral genomes occurs in vesicles formed from cellular membranes and initiates with the synthesis of complementary minus-strands that are used as templates for synthesis of plus-strands that are released into the cytoplasm (Schwartz *et al*., 2002; Buck, 1996). Replication requires the participation of *cis*-acting elements on the viral RNA that tend to cluster in the 5' and 3' untranslated regions (UTRs), exhibit sequence and/or structural specificity, and interact with proteins or other regions of viral RNA (Dreher, 1999; Duggal *et al.*, 1994). *Cis*-acting elements defined as core promoters function by recruiting replicases to plus- and minus-strand transcription initiation sites for accurate genomic and subgenomic RNA synthesis (Wang and Simon, 1997; Song and Simon, 1994; Levis *et al*., 1990; Miller *et al*., 1986; Miller *et al*., 1985). Core promoters located in the 3' UTRs of plus-strands that are involved in minus-strand synthesis include tRNA-like structures and their corresponding upstream pseudoknots (Duggal *et al*.,

1994), poly(A) tails (Hardy and Rice, 2005, Lin *et al*., 1994), and simple stem-loops (Olsthoorn and Bol, 2002; Song and Simon, 1995). The efficacy of promoters can be increased by RNA elements known as enhancers, which facilitate the recruitment of the replicase to the template. Enhancers have been identified in a number of viruses (Ranjith-Kumar *et al*., 2003; Frolov *et al*., 2001; Nagy *et al*., 1999; Ray and White, 1999; van Rossum *et al*., 1997; Quadt *et al*., 1995; Barrera *et al*., 1993; French and Ahlquist, 1987), where they are found in variable positions in relation to RNA transcription initiation start sites on both plus- and minus-strands of the viral RNAs. *Cis*-acting elements on the template RNA have also been implicated in replicase maturation by functioning as chaperones (Vlot *et al*., 2001; Quadt *et al*., 1995) with deletion of these sequences resulting in reduction of replicase stability or template recruitment to the site of replication.

As previously described in Chapter I, *Turnip crinkle virus* (TCV) is a member of the genus Carmovirus in the Family *Tombusviridae* and has been used as a model system for identifying and characterizing *cis*-acting elements important for replication. The TCV genomic RNA is 4054 bases, consisting of a plus-sense, single-stranded RNA with five overlapping open reading frames (ORFs) that encode proteins functioning in replication, movement, and packaging (Carrington *et al*., 1989; Oh *et al*., 1995; Hacker *et al*., 1992). TCV-encoded products that are required for replication *in vivo* are p28 and its readthrough product p88. p88 contains the RdRp active site and is able to promote complementary strand synthesis from cognate templates *in vitro* (Rajendran *et al*., 2002). TCV is also associated with several non-coding satellite RNAs that range in size from

194 to 356 bases with satC (356 bases) sharing its 3' terminal 166 bases with TCV (Simon and Howell, 1986).

Analysis of satC replication in protoplasts and transcription of complementary strands *in vitro* using extracts from infected plants containing partially purified RdRp led to the identification of several elements that are important for efficient satC accumulation. These elements include a core promoter (Pr) hairpin for synthesis of minus-strands that is located at the 3' terminus of plus-strands (Carpenter and Simon, 1998; Stupina and Simon, 1997; Song and Simon, 1995) and three unstructured elements on the minus-strand known as the 3' carmoviral consensus sequence (3'CCS), 3' proximal element (3'PE), and 5' proximal element (5'PE) that are important for plus-strand synthesis (Guan *et al*., 2000a; Guan *et al*., 2000b; Guan *et al*., 1997). Other replication elements include the 28-base motif-1 hairpin (M1H), which functions as a replication enhancer and hotspot for RNA recombination in its minus-sense orientation (Cascone *et al*., 1993; Nagy *et al*., 1999) and as an inhibitor of virion accumulation in its plus-sense orientation (Zhang and Simon, 2003). Two hairpins in the 3' UTR of TCV, (M3H and H4), which are not found in satC, also function as replication enhancers and recombination hotspots in their minus-sense orientation (Nagy *et al*., 1999).

In this chapter, an element (hairpin 5; H5) containing a highly conserved large symmetrical loop (LSL) has been identified near the 3' ends of nearly all carmoviral RNAs including TCV and satC. TCV H5 was found to be position-dependent and able to basepair with the 3' terminal bases, suggesting that it plays a role in regulating minus-strand synthesis. Mutations introduced into the TCV LSL resulted in a 7-fold average increase in second-site mutations positioned throughout the sequenced region with the

majority of alterations being uridylate to cytidylate and adenylate to guanylate substitutions. These results suggest that H5 may function as a maturation element to properly fold the RdRp.

Materials and Methods

Construction of TCV Mutants

C3994G, G4051C, and C3994G/G4051C (Table 2.1) were made by PCR using pTCV66 (Table 2.1; Fig. 2.1), oligonucleotide 3164, and oligonucleotide G3994S/G4051S (Table 2.2). Inserts were cut with BsmI and SmaI and ligated into similarly digested pTCV66. To generate G3991U (Table 2.1), PCR amplification was performed using pTCV66, oligonucleotide JM3, and oligonucleotide KK57 (Table 2.2). The insert was blunt-ended with Klenow and cut with SpeI and the fragment ligated into pTCV66 cut with SpeI and SmaI. For $H5_{DUP}$, pTSN-L5 (Table 2.1; a TCV construct containing a SnaBI site just downstream of H5) was cut with SnaBI and SpeI. The small DNA fragment was blunt-ended with Klenow and ligated into SnaBI-cut Sna/TCV (Table 2.1; a TCV construct containing a SnaBI site immediately downstream of the CP ORF stop codon). To create $H5_{TRANS}$ (Table 2.1), construct G3991U was digested with SpeI and SmaI and the small fragment ligated into construct $H5_{DUP}$ cut with the same enzymes. Mutations in the 5' side of the H5 LSL were made by PCR using template pTCV66, oligonucleotide KK57, and oligonucleotide JM2 (Table 2.2), which contained an equal mixture of dATP and dCTP at TCV positions 3976 to 3978. Products were kinased with T4 PNK and blunt-ended with Klenow followed by digestion with SpeI and

TABLE 2.1. Summary of TCV Constructs Used in Chapter II

Name	Description
pTCV66	Wt TCV
pTSNL5	Wt TCV with a SnaBI site created by insertion of a cytidylate, guanylate, and uridylate, downstream of position 4014
Sna/TCV	Wt TCV with a SnaBI site created by deletion of a guanylate at position 3803
C3994G	pTCV66 with a cytidylate to guanylate substitution at position 3994
G4051C	pTCV66 with a guanylate to cytidylate substitution at position 4051
C3994G/ G4051C	pTCV66 with a cytidylate to guanylate substitution at position 3994 and a guanylate to cytidylate substitution at position 4051
G3991U	pTCV66 with a guanylate to uridylate substitution at position 3991
$H5_{DUP}$	Sna/TCV with a 64b H5 insertion in the SnaBI site
$H5_{TRANS}$	Sna/TCV with a 64b H5 insertion in the SnaBI site and a guanylate to uridylate substitution at position 3991
A3976C	pTCV66 with an adenylate to cytidylate substitution at position 3976
A3978C	pTCV66 with an adenylate to cytidylate substitution at position 3978
G3991A	pTCV66 with a guanylate to adenylate substitution at position 3991
A3976C/ A3978C	pTCV66 with an adenylate to cytidylate substitution at position 3976 and 3978

TABLE 2.2. Summary of Oligonucleotides Used in Chapter II

Application	Name	Position	Sequence[b]	Polarity[c]
TCV mutagenesis	3164	3164-3181[a]	5'-ATGAGCCCTTCAACCACC	+
	G3994S/ G4051S	3983-4054[a] + 9b vector	5'-**AGGATCCCC**GGGSAGGCCCCCCCCCCGCGCGAG GGGGGAGGCTATCTTTTAGTTCGGAGGGTCACCAC ASCCCACCCTTTC	-
	KK57	4035-4054[a]	5'-GGGCAGGCCCCCCCCCCGCG	-
	JM2	3947-3993[a]	5'-GAAAACTAGTGCTCTTTGGGTAACCACTAMMMTC CCGAAAGGGTGGG	+
	JM3	3947-4006[a]	5'-GAAAACTAGTGCTCTTTGGGTAACCACTAAAATCC CGAAAGGGTNGGCTGTGGTGACCCT	+
Northern blotting	Oligo 13	3944-3963[a]	5'-AAAGAGCACTAGTTTTCCAG	-
	3892	3893-3913[a]	5'-CCGTTTTTGGTCCCTAACACA	-

[a] Positions correspond to the base number in genomic TCV

[b] Underlined letters indicate mutated bases in comparison to pTCV66 plasmid sequence. Bold letters illustrate bases derived from vector sequence. M = A or C; N = A, G, C, or T; S = G or C

[c] "+" and "-" indicate homology and complementarity, respectively, to TCV plus strands

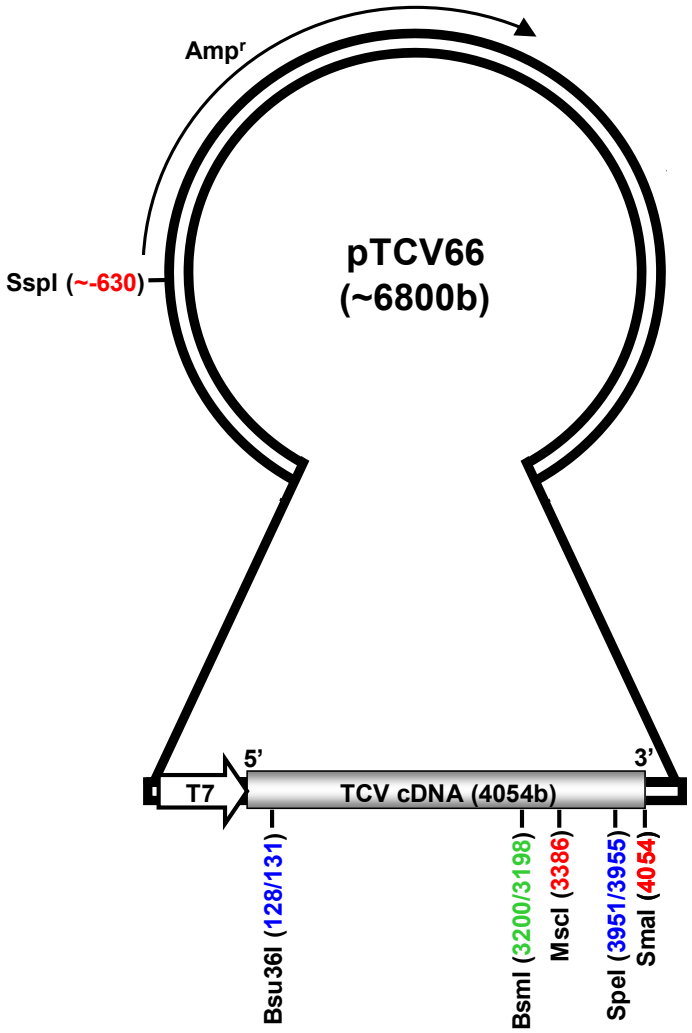

Figure 2.1. Diagram of pTCV66 Vector Containing Full-Length TCV, Massachusetts Strain, Downstream of a T7 RNA Promoter. Restriction enzyme sites are indicated by solid black lines and locations based on TCV nucleotide position are color-coded according to the type of cleavage produced: blunt-ended (red), 5' overhang (blue), 3' overhang (green).

ligation into pTCV66 cut with SpeI and SmaI. Alteration G3991A (Table 2.1) was constructed identically to the G3991U described above. Base alterations were confirmed by sequencing.

Bacterial Transformation

Fifty microliters of DH5α™ subcloning efficiency chemically competent cells (Invitrogen) were thawed and incubated on ice for 30 min with approximately 10 ng of DNA from a DNA ligation reaction mixture. Cells were then heat shocked for 45 sec at 37°C and incubated on ice for 2 min. Nine hundred fifty microliters of LB were added and the cells shaken at 225 rpm at 37°C for 1 hr. Using a microcentrifuge, cells were pulse centrifuged for 10 sec, resuspended in 100 µl of LB, and plated onto LB containing 1.5% bacteriological agar and 100 µg/ml ampicillin (prewarmed at 37°C for 1 hr). Plates were incubated for 16 to 20 hr at 37°C.

Small Scale Plasmid DNA Preparation

Three milliliters of LB containing 100 µg/ml ampicillin were inoculated with a single transformed *E. coli* bacterial colony and shaken at 225 rpm at 37°C for 16 to 20 hr. Half of the bacterial culture was subjected to pulse centrifugation and resuspended in 140 µl of STET buffer (8% (w/v) sucrose, 5% (v/v) Triton X-100, 50 mM EDTA, 50 mM Tris-HCl, pH 8). All centrifugations for this procedure were performed using a microcentrifuge. Next, 10 µl of lysozyme (10 mg/ml) was added and the mixture vortexed vigorously, incubated in boiling water for 60 sec, and immediately chilled on ice. The lysed cells were then centrifuged at 13,000 rpm for 15 min at room temperature

and the pellet discarded using a wooden toothpick. One hundred fifty microliters of isopropyl alcohol was added to the supernatant and the mixture vortexed, incubated on ice for 5 min, and centrifuged at 13,000 rpm for 5 min at 4°C. The supernatant was discarded, the pellet rinsed with 75% ethanol, and centrifuged at 13,000 rpm for 5 min at 4°C. The supernatant was discarded and the pellet dried and resuspended in 20 µl of double distilled water.

DNA Sequencing of a Small Scale Plasmid Preparation

Fourteen microliters of double distilled water, 1 µl of primer (2 pmol/µl), and 2 µl of freshly made 2 N sodium hydroxide, were added to 5 µl of a small scale plasmid DNA preparation made using the STET method. The mixture was then incubated in boiling water for 2 min and immediately chilled on ice. Three microliters of 3 M sodium acetate, pH 5.2, and 50 µl of 100% ethanol were added and the mixture vortexed and incubated at -80°C for 5 min. Next, the sample was centrifuged at 13,000 rpm for 10 min at 4°C and the supernatant discarded. All centrifugations for this procedure were performed using a microcentrifuge. The pellet was then washed with 500 µl of 70% ethanol and centrifuged at 13,000 rpm for 5 min at 4°C. The supernatant was decanted and the pellet dried, resuspended in 5 µl of 1x Sequenase buffer (40 mM Tris-HCl, pH 7.5, 20 mM magnesium chloride, 50 mM sodium chloride), and incubated for 15 min at 37°C to anneal the primer to the template. As the template was incubating, 1.25 µl of each of the dGTP termination mixes (ddA, ddG, ddC, ddT) was aliquotted separately onto one petri dish (100 x 15 mm), and a Sequenase mixture containing 1.2 µl of diluted dGTP labeling mix (1:10), 0.5 µl of DTT (100mM), 0.3 µl α-^{35}S dATP (10 mCi/ml), 0.9 µl Tris-EDTA,

pH 8, and 0.1 μl of preblended Sequenase Version 2.0 DNA polymerase containing inorganic pyrophosphatase (USB) was prepared. Both the termination mixes and Sequenase mixture were stored on ice until needed. The annealed DNA template was removed from the 37°C water bath and placed at room temperature for approximately one min. Three microliters of the Sequenase mixture were added to the annealed template, mixed by pipet, and incubated at room temperature for one min. For each termination mix, 1.8 μl of Sequenase mixture containing annealed template were added, mixed by pipet, and incubated in a 37°C water bath for 5 min. Next, the sample was placed at room temperature and 2 μl of stop solution (95% (v/v) formamide, 20 mM EDTA, bromophenol blue, xylene cyanol FF) was immediately aliquotted into each reaction and mixed by pipet. The sample was incubated in a 75°C water bath for 2 min, placed on ice, and subjected to electrophoresis through a 6% denaturing polyacrylamide gel. The gel was then transferred to Whatman gel blot paper, vacuum dried at 80°C for 20 min., and autoradiography performed using Kodak Biomax MR film.

Large Scale Plasmid DNA Preparation

Two hundred milliliters of LB containing 100 μg/ml ampicillin was inoculated with 1.5 ml of freshly amplified 3 ml bacterial culture and shaken at 225 rpm for 16 hr at 37°C. The cells were transferred to GSA bottles and subjected to centrifugation (Sorvall RC5C centrifuge, GSA rotor) at 6000 rpm for 10 min at 4°C. The supernatant was decanted and the pellet resuspended in 2.5 ml of suspension buffer (25% (w/v) sucrose, 50 mM Tris-HCl, pH 7.5) by pipet. The suspension was transferred to SS34 bottles and 400 μl of freshly prepared lysozyme (10 mg/ml) was added. The mixture was agitated

and incubated on ice for 10 min. Next, 700 µl of 0.5 M EDTA was dispensed and the mixture agitated and incubated on ice for 10 min. Lysis buffer (5.3 ml; 0.1% (v/v) Triton X-100, 62.5 mM EDTA, 50 mM Tris-HCl, pH 8.0) was then added and the mixture agitated and incubated at 42°C for 5 min. Lysed cells were next subjected to centrifugation (Sorvall RC5C centrifuge, SS34 rotor) at 17,000 rpm for 20 min at 4°C. Double distilled water was added to the supernatant to bring the volume up to 11 ml and 10.2 g of cesium chloride and 200 µl of ethidium bromide (10 mg/ml) were dissolved. The mixture was transferred to a Beckman OptiSeal ™ polyallomer centrifuge tube (16 x 67 mm) and subjected to ultracentrifugation (Beckman L8-80) at 65,000 rpm at 20°C for 3.2 to 4.2 hr. The viral cDNA band was isolated using a 5 ml syringe with an 18 gauge needle and transferred to a 15 ml centrifuge tube. The DNA was extracted 2 to 3 times with isopropyl alcohol saturated with sodium chloride. Two volumes of double distilled water were added and the mixture brought up to 15 ml with 100% ethanol. The DNA was incubated for 1 hr at -20°C and subjected to centrifugation at 3,000 rpm for 20 min at 4°C using the Beckman GPR centrifuge. The supernatant was discarded and the pellet resuspended in 400 µl of double distilled water and transferred to a 1.5 ml microcentrifuge tube. Forty microliters of 3 M sodium acetate (pH 5.2) and 880 µl of 100% ethanol were added and the mixture vortexed and incubated at -80°C for 5 min. The DNA was then centrifuged at 13,000 rpm for 10 min at 4°C and the supernatant decanted. All centrifugations for the ethanol precipitation were performed using a microcentrifuge. The pellet was then washed twice with 500 µl of 70% ethanol and subjected to centrifugation at 13,000 rpm for 5 min at 4°C. The supernatant was decanted after the second wash with 70% ethanol and the pellet dried and resuspended in 400 µl of

double distilled water. The DNA concentration was determined using a spectrophotometer.

DNA Sequencing of a Large Scale Plasmid Preparation

In a 0.5 ml microcentrifuge tube, 2 to 4 μg of plasmid DNA (prepared using the cesium chloride gradient method), 2 μl of freshly prepared 2 N sodium hydroxide, and double distilled water to a total volume of 18 μl, were combined and incubated at room temperature for 5 min. Five molar ammonium acetate (7.98 μl) and 100 μl of 100% ethanol were added and the mixture incubated at -80°C for 5 min and then centrifuged at 13,000 rpm for 10 min at 4°C. All centrifugations for this procedure were performed using a microcentrifuge. The supernatant was discarded, the pellet washed with 500 μl of 70% ethanol, and centrifuged at 13,000 rpm for 5 min at 4°C. The supernatant was removed and the pellet dried. The pellet was then dissolved in 3.5 μl of double distilled water, 1 μl of 5x Sequenase buffer (200 mM Tris-HCl, pH 7.5, 100 mM magnesium chloride, 250 mM sodium chloride), and 0.5 μl of primer (2 pmol/μl), and incubated at 37°C for 20 min to anneal the primer to the template. As the template was incubating, three procedures were performed. First, a ^{35}S mixture containing 0.5 μl of 100 mM DTT, 1 μl of dGTP labeling mix (1:10), and 0.5 μl of α-^{35}S dATP (10 mCi/ml) was prepared and stored on ice. Secondly, preblended Sequenase Version 2.0 DNA polymerase containing inorganic pyrophosphatase (USB) was diluted 1:8 using chilled Tris-EDTA, pH 8, and placed on ice. Thirdly, 1.25 μl of each dGTP termination mix (ddA, ddG, ddC, ddT) was dispensed into a petri dish (100 x 15 mm) and incubated in a 37°C water bath at 5 minutes before the completion of the incubation containing the template and primer.

The annealed template was removed from the 37°C water bath and incubated for one min at room temperature. Two microliters of the ^{35}S mixture and 1 μl of the diluted Sequenase (1:8) were added to the annealed template, mixed by pipet, and incubated for 1 min at room temperature. The dGTP termination mixes were removed from the 37°C water bath and 1.75 μl of the above mixture were added to each droplet and mixed by pipet. The sample was then incubated at 37°C for 5 min and the reaction terminated by the addition of 2 μl of stop solution (95% formamide, 20 mM EDTA, bromophenol blue, xylene cyanol FF). Prior to electrophoresis through a 6% denaturing polyacrylamide gel, the sample was incubated at 75°C for 2 min. The gel was transferred to Whatman gel blot paper and dried under vacuum for 20 min at 80°C. Autoradiography was performed using Kodak Biomax MR film.

In Vitro Transcription of Infectious Viral RNA Using T7 RNA Polymerase

To 8 μg of TCV cDNA linearized with SmaI, 29 μl of double distilled water, 6 μl of 100 mM DTT, 12 μl of a ribonucleotide mix (5 mM of each base), 12 μl of 5x T7 RNA polymerase buffer (125 mM sodium chloride, 40 mM magnesium chloride, 10 mM spermidine, 200 mM Tris-HCl, pH 8.0), 0.5 μl of RNaseOut ribouclease inhibitor (40 U/μl; Invitrogen), and 1 μl of T7 RNA polymerase (50 U/μl; Invitrogen) were added and the reaction incubated at 37°C for 1 hr. Sixty microliters of phenol/chloroform (1:1) were added, the mixture vortexed, and then subjected to centrifugation at 13,000 rpm for 2 min at room temperature. All centrifugations for this procedure were performed using a microcentrifuge. The aqueous layer was removed by pipet and 6 μl of 3 M sodium acetate and 120 μl of chilled 100% ethanol were added. The mixture was vortexed,

incubated at -80°C for 5 min, and centrifuged at 13,000 rpm for 10 min at 4°C. The supernatant was decanted, the pellet washed with 70% ethanol, and then centrifuged at 13,000 rpm for 5 min at 4°C. The supernatant was discarded and the pellet dried and resuspended in 30 µl of sterile double distilled water. Quality was assessed and concentration was calculated by subjecting the in-vitro transcripts to electrophoresis through a 1.5% agarose gel and using densitometry to compare the band intensity of the transcripts with a TCV RNA marker of a known concentration.

Culturing of Arabidopsis Callus

Approximately 300 Arabidopsis thaliana, ecotype Col-0, seeds were aliquotted into a 1.5 ml microcentrifuge tube and washed twice with 1 ml of 70% ethanol by vortexing vigorously, pulse centrifuging, and removing the alcohol by pipet. One milliliter of bleach containing 4 to 6% sodium hypochlorite followed by 50 µl of 10% (w/v) SDS were added, vortexed vigorously, incubated for 7 ½ min at room temperature, and the supernatant removed by pipet using pulse centrifugation. The seeds were then washed 5 times by suspending them in 1 ml of double distilled water, vortexing, and subjecting them to pulse centrifugation. After the final centrifugation, the seeds were resuspended in double distilled water. To create new callus, about 100 surface-sterilized seeds were placed onto CM plates and each plate individually sealed with parafilm. CM plates were made by combining 60 g sucrose, 8.8 g of MS Salts (Sigma-Aldrich), and 20 ml of 100x vitamins/glycine stock. The volume was brought up to 2 L with double distilled water and the pH adjusted to 5.8 using sodium hydroxide. Bacteriological agar was added to a concentration of 1% and the mixture autoclaved. When the temperature

of the melted agar was less than 60°C, 100 µl of 2,4-D (2 mg/ml) and 100 µl of kinetin (2 mg/ml) were added to 400 ml of medium and poured into sterile petri dishes. Every 3 weeks, callus was passaged (up to a maximum of 6 times) by using sterilized forceps to mechanically break the callus and transferring it to new CM plates. Plates were incubated in a Percival Scientific I-36LL incubator at 20°C using a photoperiod of 16 hr light and 8 hr dark, and an illuminance of 35 µmol/m^2S.

Preparation and Inoculation of Callus Culture Protoplasts with Infectious Viral RNA Using Polyethylene Glycol

Fifteen milliliters of 0.6 M mannitol (room temperature) were added to each plate of callus in a sterile environment. The callus was broken into smaller pieces using a 14.6 cm Pasteur pipet melted into an L-shape. Callus and mannitol were then poured into a 50 ml centrifuge tube and agitated at room temperature using a rotating shaker for 20 min at 100 rpm. For each plate of callus being processed, 50 ml of PIM was dispensed into a sterile 125 ml glass bottle along with 0.5 g cellulase (10 KU/g dry weight; Calbiochem) and 0.1 g pectinase (3 KU/g dry weigh; Calbiochem). PIM was made by combining 1 ml of 1000x vitamin stock (prepared by adding 0.02 g thiamine HCl, 0.01 g pyridoxine HCl, 0.01 g nicotinic acid, and 2 g myo-inositol to double distilled water, volume was adjusted to 20 ml), 0.5 ml of 2000x hormone stock (prepared by adding 0.004 g 2,4-D, 0.004 g kinetin, and 0.5 ml 1 N potassium hydroxide to double distilled water, volume was adjusted to 10 ml), 4.4 g of MS salts, 34.2 g of sucrose, 0.585 g of MES, 91 g of mannitol, and 0.555 g calcium chloride. The volume was brought up to 1 L with double distilled water and the pH adjusted to 5.8 with potassium hydroxide. The mixture

containing the PIM and enzymes was incubated on a rotating shaker at 100 rpm until completely dissolved (about 20 minutes) at room temperature. The callus was subjected to centrifugation at 2,000 rpm for 4 min at 4°C and the supernatant poured off. All centrifugations in this procedure were performed with the brake off in a Beckman GPR centrifuge. Fifty milliliters of PIM containing the dissolved enzymes were added to the callus and transferred to a 125 ml glass bottle. The bottle was then wrapped completely in aluminum foil and incubated at room temperature for 3.5 hr on a rotating shaker at 100 rpm. The turbid solution was filtered into a 50 ml centrifuge tube using a sterile funnel and 53 μm nylon mesh (Small Parts).

Protoplasts were centrifuged at 1,000 rpm for 4 min at 4°C. The supernatant was decanted leaving about 10 ml of solution and the pellet resuspended by gentle shaking of the tube. Twenty milliliters of cold (4°C) 0.6 M mannitol was added and the tube inverted several times to wash the protoplasts. The cells were centrifuged at 1,000 rpm for 4 min at 4°C. The washes were repeated for a total of three times. After the final wash and centrifugation, protoplasts were resuspended in a volume adjusted to 20 ml by cold 0.6 M mannitol and kept on ice. Protoplasts were then enumerated using a hemacytometer and 5 x 10^6 cells were aliquotted into 50 ml centrifuge tubes, one for each inoculation. Each tube was centrifuged at 1,000 rpm for 5 min at 4°C and the supernatant poured off leaving about 100 μl of solution. Protoplasts were kept on ice until inoculation. For each inoculation, 20 μg of TCV in-vitro transcribed RNA was combined with 8 μl of 1 M calcium chloride and the volume brought up to 430 μl with double distilled water. Each inoculation mix was kept on ice until needed. The inoculation mix was then added to the tube containing the protoplasts and pipetted gently up and down

twice. Next, 2.2 ml of 50% (w/v) PEG (prepared by dissolving 25 g of PEG 1540 in 50 mM Tris-HCl, pH 7.5, volume was adjusted to 50 ml) was added, mixed well by shaking for 15 sec, and incubated at room temperature for 20 sec. Cold 0.6 M mannitol containing 1 mM calcium chloride was added to a volume of 30 ml and tube incubated on ice for 15 min. Protoplasts were then centrifuged at 1,000 rpm for 5 min at 4°C and the supernatant decanted leaving 10 ml of residual liquid. Ten milliliters of cold 0.6 M mannitol containing 1 mM calcium chloride was added, centrifuged at 1,000 rpm for 5 min at 4°C, and the supernatant decanted. The wash and centrifugation were repeated two more times. After the final centrifugation, the supernatant was completely decanted and each tube of protoplasts was resuspended in protoplast culture medium (PCM). PCM was prepared by combining 1 ml 1000x vitamin stock, 0.5 ml 2000x hormone stock, 4.4 g MS salts, 34.2 g sucrose, 0.585 g MES, and 72.8 g mannitol. The volume was brought up to 1 L with double distilled water and pH adjusted to 5.8 using 1 N potassium hydroxide. The protoplasts were then poured into a 60 x 15 mm petri dish, covered in aluminum foil, and incubated at room temperature for 40 hr.

Extraction of Total RNA from Arabidopsis Protoplasts

Condition of the protoplasts at 40 hpi was checked by examining the plates under a light microscope. Plates were tilted to evenly distribute the cells and collected by transferring to two 1.5 ml microcentrifuge tubes. They were then subjected to centrifugation at 5,000 rpm for 3 min at room temperature. All centrifugations were performed for this procedure using a microcentrifuge. The supernatant was removed by pipet leaving 100 μl of medium and one of the tubes was stored as a backup sample by

freezing at -80°C. Two hundred microliters of 1:1 phenol/chloroform containing 0.1% (w/v) 8-hydroxyquinoline and 200 µl of RNA special extraction buffer (50 mM Tris-HCl, pH 7.5, 5 mM EDTA, pH 8.0, 100 mM sodium chloride, 1% (w/v) SDS) were added to each tube and the mixture vortexed for 10 sec. The samples were centrifuged at 13,000 rpm for 2 min at 4°C and the upper layer transferred to a new tube. Twenty five microliters of 3 M sodium acetate, pH 5.2, and 575 µl of 100% ethanol were added and the mixture vortexed and incubated at -80°C for 5 min. The cells were then centrifuged at 13,000 rpm for 10 min at 4°C. The supernatant was discarded by pipet and 500 µl of 70% ethanol was added and the sample centrifuged at 13,000 rpm for 5 min at 4°C. The supernatant was removed and the pellet dried and resuspended in 20 µl of double distilled water. RNA concentration was determined using a spectrophotometer at an optical density (OD) of 260.

Northern Blotting Using RNA Gels

One and a half micrograms of total RNA and double distilled water up to 5 µl were combined with 5 µl of 2x formamide loading buffer (prepared by mixing 800 µl of formamide with 200 µl of 10x formaldehyde gel-loading buffer (50% (v/v) glycerol, 1 mM EDTA, pH 8.0, 0.25% bromophenol blue, 0.25% xylene cyanol FF)). The mixture was incubated at 65°C for 5 min, quenched on ice, and subjected to electrophoresis through a freshly prepared 1.3% agarose gel. The gel was then rinsed briefly with double distilled water and soaked completely in 6% formaldehyde solution for 1 hr with shaking. The formaldehyde was decanted and the gel soaked in 10x SSC for 10 min followed by another 15 min in 10x SSC with a 45 µm pure nitrocellulose membrane. The 10x SSC

solution was prepared by combining 350.5 g of sodium chloride and 176.4 g of sodium citrate, trisodium salt, dihydrate, and bringing the volume to 2 L with double distilled water. The pH was adjusted to 7.0 with HCl. RNA was transferred to the membrane using the capillary transfer method and the membrane rinsed with 10x SSC. The membrane was then placed, face-down, on an ultraviolet light box for 2 min and dried at 80°C for 5 min. Both the membrane and gel were analyzed under ultraviolet light to verify the transfer. To probe for TCV plus-strands, the membrane was prehybridized for at least 1 hr at 42°C using a 30% (v/v) formamide prehybrization buffer. Prehybridization buffer was prepared by combining 3 ml of formamide, 2 ml of 50x Denhardt's reagent (contains 5g of Ficoll, Type 400, 5 g of polyvinylpyrrollidone, 5 g of bovine serum albumin, Fraction V, and double distilled water to 500 ml), 2.5 ml of 20x SSPE (combined 175.3 g sodium chloride, 27.6 g of sodium phosphate, anhydrate, monobasic, 40 ml of 0.5 M EDTA, pH 8, and adjusted to pH 7.4 with sodium hydroxide and to a volume of 1 L with double distilled water), 2.1 ml of double distilled water, 200 µl of 10 mg/ml single-stranded DNA, and 200 µl of 10% (w/v) SDS. During the prehybridization incubation, oligonucleotides were radiolabeled by combining 9.5 µl of double distilled water, 6 µl of 10 pmol/µl oligonucleotide, 2 µl of 10x T4 polynucleotide kinase buffer (700 mM Tris-HCl, pH 7.6, 100 mM magnesium chloride, 50 mM DTT), 1.5 µl of γ-^{32}P ATP (10 mCi/ml), and 1 µl of T4 polynucleotide kinase (10,000 U/ml; New England Biolabs), and the mixture incubated for 10 min at 37°C. The radiolabeled oligonucleotide was added to the prehybridization buffer and incubated for at least 2 hrs at 42°C. The prehybridization buffer was decanted and the membrane washed briefly with Northern wash I (made by combining 690 ml of double distilled water, 300 ml of

20x SSPE, and 10 ml of 10% (w/v) SDS) and washed a second time with Northern wash I for 10 min at 42°C. Next, the membrane was rinsed briefly with Northern wash II (made by combining 985 ml of double distilled water, 5 ml of 20x SSPE, and 10 ml of 10% (w/v) SDS) and washed a second time with Northern wash II for 15 min at 42°C. The membrane was allowed to dry at room temperature for 3 min, covered in plastic wrap, and audioradiography performed at -80°C for at least 12 hr.

The oligonucleotide was removed from the probed membrane by incubating it at 65°C for 2 hr in 200 ml of mild stripping solution made by combining 198 ml of double distilled water, 1 ml of 1 M Tris-HCl, pH 8.0, 800 µl of 0.5 M EDTA, pH 8.0, and 400 µl of 50x Denhardt's reagent. To probe for ribosomal RNA, the membrane was incubated at 42°C for 1 hr in a 50% formamide prehydrization buffer containing 5 ml of formamide, 2 ml of 50x Denhardt's reagent, 2.5 ml of 20x SSPE, 200 µl of single-stranded DNA (10 mg/ml), and 200 µl of 10% (w/v) SDS. The ribonucleotide probe was prepared by combining 5 µl of 5x T7 RNA polymerase transcription buffer, 2.5 µl of 100 mM DTT, 1 µl of SmaI-digested pT7C(+), which contains full-length satC downstream of a T7 promoter, 2 µl of a 5mM ribonucleotide mix (rATP, rGTP, rCTP), 2.5 µl of α-^{32}P UTP (20 mCi/ml), and 0.5 µl of T7 RNA polymerase (50 U/µl; Invitrogen) and incubated at 37°C for 30 min. The template DNA was digested by adding 2 µl of RQ1 RNase-free DNase (1 U/µl; Promega) and incubated at 37°C for 15 min. The riboprobe was then added to the prehybridization buffer and incubated at 42°C overnight. The buffer was decanted and the membrane briefly washed with Ribowash I (2x SSC buffer, 0.1% (w/v) SDS) and then washed again with Ribowash I for 15 min at 42°C. Next, the membrane was briefly washed using Ribowash II (0.1x SSC buffer, 0.1% (w/v) SDS) and then

washed again with Ribowash II for 15 min at 42°C. The membrane was then dried at room temperature for 3 min, covered in plastic wrap, and autoradiography performed at -80°C for at least 30 min.

Inoculation of Turnip Seedlings with In Vitro RNA Transcripts

To inoculate 6 turnip seedlings, 12 μg of purified TCV in vitro RNA transcripts were suspended in 60 μl of double distilled water. Immediately before inoculation, the RNA was mixed with 60 μl of 2x infection buffer (0.05 M glycine, 0.03 M dipotassium hydrogen phosphate, dibasic, anhydrous, pH 9.2, 1% cleaned bentonite, 1% celite) and rubbed into two leaves of each seedling (10 μl each leaf) using gloved hands.

Extraction and Sequencing of Viral Progeny RNA from Infected Turnip Plants

A two inch long leaf was removed from an inoculated turnip plant and its midrib removed using a razor blade. The leaf was finely ground in liquid nitrogen using a spatula and 0.5 ml of crushed leaf transferred to a 1.5 ml microcentrifuge tube. RNA extraction buffer (0.55 ml; 0.2 M Tris-HCl, pH 9, 0.4 M lithium chloride, 25 mM EDTA, 1% SDS) and 0.55 ml of water-saturated phenol were immediately added, the sample vortexed for 15 sec., and placed on ice. Samples were vortexed intermittently until all samples were processed. After the last sample was processed, all extractions were incubated on ice for 10 min. Samples were then subjected to centrifugation at 13,000 rpm for 2 min at 4°C. All centrifugations in this procedure were performed using a microcentrifuge. The aqueous layer was removed by pipet, transferred to another microcentrifuge tube, and extracted again with water-saturated phenol as described

above. Chloroform was next added to the aqueous layer and the RNA extracted using a procedure identical to the phenol extraction. Fifty microliters of 3 M sodium acetate, pH 5.2, and 1100 µl of 100% ethanol were added to the aqueous layer and vortexed. The samples were incubated at -80°C for 5 min and centrifuged at 13,000 rpm for 10 min at 4°C. The supernatant was decanted and the pellet resuspended in 300 µl of 2 M lithium chloride by pipet. The extractions were vortexed, centrifuged at 5 min at 4°C, and the supernatant discarded by pipet. The pellet was next resuspended in 300 µl of double distilled water and 30 µl of sodium acetate, pH 5.2, and 660 µl of 100% ethanol were added. Samples were vortexed, incubated at -80°C for 5 min, and centrifuged at 13,000 rpm for 10 min at 4°C. The supernatant was removed by pipet and 500 µl of 70% ethanol added to the pellet. The extracted viral RNA was subjected to centrifugation at 13,000 rpm for 5 min at 4°C and the supernatant pipetted out. The pellet was dried, resuspended in 50 µl of double distilled water, and stored at -80°C.

Viral progeny RNA was prepared for reverse transcription by mixing 1 µl of oligonucleotide (10 pmol/µl) and 9 µl (out of 50 µl) of extracted viral progeny RNA. Samples were heated at 75°C for 5 min, incubated on ice for 1 min, and subjected to pulse centrifugation. Next, 4 µl of 5x first-strand buffer (250 mM Tris-HCl, pH 8.3, 375 mM potassium chloride, 15 mM magnesium chloride), 4 µl of 5 mM dNTPs, 2.3 µl of double distilled water, 0.2 µl of RNaseOut ribouclease inhibitor (40 U/µl; Invitrogen), and 1.5 µl of MMLV (200 U/µl; Invitrogen) were added. The reactions were incubated at 42°C for 1 ½ hr followed by incubation at 75°C for 10 min. Six microliters of the reverse transcription reaction were used for PCR. PCR products were kinased with T4

PNK, treated with klenow, and ligated into pUC19 digested with SmaI. DNA sequencing was performed on small-scale preparations.

Results

Comparison of Carmoviral 3' UTRs Using Phylogenetic Analysis

Although the 3' UTRs of carmoviruses are poorly conserved (sequence similarity with TCV 3' UTR ranges from 24% for *Cowpea mottle virus* (CPMoV) to 50% for *Cardamine chlorotic fleck virus* (CCFV); Huang *et al*., 2000; Takemoto *et al*., 2000; Weng and Xiong, 1997; Skotnicki *et al*., 1993; Guilley *et al*., 1985, You *et al*., 1995; Riviere and Rochon, 1990; Suzuki *et al*., 2002; Rico and Hernandez, 2004; Ciuffreda *et al*., 1998), comparative RNA structural analysis using the *mfold* secondary structure prediction program (Mathews *et al*., 1999) revealed striking structural similarities. With the exception of *Galinsoga mosaic virus* (GaMV), all carmoviruses contain a 3' terminal hairpin (Pr) previously identified as the core promoter for TCV minus-strand synthesis (Song and Simon, 1995). In addition, all carmoviruses except GaMV have a second hairpin located 16 to 27 bases upstream of Pr that contains a highly conserved LSL (Fig. 2.2). Four of the carmoviruses (including TCV) have identical sequence in this internal loop (5'-UAAAAU and 5'-UGGGCU), whereas most others differ symmetrically from this sequence. The hairpin stems are poorly conserved and upper stems range from two to seven basepairs and most are capped by either the main classes of stable tetraloops (GNRA, UNCG or CUYG; Moore, 1999), or pentaloops. This carmovirus hairpin has been given the designation of H5.

TCV H5 is a Position-Dependent Element That Basepairs with the 3' Terminus To Regulate Minus-Strand Synthesis

In satC, basepairing of the 3' terminal cytidylates with the 3' side of the H5 LSL regulates and promotes correct initiation of minus-strand synthesis *in vitro* (Zhang *et al*., 2004a). To test whether this interaction occurs in TCV *in vivo,* constructs were made that contained either a substitution in the LSL (C3994G), the 3' end (G4051C), or in both regions (C3994G/G4051C; Fig. 2.3A) and tested in protoplasts. Protoplasts are individual plant cells that have been enzymatically treated to remove their cell walls, but contain intact cell membranes. The cell membranes were made permeable by calcium chloride, the infectious viral RNA manually inoculated by brief shaking with polyethylene glycol (PEG), and the cells incubated for 40 hours. Total RNA was then extracted, subjected to electrophoresis on an agarose gel, and the levels of viral RNA accumulation quantified by Northern blotting and densitometry. Inoculations performed in triplicate revealed that C3994G had a 93% reduction and G4051C had a 71% reduction in accumulation in comparison to wt, showing that alterations within either of these regions were detrimental. For C3994G/G4051C, accumulation in protoplasts was reduced by only 50%, a level that is almost 2-fold higher than the most fit single-site alteration (Fig. 2.3B). These results indicate that the 3' end of TCV likely basepairs with the 3' side of the LSL *in vivo*. In contrast, equivalent changes made in satC failed to show an interaction *in vivo,* suggesting that the specificity of these sequences in satC are more stringent than in TCV (Zhang *et al*., 2004a). Since similar interactions between equivalent structures in TBSV and satC function to mediate minus-strand synthesis *in*

Figure 2.2. Conserved Structures in the 3' Ends of Carmoviruses. 3' UTRs of the following carmoviruses were subjected to computer structural predictions using *mfold*: *Turnip crinkle virus* (TCV), *Cardamine chlorotic fleck virus* (CCFV), *Japanese iris necrotic ring virus* (JINRV), *Hibiscus chlorotic ringspot virus* (HCRSV), *Saguaro cactus virus* (SCV), *Carnation mottle virus* (CarMV), *Cowpea mottle virus* (CPMoV), *Melon necrotic spot virus* (MNSV), *Pea stem necrosis virus* (PSNV), and *Pelargonium flower break virus* (PFBV). Bases identical to those in TCV are in black. Putative interacting bases are indicated with solid black lines (Zhang *et al*., 2004a).

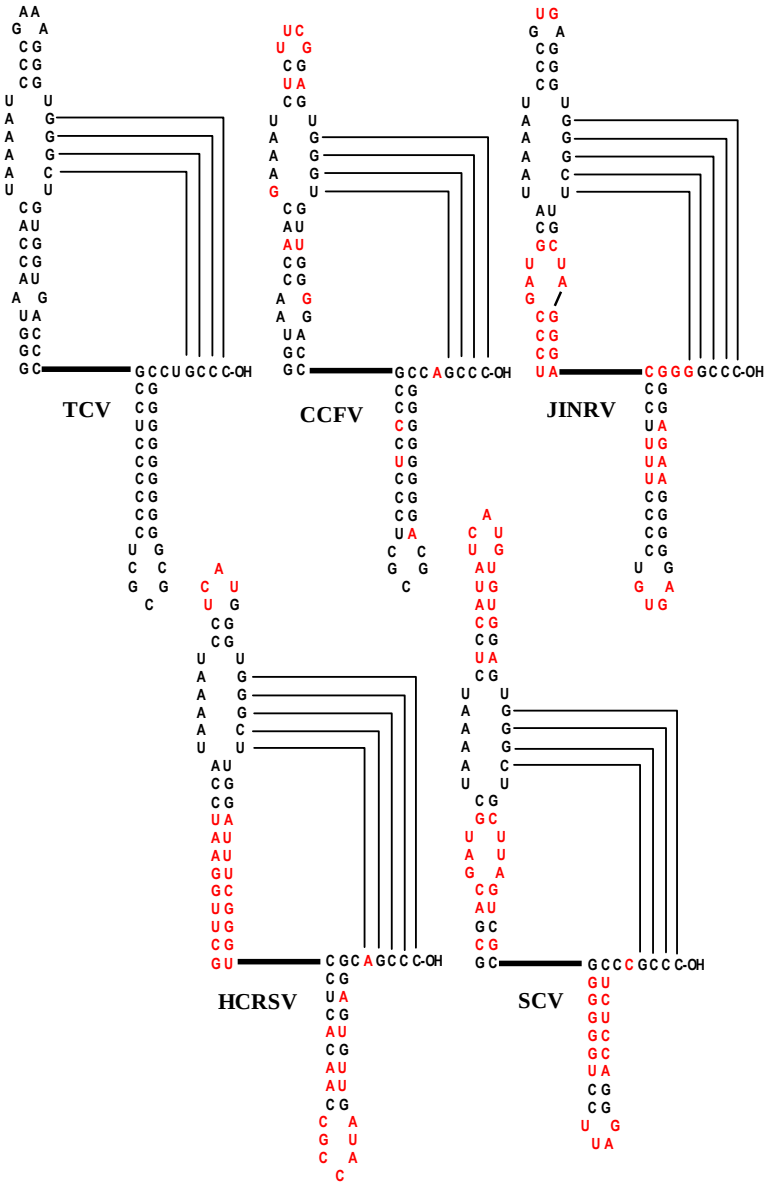
TCV
CCFV
JINRV
HCRSV
SCV

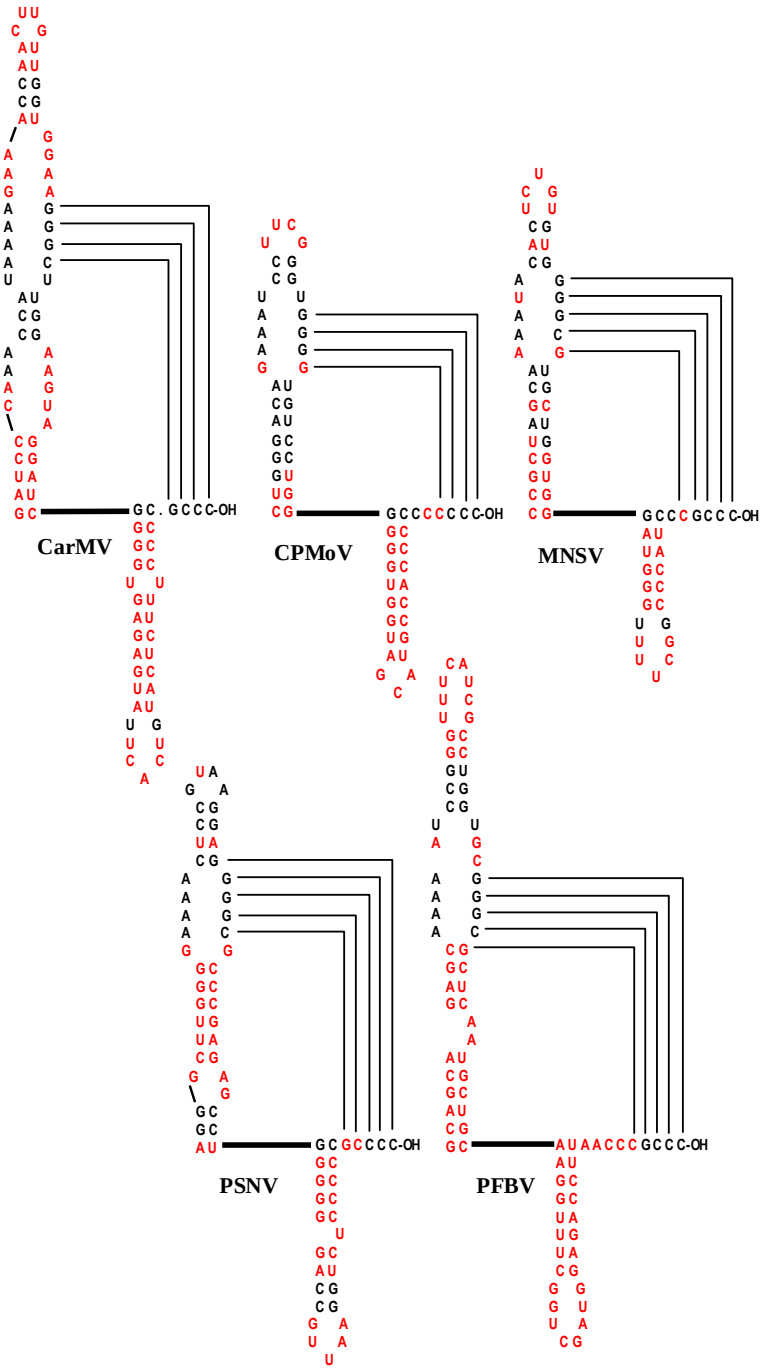
CarMV
CPMoV
MNSV
PSNV
PFBV

vitro (Pogany *et al*, 2003, Zhang *et al*., 2004a), TCV basepairing is assumed to be involved in replication as well.

Replication enhancers are dispensable *cis*-acting elements that can function independently of position on both plus- and minus-strands (Nagy *et al*., 1999). To ascertain whether H5 exhibits enhancer activity, this hairpin was ectopically positioned within the 3' UTR to a region approximately 200 bases upstream from its original location. To test if the upstream region was tolerant of large inserts, H5 was first duplicated ($H5_{DUP}$; Fig. 2.4A,B) and accumulation levels quantified in protoplasts. Results revealed that $H5_{DUP}$ accumulated to almost wt levels (Fig. 2.4C), showing that the upstream region was tolerant of changes. H5 was then translocated to the upstream region ($H5_{TRANS}$) by inactivating the natural H5 with a single-site alteration that is critical for H5 function (G3991U; Fig. 2.4A,B). For $H5_{TRANS}$, undetectable levels of accumulation (Fig. 2.4C) showed that H5 translocated to a position 200 bases upstream is not functional and does not support the role of this element as a simple replication enhancer.

Alterations in TCV H5 LSL Lead to a Reduction of Accumulation in Protoplasts

To further determine the importance of TCV H5 *in vivo*, several single and double point mutations were constructed in the LSL (Fig. 2.5A) and accumulations tested in protoplasts. TCV containing an adenylate to cytidylate substitution at position 3976 on the 5' side of the LSL (A3976C) accumulated to 74% of wt levels, whereas A3978C, either alone (A3978C) or in combination with A3976C (A3976C/A3978C), reduced the

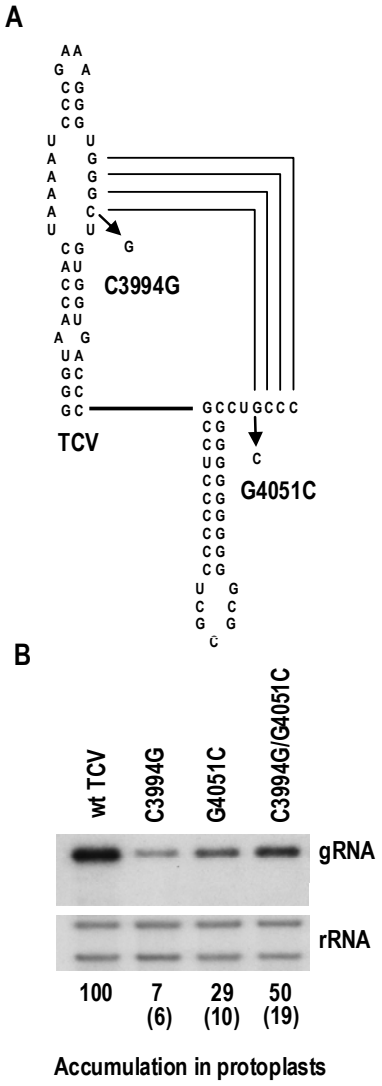

Figure 2.3. RNA-RNA Interaction Between TCV H5 LSL and the 3' Terminal Bases. (A) Compensatory mutational analysis was performed by introducing alterations into either the LSL (C3994G), the 3' terminus (G4051C), or both regions (C3994G/G4051C). (B) In vitro RNA transcripts of each construct were inoculated into protoplasts from *Arabidopsis thaliana* using the polyethylene glycol method as previously described (Kong et. al, 1997). Total RNA was extracted at 40 hours post-inoculation (hpi) and the genomic RNA (gRNA) and ribosomal RNA (rRNA) probed. Accumulation levels of each construct, in comparison to wt TCV levels, were normalized against the rRNA loading control and are given below the blots. The numbers within parentheses indicates standard deviation. Levels of TCV were determined with a scanning laser densitometer.

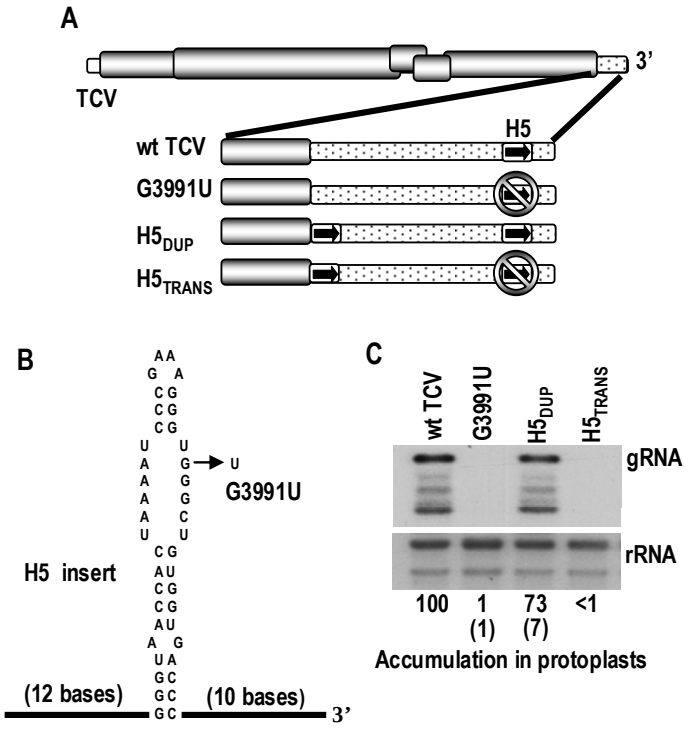

Figure 2.4. H5 Duplication and Translocation. (A) H5 was duplicated by introducing an insert into a region of the TCV 3' UTR just downstream of the CP ORF stop codon ($H5_{DUP}$). To inactivate H5, a single-site mutation that reduced accumulation levels to almost undetectable levels in protoplasts was introduced into the LSL. H5 containing G3991U was inactivated either by itself or in combination with the duplicated H5 ($H5_{TRANS}$), which moved a wt copy of H5 to the upstream region. (B) The insert used contained H5 in addition to 12 upstream and 10 downstream bases derived from TCV. The alteration made to inactivate the function of H5 is shown by the black arrow. (C) Accumulation levels of H5 constructs in protoplasts are given below the blots and standard deviations are indicated by the numbers within parentheses. Levels of TCV were determined with a scanning laser densitometer and normalized to the level of rRNA.

level of virus to below detectability. TCV containing G3991A on the 3' side of the LSL also did not accumulate to detectable levels (Fig. 2.5B), which was similar to the accumulation levels observed for G3991U (Fig. 2.4C). These results support an important function for both sides of the H5 LSL in TCV and correlate with results obtained in satC, which show the sequence specificity of both sides of H5 in accumulation (Zhang *et al*., 2004b).

H5 LSL Mutants in Inoculated Turnip Plants Frequently Revert and Are Associated with Second-Site Alterations

To determine if TCV containing LSL mutations accumulated in host plants, either mutant or wild-type TCV was inoculated onto six turnip seedlings. At 20 dpi, total RNA was extracted from leaves and subjected to reverse transcription (RT) and PCR amplification to detect TCV accumulation. Cloned cDNAs derived from progeny of A3976C (42 clones from six plants), G3991A (11 clones from one plant), A3976C/A3978C (25 clones from five plants), and wild-type TCV (31 clones from five plants) were sequenced between positions 3800 and 4000 and progeny of A3978C (26 clones from five plants) were sequenced between positions 3700 and 4000.

Sequence analysis of A3976C progeny revealed that the original alteration was stably maintained in all cloned progeny, which supported finding only marginally reduced accumulation in protoplasts. In addition, four of 42 clones contained unique second site mutations, three of which were uridylate to cytidylate transitions (Fig. 2.6; Table 2.3). The second site changes were located in two nearby hairpins (M3H and H4) that have enhancer function in their minus-sense orientations (Carpenter *et al*., 1995).

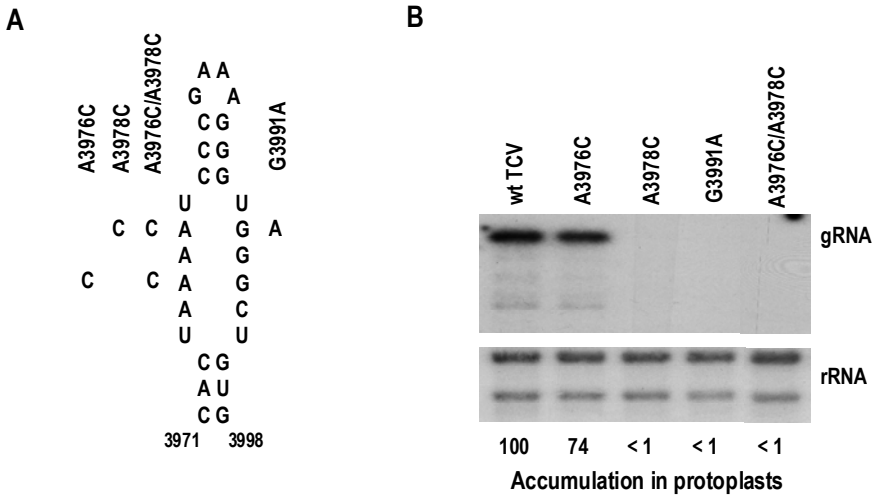

Figure 2.5. Accumulation of TCV H5 LSL Mutants in Protoplasts at 40 hpi. (A) Location of the mutations in the LSL. Designations of the mutants are given. (B) (Top) RNA gel blot of TCV genomic RNA. (Bottom) RNA gel blot of rRNA loading control. Levels of TCV (expressed below the gels as percentages of the wt level, taken as 100%) were determined with a scanning laser densitometer and normalized to the level of rRNA.

There was no discernable relationship between the regions that contained the additional changes and no obvious interactions possible with H5.

Three of six plants inoculated with A3978C accumulated virus at or near wt levels and two additional plants accumulated TCV-specific RNA, as detected by RT-PCR (data not shown). All 25 cloned progeny contained either a reversion to wt (15/25) or a primary site alteration to a uridylate (10/25). Unexpectedly, 3 of 25 clones contained two second-site mutations and 8 of 25 clones contained single second site mutations that were unique for each clone in the 300 bases that were sequenced (Fig. 2.6; Table 2.3). One mutation located at the first position of the CP ORF termination codon extended the C-terminus of the CP by 10 amino acids. Other mutations in the CP ORF led to conservative amino acid substitutions. The remaining mutations were scattered throughout the 3' UTR, mostly in putative single-stranded regions between hairpins or in internal and terminal loops within hairpins. Of the 14 base changes, 9 were uridylate to cytidylate transitions and 4 were adenylate to guanylate transitions (Table 2.3).

Plants inoculated with G3991U failed to accumulate viral RNA detectable by PCR (data not shown). However, one of six plants inoculated with G3991A contained PCR-detectable RNA (data not shown). All 11 clones sequenced contained a reversion to the wt guanylate and 2 clones had second site mutations in the 200 bases sequenced (Fig. 2.6). The second site alteration in the 5' side of H5 would expand the LSL, possibly helping to stabilize the interaction between the 3' LSL and the 3' terminal bases, which would be weakened in G3991A. The other second site alteration was near the beginning of the UTR, with no discernable connection between this sequence and H5.

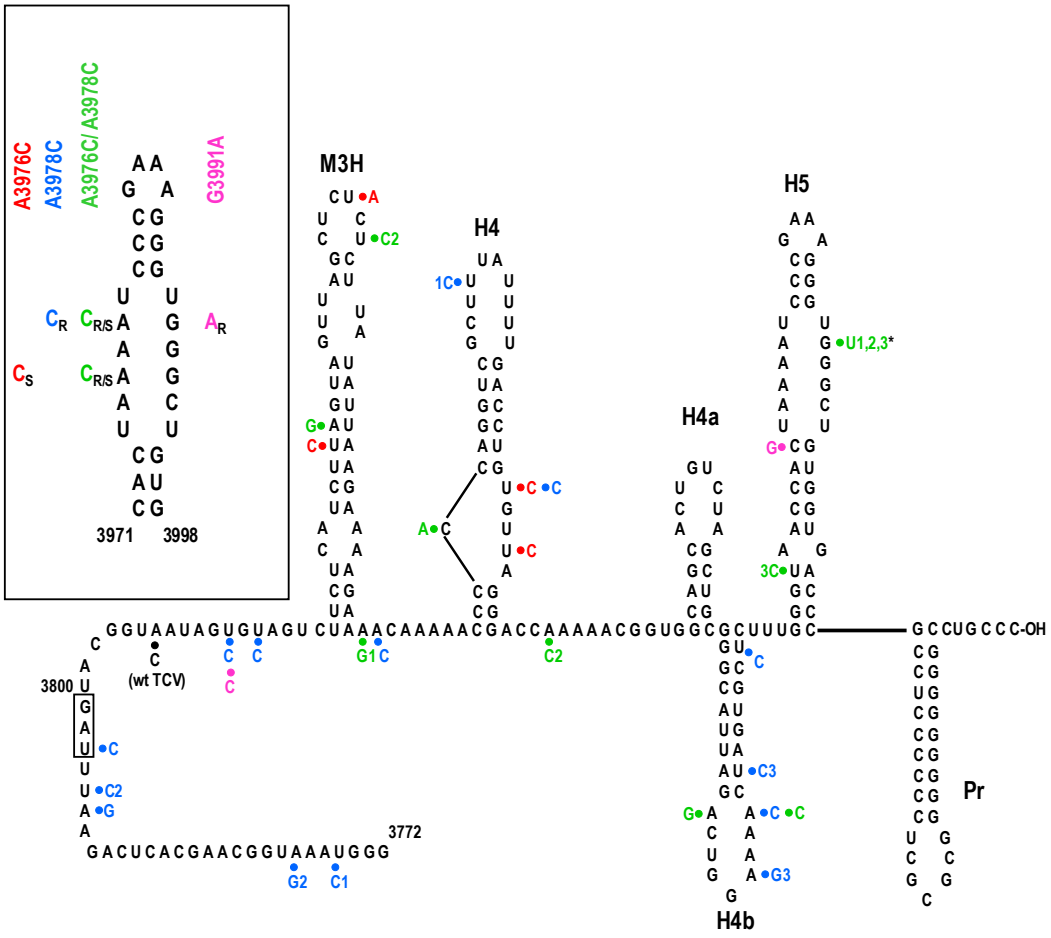

Figure 2.6. Locations of Second-Site Mutations in the 3' End of LSL Mutant Progeny at 20 dpi. (Inset) The primary mutations in H5 that gave rise to second-site mutations. R, S, R/S indicate mutations that either reverted to wt, were stable, or were partially stable in progeny virus, respectively. Designations of the mutant TCV constructs are given. Second-site mutations and their primary-site mutant progenitors are color-coded. The single alteration found in wt TCV progeny is shown in black. Identically colored numbers associated with some second-site mutations indicate their presence in the same clone. The termination codon of the CP is boxed. Asterisk indicates mutation found in five TCV clones isolated from three plants. All other second-site mutations were found only once in independent clones.

TABLE 2.3. Characterization of second site mutations in clones derived from TCV mutant and wild type constructs

Construct(s)	No. of substitution types							# clones with second site changes	Total mutations/ bases sequenced	Mutation frequency ($x 10^{-3}$)
	U to C	A to G	U to A	A to C	C to G	C to A	G to U			
A3976C	3	0[c]	1	0[c]	0[c]	0[c]	0[c]	4/42	4/8400[a]	0.5
A3978C	9	4	0[c]	1	0[c]	0[c]	0[c]	11/25	14/7500[b]	1.9
G3991A	1	0[c]	0[c]	0[c]	1	0[c]	0[c]	2/11	2/2200[a]	0.9
A3976C/A3978C	2	3	0[c]	2	0[c]	1	5	9/27	13/5400[a]	2.4
All mutants	15	7	1	3	1	1	5	26/105	33/23500	1.4
TCV wt	0[c]	0[c]	0[c]	1	0[c]	0[c]	0[c]	1/31	1/6200[a]	0.2

[a]TCV clones sequenced between bases 3800 to 4000 within the 3' UTR

[b]TCV clones sequenced between bases 3800 to 4000 within the 3' UTR and between bases 3700 to 3800 within the p38 coding region

[c]no mutations found for possible base change

Sequencing of 27 clones for mutant A3976C/A3978C, which contained 5'-UACACU in its LSL, resulted in the recovery of the following sequences in this location: no change (maintained both mutations), 6/27; wt (reversion at both positions), 16/27; reversion at a single position (5'-UACAAU), 1/27; primary site alteration with a reversion at the other original position (5'-AAAUU), 4/27. In addition, within the 200 bases sequenced, six clones contained single second site mutations, two had double mutations and one had three mutations. Five of these alterations, found in clones derived from three plants, were guanylate to uridylate changes at position 3991 in the 3' side of the LSL (Fig. 2.6; Table 2.3). Since a uridylate in this location was highly detrimental to TCV accumulation (G3991U; Fig. 2.4C), this alteration is likely compensating for changes to the 5' side of the LSL. With this exception, all other second site changes were scattered throughout the sequenced region and were biased towards uridylate to cytidylate (2 of 8) and adenylate to guanylate (3 of 8) transitions (Fig. 2.6; Table 2.3).

In all, 33 second-site mutations were recovered in 23,500 bases sequenced, which corresponds to a mutation frequency of 1.4×10^{-3} (Table 2.3). Since most of the region sequenced was in the 3' UTR, a lower mutation frequency may exist in coding regions. To determine if mutation frequencies for the TCV LSL constructs and the mutation bias noted above were unusual compared with wt TCV, wt TCV progeny from identically infected plants were subjected to RT-PCR and 31 clones were sequenced. Only one alteration at position 3806 (adenylate to cytidylate) was found in the 6200 bases sequenced, corresponding to an approximate mutation frequency of 0.2×10^{-3} (Fig. 2.6; Table 2.3). This value is consistent with the 0.2×10^{-3} mutation frequency determined for some picornaviruses (de la Torre *et al*., 1990; Holland *et al*., 1992). Therefore, alterations

in H5 increased the mutation frequency 2.5-fold for A3976C to 12-fold for A3976C/A3978C with an overall increase for all mutants of 7-fold (Table 2.3). Surprisingly, similar lesions introduced into the satC LSL did not lead to such a large increase in mutation frequency (Zhang *et al*., 2004b). However, the small size of satC may impose sequence constraints on the molecule that are more rigid than constraints for the 3' UTR of TCV.

Discussion

While the effects of individual second site mutations have not been evaluated for the TCV H5 LSL constructs, several observations lead to the possibility that the vast majority of second site changes are not compensatory. First, these mutations were found in 26 different positions scattered throughout the sequenced region (Fig. 2.6). Second, the composition of the changes was strongly biased towards uridylate to cytidylate (15/33) and adenylate to guanylate (7/33) transitions (Table 2.3), suggesting a specific replication defect. Third, the second site changes were nearly all coupled with reversion of the original alterations, suggesting that the second site changes were not compensating for the original defects in the H5 LSL. Finally, although A3976C accumulated to 74% of wt TCV levels in protoplasts (Fig. 2.5B), the progeny still exhibited an increased mutation frequency, suggesting that this phenomenon is more complex than a simple association between poorly replicating constructs and enhanced mutation frequency.

One explanation for the biased second site alterations may be that poorly replicating mutant viruses multiply undetectably until a mutation occurs in the RdRp that

allows for reversion of the original LSL alteration while reducing RdRp fidelity. A second explanation is that these mutations may arise from the activity of cellular adenosine deaminases (ADARs), which convert adenosines to inosines in double stranded RNAs during the replication of negative-stranded RNA viruses (Bass *et al*., 1989; Cattaneo, 1994). However, ADARs have only been found in a subset of animal hosts and have not been identified in plants (Bass, 2002). A third explanation is that H5 functions as a chaperone that nucleates the formation of an active RdRp complex. An incorrectly assembled or misfolded RdRp could have lower fidelity and more readily mispair templated uridylates with guanylates during transcription of plus- and minus-strands. RNA elements in the 3' UTR of *Alfalfa mosaic virus* (AlMV; Vlot *et al*., 2001) and the 3' UTR and intercistronic regions in RNA 3 of *Brome mosaic virus* in yeast (BMV; Quadt *et al*., 1995) are known to be required for the formation of an active RdRp. In addition, studies using BMV replicase suggest that RdRp is inherently flexible and able to adjust its structure based on contact with a few key nucleotides (Stawicki and Kao, 1999).

Since RNA templates are not substrates for post-polymerization mismatch repair, RNA replication leads to a dynamic quasispecies population consisting of a dominant "master" sequence, and master sequence variants that differ in abundance and level according to the intrinsic properties of the virus and perturbations in the host microenvironment (Domingo and Holland, 1997; Holland *et al*., 1982; Schneider and Roossinck, 2001). Increases in the mutation frequency of poliovirus by as little as 1.2-fold following treatment with nucleoside analogues resulted in steep losses in virus viability and rapid population extinction (error catastrophe) (Sierra *et al*., 2000; Crotty *et*

al., 2001). These observations led to the suggestion that RNA viruses exist precariously close to the error threshold in order to maximize the genetic diversity of their viral population (quasispecies cloud size) and their potential for adaptation to fluctuating environmental conditions (Crotty *et al*., 2001; Drake and Holland, 1999). A mechanism that could transiently increase the mutation frequency in excess of the error threshold while avoiding extinction of the population by high frequency reversion of the original mutation would increase the rate of evolution and its quasispecies cloud size, thereby enhancing adaptive potential without permanently altering the RdRp. Observations presented in this study suggest that this novel attribute may exist for TCV.

At the time that this work was completed in 2004, the function of the TCV 3' UTR had not been thoroughly investigated. As of 2007, mutagenesis of the adenylates in the 5' side of TCV H5 LSL were shown to abolish detectable levels of RdRp binding to an RNA fragment spanning TCV positions 3858-4017 *in vitro* (M. Young and A.E. Simon, unpublished results). These results support the role of H5 in functioning as an RdRp chaperone. However, H5 along with H4a and H4b form a domain that may cooperatively function with M3H and H4, which brings into question whether some of the second-site mutations described in this chapter are compensating for structural changes made in this domain.

CHAPTER III

AN INTERNAL tRNA-LIKE STRUCTURE IN THE 3' UTR OF AN RNA VIRUS IS A TRANSLATIONAL ENHANCER THAT BINDS THE 60S RIBOSOMAL SUBUNIT

Introduction

Translating RNA sequences into functional proteins is a central activity for all organisms. While the elongation phase of translation (e.g., the peptidyltransferase reaction) is virtually identical across kingdoms, translation initiation varies widely and is intimately connected with kingdom-specific avenues of gene expression (Kozak, 1999). Translation initiation in eukaryotic mRNAs requires that the template assume a closed loop structure, mediated by eukaryotic initiation factor eIF4E binding to the 5' cap and poly(A)-binding protein binding to the poly(A) tail (Wells *et al*., 1998). Since both translation factors bind to the scaffold protein eIF4G, a bridge is formed between the 5' and 3' ends. eIF4G and associated proteins, known as eIF4F, recruits the 40S small ribosomal subunit and associated ternary complex (eIF2-GTP/Met-tRNA$_i$) to the cap region of the mRNA. The complex then "scans" in a 5' → 3' direction to the initiation codon, followed by release of specific initiation factors and recruitment of the 60S subunit to form the 80S ribosome followed by translation initiation (Merrick 2004; Preiss and Hentze 2003).

Many plant and animal viral RNAs have no 5' cap and about 3% of animal mRNAs also can use cap-independent mechanisms for translation under conditions when cap-dependent translation is impaired (Hellen and Sarnow, 2001; Merrick, 2004). Animal plus-strand RNA viruses that lack 5' caps contain large internal ribosome entry sites (IRES) that are located either in extensive (300 to 1500 nt) 5' UTRs or upstream of internal ORFs and use different mechanisms to attract ribosomes (Hellen and Sarnow, 2001). For example, *Encephalomyocarditis virus* (EMCV) IRES (~600 nt) interacts with canonical initiation factors to recruit the 40S ribosomal subunit, whereas the *Hepatitis C virus* (HCV) IRES (~360 nt) directly binds eIF/ternary complex-free 40S subunits (Fraser and Doudna, 2007). Dicistrovirus IRESes are unusual in that they can assemble 80S ribosomes without eIFs and a portion directly serves as the initiator tRNA (Hellen and Sarnow, 2001). Efficient translation using viral IRESes may also require sequences in the 3' UTR of unknown function (Bradrick *et al*., 2006; Song *et al*., 2006), host proteins (Baird *et al*., 2006) and/or additional viral-encoded proteins (Dobrikova *et al*., 2006).

Less than 20% of plant plus-strand RNA viruses have 5' and 3' ends that terminate with both 5' caps and 3' poly(A) tails (Dreher and Miller, 2006). Aminoacylated tRNA-like structures are found at the 3' termini of many plant virus genera that contain 5' caps (Dreher and Miller, 2006). A proposal has been made that the TLS of *Turnip yellow mosaic virus* (TYMV) functionally replaces Met-$tRNA_i$ during translation resulting in (or promoting) incorporation of the TLS amino acid at the N-terminus of the viral polyprotein (Barends *et al*., 2003). However, other studies are contradictory with the overlapping 5' proximal TYMV ORFs being translated by a canonical cap-dependent

recruitment of ribosomes that then scan to the closely spaced initiation codons (Matsuda and Dreher 2006). Cap-independent translation of many plant viruses differs from those of animal viruses by involving elements in the 3' UTR that enhance translation through unknown mechanisms (Fabian and White 2004; Karetnikov *et al*., 2006; Shen and Miller, 2004). Such elements can bind to specific translation factors and either encompass or are associated with a nearby sequence that forms an RNA-RNA bridge with single-stranded complementary sequences near the 5' end (Miller and White, 2006).

Turnip crinkle virus (TCV), a member of the Carmovirus genus in the Family *Tombusviridae*, contains a single 4054 nt plus-sense genomic RNA with five overlapping ORFs, as previously stated in Chapter I (Fig. 1.3; Hacker *et al*., 1992). TCV RNAs are not capped (Qu and Morris, 2000), and terminate with a 3' hydroxyl group. The viral genomic and two subgenomic RNAs are highly efficient templates for replication and translation, with viral RNAs reaching levels in cells comparable to ribosomal RNAs. The TCV 3' UTR was reported to contain an unidentified element that synergistically enhances translation in the presence of the viral 5' UTR (Qu and Morris, 2000; Yoshii *et al*., 2004).

A region in the TCV 3' UTR was determined to fold into a novel domain that structurally resembles a tRNA. The internal tRNA-like structure (iTLS) binds to 60S ribosomal subunits and the P-site of 80S ribosomes in the absence of eIFs. These results identify the first known example of an RNA element that specifically binds 60S ribosomal subunits.

Materials and Methods

Construction of TCV Mutants

G3913C, C3922G, and G3913C/C3922G (Table 3.1), were made by PCR using pTCV66 template, which contains wt TCV sequence downstream of a T7 promoter, oligonucleotide 3164, and oligonucleotide G3913S/C3922S (Table 3.2). PCR products were cleaved using BsmI and Spe I and ligated into similarly digested pTCV66. To generate G3912U and G3912U/U3923G (Table 3.1), PCR was performed using pTCV66 template, oligonucleotide 3164, and oligonucleotide G3912K/T3923K (Table 3.2). Products were digested using BsmI and SpeI and ligated into pTCV66 digested with the same enzymes. For U3923G (Table 3.1), the above PCR and digestions were performed, except oligonucleotide T3923G was used in place of oligonucleotide G3912K/T3923K (Table 3.2).

U3945A, U3945G, U3945C, G3946A, G3946C, G3946U, G3947A, G3947C, and G3947U (Table 3.1) were created by PCR using pTCV66 template, oligonucleotide 3164, and either oligonucleotide T3945V for the 3945 mutant series, G3946H for the 3946 mutant series, or G3947H for the 3947 mutant series (Table 3.2). PCR products were treated with BsmI and SpeI and inserted into similarly digested pTCV66. For C4007G and C4008G (Table 3.1), PCR was performed using pTCV66 template, oligonucleotide 3164, and either oligonucleotides C4007G or C4008G (Table 3.2). PCR products were treated with T4 PNK and Klenow followed by digestion with SpeI and the small fragment ligated into pTCV66 digested with SmaI and SpeI. The above PCR products were also ligated into G3946C and G3947C digested with SmaI and SpeI to create constructs G3946C/C4008G and G3947C/C4007G (Table 3.1). G3924C (Table 3.1) was created by

PCR using pTCV66 template, oligonucleotide 3331, and oligonucleotide G3924C (Table 3.2). PCR products were cleaved with MscI and SpeI and introduced into pTCV66 digested with the same enzymes. U3925A, U3925C, C3926A, and C3926U (Table 3.1) were constructed by PCR using pTCV66 template, oligonucleotide 3164, and either oligonucleotide T3925M for the 3925 mutant series or C3926W for the 3926 mutant series (Table 3.2). PCR products were treated with BsmI and SpeI and ligated into similarly digested pTCV66.

A3950U (Table 3.1) was generated by PCR using pTCV66 template, oligonucleotide 3164, and oligonucleotide A3950T (Table 3.2). Product was digested with BsmI and SpeI and inserted into pTCV66 digested with the same enzymes. U3962 (Table 3.1) was constructed by PCR using pTCV66 template, oligonucleotide KK57, and oligonucleotide T3962A (Table 3.2). Product was treated with T4 PNK and Klenow, digested with SpeI, and ligated into pTCV66 cleaved with SpeI and SmaI. To make A3950U/U3962A , constructs A3950U and U3962A were digested with BsmI and SpeI and the small fragment of A3950U ligated into the large fragment of U3962A (Table 3.1). A3951U, U3963A, and A3951U/U3963A (Table 3.1) were generated by PCR using template pTCV66, oligonucleotide 3164, and oligonucleotide A3951W/T3963W (Table 3.2). Inserts were treated with T4 PNK and Klenow, digested with BsmI, and introduced into pTCV66 cleaved with BsmI and SmaI.

U3885A (Table 3.1)was created by PCR using pTCV66 template, oligonucleotide 3164, and oligonucleotide T3885A (Table 3.2). Product was digested with BsmI and SpeI and ligated into similarly cleaved pTCV66. A3978U (Table 3.1) was generated by PCR using pTCV66 template, oligonucleotide KK57, and oligonucleotide A3978T

(Table 3.2). Product was treated with T4 PNK, blunt-ended with Klenow, digested with SpeI, and introduced into pTCV66 digested with SpeI and SmaI. U3885A/A3978U was constructed by digesting constructs U3885A and A3978U with BsmI and SpeI and ligating the small fragment of U3885A with the large fragment of A3978U (Table 3.1).

A33U (Table 3.1) was made by PCR using pTCV66 template, oligonucleotide SspIpUC19, and oligonucleotide 5UTR-TAAAAT (Table 3.2). PCR product was treated with T4 PNK and Klenow, digested with Bsu36I, and inserted into pTCV66 digested with SspI and Bsu36I. Blunt-ending the PCR product destroyed the SspI site. A33U/U3885A was generated by digesting constructs A33U and U3885A with BsmI and SpeI and ligating the small fragment of U3885A into the large fragment of A33U (Table 3.1). A33U/U3885A/A3978U was constructed by digesting A33U/U3885A and A3978U with SpeI and SmaI and ligating the small fragment of A3978U with the large fragment of A33U/U3885A (Table 3.1).

M10, H4Linkmut, and M10/H4Linkmut (Table 3.1), were created by PCR using template pTCV66, oligonucleotide 3164, and a respectively labeled mutant oligonucleotide (Table 3.2). PCR products were cleaved with BsmI and SpeI and ligated into similarly digested pTCV66. J5UTR and C5UTR (Table 3.1) were made by PCR using template pTSNL5, oligonucleotide SspIpUC19, and either JINV5UTR or CCFV5UTR oligonucleotide, respectively (Table 3.2). Products were treated with T4 PNK, Klenow, and Bsu36I, and ligated into pTSNL5 digested with SspI and Bsu36I. Blunt-ending the PCR products destroyed the SspI site.

Construction of TCV iTLS RNA Fragments

Amplification of a 117 b sequence between TCV positions 3901 and 4017 was performed by PCR using oligonucleotide T7-H4M1H, which contains a T7 promoter, and oligonucleotide TCV-Linker (Table 3.2). Template pTCV66 was used for iTLS PCR and templates G3913C, C3922G, G3913C/C3922G, A3951U, U3963A, or A3951U/U3963A, were used for the respectively labeled TCV mutant PCRs (Table 3.3).

Generation of fragments corresponding to TCV positions 3858 to 4017 were made using oligonucleotides T7-M3HLinkerH4 and TCV-Linker (Table 3.2). Template pTCV66 was used for iTLS+H4 and templates A3978C, U3885A, A3978U, U3885A/A3978U, H4Linkmut, and M10/H4Linkmut, were used for the respectively labeled TCV mutant PCRs (Table 3.3). Fragments m10, m11, U3886A, U3887A, and H4bulgemut (Table 3.3) were PCRed between positions 3858 and 4017 using pTCV66 template, oligonucleotide TCV-Linker, and either T7-m10, T7-m11, T7-U3886A, T7-U3887A, or T7-H4bulgemut oligonucleotide, respectively (Table 3.2). For PCRs of mutants A3976U and A3977U (Table 3.3), template TCV66, oligonucleotide T7-M3HLinkerH4, and a respectively named mutant oligonucleotide, were used (Table 3.2). U3886A/A3977U and U3887A/A3976U PCR fragments (Table 3.3) were generated using pTCV66 template and either oligonucleotides T7-U3886A and A3977U or T7-U3887A and A3976U, respectively (Table 3.2). A PCR fragment of H4bulgemut/A3978C (Table 3.3) was created using A3978C template, T7-H4bulgemut oligonucleotide, and TCV-Linker oligonucleotide (Table 3.2).

PCR of iTLS+3' and iTLS+3'mut (Table 3.3), between TCV positions 3901 and 4054, were performed using pTCV66, oligonucleotide T7-H4M1H and either oligonucleotide KK57 or C4052A/C4053A/C4054A, respectively (Table 3.2). Sequence

TABLE 3.1. Summary of Full-Length TCV Mutants Used in Chapter III

Name	Description
pTCV66	Wt TCV
pTSNL5	Wt TCV with a SnaBI site created by insertion of a cytidylate, guanylate, and uridylate, downstream of position 4014
G3913C	pTCV66 with a guanylate to cytidylate substitution at position 3913
C3922G	pTCV66 with a cytidylate to guanylate substitution at position 3922
G3913C/ C3922G	pTCV66 with a guanylate to cytidylate substitution at position 3913 and a cytidylate to guanylate substitution at position 3922
G3912U	pTCV66 with a guanylate to uridylate substitution at position 3912
U3923G	pTCV66 with a uridylate to guanylate substitution at position 3923
G3912U/ U3923G	pTCV66 with a guanylate to uridylate substitution at position 3912 and a uridylate to guanylate substitution at position 3923
G3946C	pTCV66 with a guanylate to cytidylate substitution at position 3946
C4008G	pTCV66 with a cytidylate to guanylate substitution at position 4008
G3946C/ C4008G	pTCV66 with a guanylate to cytidylate substitution at position 3946 and a cytidylate to guanylate substitution at position 4008
G3947C	pTCV66 with a guanylate to cytidylate substitution at position 3947
C4007G	pTCV66 with a cytidylate to guanylate substitution at position 4007
G3947C/ C4007G	pTCV66 with a guanylate to cytidylate substitution at position 3947 and a cytidylate to guanylate substitution at position 4007
G3924C	pTCV66 with a guanylate to cytidylate substitution at position 3924
U3925A	pTCV66 with a uridylate to adenylate substitution at position 3925
U3925C	pTCV66 with a uridylate to cytidylate substitution at position 3925
C3926A	pTCV66 with a cytidylate to adenylate substitution at position 3926
C3926U	pTCV66 with a cytidylate to uridylate substitution at position 3926
U3945A	pTCV66 with a uridylate to adenylate substitution at position 3945
U3945G	pTCV66 with a uridylate to guanylate substitution at position 3945
U3945C	pTCV66 with a uridylate to cytidylate substitution at position 3945

Name	Description
G3946A	pTCV66 with a guanylate to adenylate substitution at position 3946
G3946U	pTCV66 with a guanylate to uridylate substitution at position 3946
G3947A	pTCV66 with a guanylate to adenylate substitution at position 3947
G3947U	pTCV66 with a guanylate to uridylate substitution at position 3947
A3950U	pTCV66 with an adenylate to uridylate substitution at position 3950
U3962A	pTCV66 with a uridylate to adenylate substitution at position 3962
A3950U/ U3962A	pTCV66 with an adenylate to uridylate substitution at position 3950 and a uridylate to adenylate substitution at position 3962
A3951U	pTCV66 with an adenylate to uridylate substitution at position 3951
U3963A	pTCV66 with a uridylate to adenylate substitution at position 3963
A3951U/ U3963A	pTCV66 with an adenylate to uridylate substitution at position 3951 and a uridylate to adenylate substitution at position 3963
U3885A	pTCV66 with a uridylate to adenylate substitution at position 3885
A3978U	pTCV66 with an adenylate to uridylate substitution at position 3978
U3885A/ A3978U	pTCV66 with a uridylate to adenylate substitution at position 3885 and an adenylate to uridylate substitution at position 3978
M10	pTCV66 with uridylate to adenylate substitutions at positions 3897 and 3898
H4Linkmut	pTCV66 with adenylate to uridylate substitutions at positions 3906-3910
M10/ H4Linkmut	pTCV66 with uridylate to adenylate substitutions at positions 3897 and 3898 and adenylate to uridylate substitutions at positions 3906-3910
A33U	pTCV66 with an adenylate to uridylate substitution at position 33
A33U/ U3885A/	pTCV66 with an adenylate to uridylate substitution at position 33 and a uridylate to adenylate substitution at position 3885
A33U/U3885A/ A3978U	pTCV66 with an adenylate to uridylate substitution at position 33, a uridylate to adenylate substitution at position 3885, and an adenylate to uridylate substitution at position 3978
J5UTR	pTSNL5 with the 5’ UTR of JINRV
C5UTR	pTSNL5 with the 5’ UTR of CCFV (Blue lake)

TABLE 3.2. Summary of Oligonucleotides Used in Chapter III

Application	Name	Position	Sequence[d]	Polarity[b]
TCV mutagenesis	3164	3164-3181[a]	5'-ATGAGCCCTTCAACCACC	+
	G3913S/ C3922S	3898-3960[a]	5'-GAGCACTAGTTTTCCAGTCTAATGCCCGCAGCTA GACAS<u>S</u>TGCTGCCA<u>S</u>CGTTTTTGGTCCCTA	-
	G3912K/ T3923K	3898-3960[a]	5'-GAGCACTAGTTTTCCAGTCTAATGCCCGCAGCTA GAC<u>M</u>GTGCTGCCAC<u>M</u>GTTTTTGGTCCCTA	-
	T3923G	3903-3960[a]	5'-GAGCACTAGTTTTCCAGTCTAATGCCCGCAGCTA GAC<u>C</u>GTGCTGCCACCGTTTTTGGT	-
	C4007G	3990-4054[a]	5'-GGGCAGGCCCCCCCCCCGCGCGAGGGGGGAGG CTATCTTTTAGTTCG<u>C</u>AGGGTCACCACAGCCCA	-
	C4008G	3990-4054[a]	5'-GGGCAGGCCCCCCCCCCGCGCGAGGGGGGAGG CTATCTTTTAGTTC<u>C</u>GAGGGTCACCACAGCCCA	-
	3331	3331-3348[a]	5'-TGTGGCGGATGGTATCAG	+
	G3924C	3915-3960[a]	5'-GAGCACTAGTTTTCCAGTCTAATGCCCGCAGCTA GA<u>G</u>AGTGCTGCC	-
	T3925M	3915-3960[a]	5'-GAGCACTAGTTTTCCAGTCTAATGCCCGCAGCTA G<u>K</u>CAGTGCTGCC	-
	C3926W	3915-3960[a]	5'-GAGCACTAGTTTTCCAGTCTAATGCCCGCAGCTA <u>W</u>ACAGTGCTGCC	-
	T3945V	3925-3967[a]	5'-ACCCAAAGAGCACTAGTTTTCC<u>B</u>GTCTAATGCCC GCAGCTAGA	-
	G3946H	3925-3967[a]	5'-ACCCAAAGAGCACTAGTTTTC<u>D</u>AGTCTAATGCCC GCAGCTAGA	-
	G3947H	3925-3967[a]	5'-ACCCAAAGAGCACTAGTTTT<u>D</u>CAGTCTAATGCCC GCAGCTAGA	-
	A3950T	3928-3960[a]	5'-GAGCACTAGT<u>A</u>TTCCAGTCTAATGCCCGCAGCT	-
	T3962A	3947-3977[a]	5'-GAAAACTAGTGCTCT<u>A</u>TGGGTAACCACTAAA	+

Application	Name	Position	Sequence[d]	Polarity[b]
	KK57	4035-4054[a]	5'-GGGCAGGCCCCCCCCCGCG	-
	A3951W/ T3963W	3931-4054[a]	5'-GGGCAGGCCCCCCCCCGCGCGAGGGGGGAGGCT ATCTTTTAGTTCGGAGGGTCACCACAGCCCACCCTT TCGGGATTTTAGTGGTTACCCWAAGAGCACTAGWT TTCCAGTCTAATGCCCGCA	-
	T3885A	3865-3960[a]	5'-GAGCACTAGTTTTCCAGTCTAATGCCCGCAGCTAGA CAGTGCTGCCACCGTTTTTGGTCCCTAACACAGGT CAAATTAAAGCGACCTGGGGGTTTT	-
	A3978T	3947-3998[a]	5'-GAAAACTAGTGCTCTTTGGGTAACCACTAAATTCCC GAAAGGGTGGGCTGTG	+
	M10	3877-3960[a]	5'-GAGCACTAGTTTTCCAGTCTAATGCCCGCAGCTAGA CAGTGCTGCCACCGTTTTTGGTCCCTTTCACAGGTC AAAATAAAGCGA	-
	H4Link mut	3886-3960[a]	5'-GAGCACTAGTTTTCCAGTCTAATGCCCGCAGCTAGA CAGTGCTGCCACCGAAAAAGGTCCCTAACACAGGT CAAA	-
	M10/H4 Linkmut	3877-3960[a]	5'-GAGCACTAGTTTTCCAGTCTAATGCCCGCAGCTAGA CAGTGCTGCCACCGAAAAAGGTCCCTTTCACAGGTC AAAATAAAGCGA	-
	5UTR-TAAAAT	10-137[a]	5'-TGAACCTCAGGGTAGTACCTGGCTCCTAGGAGTCCC ACTGCGAGCGCTGTGTTGAGTGTGTGTAGAAGAGG CATCGTGAATAGAGAGAAGGTTGATGAGGGCAAWWW WAGGCGGGTGCCAGGGATTTG	-
	JINV 5UTR	1-137[c]	5'-TGAACCTCAGGGTAGTACCTGGCTCCTAGGAGTCCC ACTGCGAGCGCTGTGTTGAGTGTGTGTAGAAGAGG CATGGGTTCACGTTGTATATATACTCGTTTACCC*TA TAGTGAGTCGTATTA*	-
	CCFV 5UTR	1-137[c]	5'-TGAACCTCAGGGTAGTACCTGGCTCCTAGGAGTCCC ACTGCGAGCGCTGTGTTGAGTGTGTGTAGAAGAGG CATGAGGGTTAAGAAGAAGAATTTGGGTTCTATGGAA AACC*TATAGTGAGTCGTATTA*	-
Generation of iTLS fragments	T7-H4M1H	3901-3912[a]	5'-*TAATACGACTCACTATAG*GGACCAAAAACG	+
	TCV-Linker	3998-4017[a]	5'-TTTTAGTTCGGAGGGTCACC	-

Application	Name	Position	Sequence[d]	Polarity[b]
	T7-M3H LinkerH4	3858-3877[a]	5'-*TAATACGACTCACTATAG*GAAAACAAAAACCCCCAG GT	+
	C4052A/ C4053A/ C4054A	4032-4054[a]	5'-TTTCAGGCCCCCCCCCCGCGCGA	-
	T7-M11	3858-3907[a]	5'-*TAATACGACTCACTATAG*GAAAACAAAAACCCCCAG GTCGCTTATATATGACCTGTGTTAGGGACCAA	+
	A3977T	3956-4017[a]	5'-TTTTAGTTCGGAGGGTCACCACAGCCCACCCTTTCG GGATATTAGTGGTTACCCAAAGAGCA	-
	T7-T3886A	3858-3908[a]	5'-*TAATACGACTCACTATAG*GAAAACAAAAACCCCCAG GTCGCTTTATATTGACCTGTGTTAGGGACCAAA	+
	A3976T	3956-4017[a]	5'-TTTTAGTTCGGAGGGTCACCACAGCCCACCCTTTCG GGATTATAGTGGTTACCCAAAGAGCA	-
	T7-T3887A	3858-3908[a]	5'-*TAATACGACTCACTATAG*GAAAACAAAAACCCCCAG GTCGCTTTATTATGACCTGTGTTAGGGACCAAA	+
	T7-M10	3858-3918[a]	5'-*TAATACGACTCACTATAG*GAAAACAAAAACCCCCAG GTCGCTTTATTTTGACCTGTGAAAGGGACCAAAAACG GTGGCA	+
	T7-H4bulge mut	3858-3918[a]	5'-*TAATACGACTCACTATAG*GAAAACAAAAACCCCCAG GTCGCTTTATTTTGACCTGTGACTGGGACCAAAAACG GTGGCA	+
Northern blotting	3181	3181-3199[a]	5'-CCAGAGCCACCTTGCCTCCG	-
	551	551-570[a]	5'-GTGGCTGTCTACGACATGTC	-

[a] Positions correspond to the base number in genomic TCV

[b] "+" and "-" indicate homology and complementarity, respectively, to either TCV, CCFV (Blue lake), or JINRV.

[c] Base positions were determined using TCV sequence and analogous nucleotide positions to TCV for either CCFV (Blue lake) or JINRV sequence

[d] Underlined letters indicate mutated bases in comparison to pTCV66 plasmid sequence. Uppercase bold italicized letters correspond to T7 RNA polymerase promoter sequence. Lowercase bold letters indicate bases added for in vitro RNA transcription. S = C or G; K = G or T; M = A or C; D = A, G, or T; W= A, T; B= C, G, or T

TABLE 3.3. Summary of iTLS RNA Fragments Used in Chapter III

Name	Description
iTLS	TCV wt fragment (position 3901-4017)
iTLS+3'	TCV wt fragment (position 3901-4054)
iTLS+H4	TCV wt fragment (position 3858-4017)
iTLS+H4+3'	TCV wt fragment (position 3858-4054)
iTLS+3'mut	TCV fragment (position 3901-4054) containing cytidylate to adenylate substitutions at positions 4052, 4053, and 4054
iTLS+H4+3'mut	TCV fragment (position 3858-4054) containing cytidylate to adenylate substitutions at positions 4052, 4053, and 4054
A3978C	TCV fragment (position 3858-4017) containing an adenylate to cytidylate substitution at position 3978
m11	TCV fragment (position 3858-4017) containing uridylate to adenylate substitutions at positions 3883, 3885, and 3887 and an adenylate to uridylate substitution at position 3884
U3885A	TCV fragment (position 3858-4017) containing a uridylate to adenylate substitution at position 3885
A3978U	TCV fragment (position 3858-4017) containing an adenylate to uridylate substitution at position 3978
U3885A/ A3978U	TCV fragment (position 3858-4017) containing a uridylate to adenylate substitution at position 3885 and an adenylate to uridylate substitution at position 3978
U3886A	TCV fragment (position 3858-4017) containing a uridylate to adenylate substitution at position 3886
A3977U	TCV fragment (position 3858-4017) containing an adenylate to uridylate substitution at position 3977
U3886A/ A3977U	TCV fragment (position 3858-4017) containing a uridylate to adenylate substitution at position 3886 and an adenylate to uridylate substitution at position 3977
U3887A	TCV fragment (position 3858-4017) containing a uridylate to adenylate substitution at position 3887
A3976U	TCV fragment (position 3858-4017) containing an adenylate to uridylate substitution at position 3976
U3887A/ A3976U	TCV fragment (position 3858-4017) containing a uridylate to adenylate substitution at position 3887 and an adenylate to uridylate substitution at position 3976
m10	TCV fragment (position 3858-4017) containing uridylate to adenylate substitutions at positions 3897 and 3898

Name	Description
H4bulgemut	TCV fragment (position 3858-4017) containing a uridylate to adenylate substitution at position 3897, a uridylate to cytidylate substitution at position 3898, and an adenylate to uridylate substitution at position 3899
H4bulgemut/ A3978C	TCV fragment (position 3858-4017) containing a uridylate to adenylate substitution at position 3897, a uridylate to cytidylate substitution at position 3898, an adenylate to uridylate substitution at position 3899, and an adenylate to cytidylate substitution at position 3978
G3913C	TCV fragment (position 3901-4017) containing a guanylate to cytidylate substitution at position 3913
C3922G	TCV fragment (position 3901-4017) containing a cytidylate to guanylate substitution at position 3922
G3913C/ C3922G	TCV fragment (position 3901-4017) containing a guanylate to cytidylate substitution at position 3913 and a cytidylate to guanylate substitution at position 3922
A3951U	TCV fragment (position 3901-4017) containing an adenylate to uridylate substitution at position 3951
U3963A	TCV fragment (position 3901-4017) containing a uridylate to adenylate substitution at position 3963
A3951U/ U3963A	TCV fragment (position 3901-4017) containing an adenylate to uridylate substitution at position 3951 and a uridylate to adenylate substitution at position 3963
H4Linkmut	TCV fragment (position 3901-4017) containing adenylate to uridylate substitutions at positions 3906-3910
m10/ H4Linkmut	TCV fragment (position 3901-4017) containing uridylate to adenylate substitutions at positions 3897 and 3898 and adenylate to uridylate substitutions at positions 3906-3910

between positions 3858 and 4054 was amplified for iTLS+H4+3' and iTLS+H4+3'mut (Table 3.3) using pTCV66 template, T7-M3HLinkerH4 oligonucleotide, and either KK57 or C4052A/C4053A/C4054A oligonucleotide, respectively (Table 3.2).

Determining TCV Accumulation Levels in Protoplasts

Preparation and inoculation of protoplasts and Northern blotting of TCV RNA were previously described in Chapter II.

Results

A 100 nt Region in the TCV 3' UTR Contains Two Pseudoknots and Three Hairpins

MPGAfold, a massively parallel genetic algorithm that predicts secondary and limited tertiary RNA structures (H-type pseudoknots; Shapiro *et al*., 2001), coupled with phylogenetic analyses were used to identity structural elements within the 3' terminal region of TCV (positions 3895-4054) that might contribute to replication and/or translational enhancement (Fig. 3.2A). The 3' terminal Pr was identified as the core promoter based on its ability to bind the RNA dependent RNA polymerase (RdRp) and direct complementary strand synthesis *in vitro* (Sun and Simon, 2006). The 3' side of the large symmetrical loop (LSL) of H5 forms an RNA-RNA interaction with four bases at the 3' terminus (termed Ψ_1) that is important for efficient accumulation *in vivo* (Fig. 2.3B). The juxtaposed hairpins H4a and H4b are structurally and spatially conserved in the most closely related carmoviruses, *Cardamine chlorotic fleck virus* (CCFV; Fig. 4.1B; Zhang *et al*., 2006a) and *Japanese iris necrotic ring virus* (JINRV; Fig. 4.1C).

To assess the importance of TCV H4a and H4b *in vivo*, mutations were introduced into the terminal loops and viral accumulation levels determined in protoplasts. In H4a, mutagenesis of a guanylate to cytidylate at position 3924 (G3924C) resulted in a 98% reduction in accumulation, whereas viral RNA levels for alterations at positions 3925 (U3925A and U3925C) and 3926 (C3926A and C3926U) were between 20% and 42%, in comparison to wt TCV (Fig. 3.1A,B). These results show the importance of TCV H4a terminal loop sequence in promoting high levels of viral RNA accumulation. For H4b, mutants U3945G and U3945C accumulated to wt TCV levels and construct U3945A showed a reduction in accumulation of 51%, in comparison to wt TCV RNA (Fig. 3.1C). The 3946 (G3946A and G3946U) and 3947 (G3947A and G3947U) mutant series ranged from 29% to 74% of wt TCV levels (Fig. 3.1C). These data suggest that the guanylates at positions 3946 and 3947 are an important feature of H4b.

SatC, an untranslated subviral RNA that participates in a mutualistic association with TCV, shares 151 3' co-terminal bases with TCV (90% sequence similarity) (Zhang *et al*., 2006b). SatC contains an important pseudoknot (Ψ_2) between its H4b loop sequence (5'-UGGA) and sequences flanking the 3' side of H5 (3'-GCCU) (Zhang *et al*., 2006a). To determine if a similar pseudoknot exists in TCV, two sets of compensatory mutations were generated (Fig. 3.2A). Converting a guanylate to a cytidylate at position 3947 in the H4b loop (G3947C) or a cytidylate to guanylate in its putative partner at the base of H5 (C4007G) reduced TCV accumulation in Arabidopsis protoplasts to 31 and 34% of wt, respectively (Fig. 3.2B). In contrast, the mutations together (G3947C/C4007G) had a compensatory effect, with mutant TCV accumulating to 80%

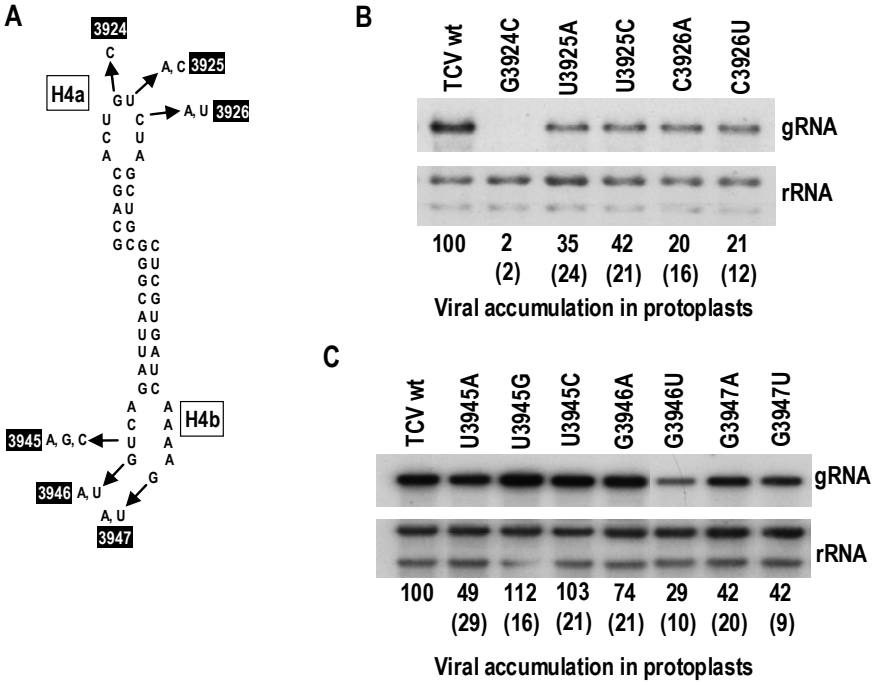

Figure 3.1. Accumulation in Protoplasts of TCV Containing Mutations in H4a and H4b Terminal Loops. (A) Depiction of H4a and H4b region with individual mutations shown. Black boxes contain the partial names of the mutant series. (B) RNA accumulation of H4a mutants in protoplasts at 40 hpi. Names of constructs are designated based on mutation position and substitution type. Average relative accumulations from 3 trials and standard deviations in parentheses are given. gRNA = genomic TCV RNA; rRNA = ribosomal RNA (C) H4b mutant accumulations in protoplasts at 40 hpi. Blot is labeled similarly as the one shown in (B).

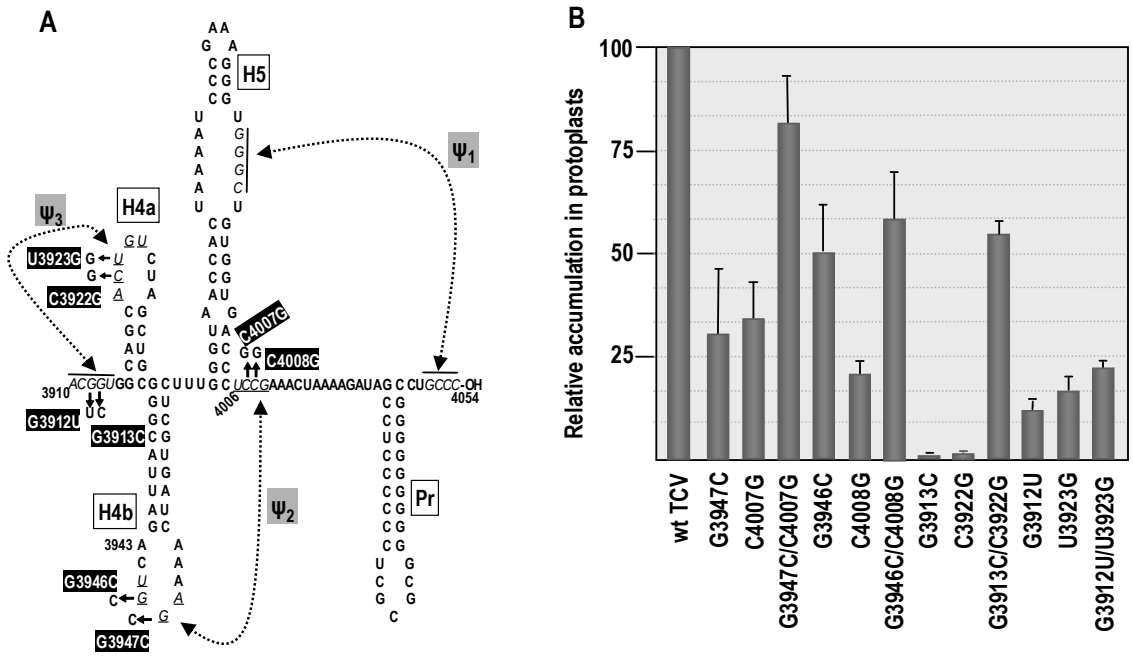

Figure 3.2. Structure of the 3' Terminal Region of TCV RNA. (A) MPGAfold-predicted secondary structure of the 3' region of the TCV 3' UTR. Ψ_1 was previously identified (Fig. 2.3B), whereas Ψ_2 was identified as important for replication of TCV-associated satC (Zhang *et al*., 2006a). Ψ_3 was predicted by MPGAfold. Names of mutations are boxed in black. **(**B**)** Effect of mutations in the presumptive pseudoknots Ψ_2 and Ψ_3 on accumulation of TCV in protoplasts at 40 hpi. All mutants were subjected to three independent assays, and standard deviation bars are shown.

of wt (Fig. 3.2B). Alteration of H4b loop position G3946C was less deleterious to TCV accumulation (50% of wt), possibly due to a 3 bp Ψ_2 interaction that can exist if pairing with sequence at the base of H5 is shifted one nucleotide downstream. Altering the putative partner residue at the base of H5 (C4008G) reduced accumulation 5-fold, whereas both alterations improved TCV accumulation to 58% of wt. These results support the existence of Ψ_2 in TCV (Fig. 3.2B).

MPGAfold revealed a possible H-type pseudoknot between 5 nt in the loop of H4a and upstream flanking sequence in TCV, labeled as Ψ_3 in Fig. 3.2A. TCV containing G3913C at the base of H4a or C3922G in the H4a loop accumulated to barely detectable levels, whereas virus containing mutations (G3913C/C3922G) that should reform Ψ_3, accumulated to 55% of wt (Fig. 3.2B). The second pair of mutations, G3912U and U3923G, individually reduced TCV levels to 11 and 16% of wt, respectively, whereas TCV containing both mutations (G3912U/U3923G) accumulated slightly better (22% of wt). Together, these results support the presence of Ψ_3 in TCV, and also suggest that partner sequences comprising Ψ_3 are sequence specific (Fig. 3.2B).

Region Encompassed by Ψ_2 and Ψ_3 Structurally Resembles a tRNA

Viral RNAs can adopt mutually exclusive conformations important for different requirements during the virus life cycle (Zhang *et al*., 2006a). To determine if H4a/H4b/H5 along with Ψ_2 and Ψ_3 are capable of simultaneous existence, a 3-D molecular modeling protocol was employed by collaborators Yara G. Yingling and Bruce A. Shapiro and involved initial prediction by the program RNA2D3D followed by molecular modeling (Yingling and Shapiro, 2006). Several starting structures for the

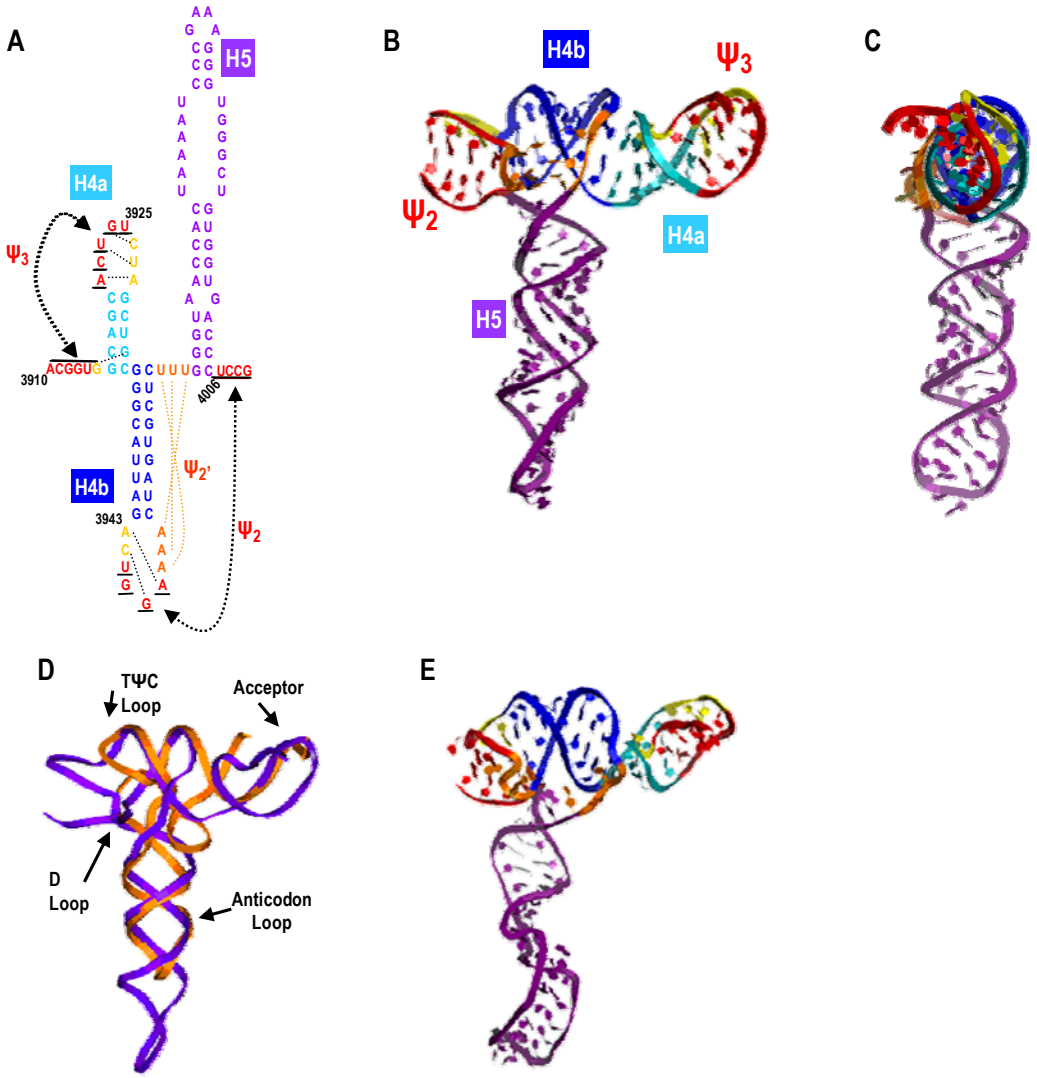

Figure 3.3. tRNA-Like Structure Predicted by RNA2D3D and Molecular Modeling. (A) Region of TCV subjected to RNA2D3D and molecular modeling. Secondary structure of the TCV modeled region with predicted tertiary interactions indicated by dotted lines. **(**B**)** Predicted tertiary structure of TCV color-coded according to secondary structure shown in (A). Ψ_2 and Ψ_3 are in red and unpaired bases are in yellow. Ψ_2' is in orange. **(**C**)** Side view of the predicted TCV structure. **(**D**)** Superimposed structures of the TCV iTLS (purple) and Phe-tRNA (orange). tRNA sites are indicated. **(**E**)** Predicted structure of TCV iTLS containing single base mutation G3913C (see Fig. 3.2A). Note significant disorder of all tertiary interactions.

Performed by Yaroslava G. Yingling

TCV model were used with different positions of the bases not participating in the secondary structure base pairing. The region encompassed by Ψ_2 and Ψ_3 stably folded into a single structural domain that strongly resembled a canonical tRNA (Fig. 3.3B,C,D). Molecular modeling also suggested that the internal tRNA-like structure (iTLS) is stabilized by parallel tertiary interactions (labeled Ψ_2' ; Fig. 3.3A), a structural feature also found in canonical tRNAs (Quigley and Rich, 1976).

The iTLS Binds 80S Ribosomes at the P-site

To determine if structural tRNA mimicry implied some degree of functional mimicry, a 117 nt RNA fragment containing the iTLS was subjected to filter binding assays using 80S yeast ribosomes, which were performed by Arturas Meskauskas. Wild-type (wt) iTLS bound ribosomes with high affinity (K_d=0.45 μM; Fig. 3.4A), comparable to the binding constants of yeast aminoacylated-tRNA for yeast 80S ribosomes (K_d=0.05 μM; Petrov *et al*., 2004) and of deacylated tRNA for *E. coli* ribosomes (0.1-0.25 μM; Schilling-Bartetzko *et al*., 1992). The K_d of iTLS binding was not affected by salt washing the ribosomes, indicating that binding was independent of translation factors (Fig. 3.4A). To determine the 80S ribosome binding site of the iTLS, competition assays were performed using uncharged (non-acylated) $tRNA_{Phe}$, which binds to P- and E-sites, charged Phe-tRNA (Phe-tRNA), which binds to P- and A-sites and acetylated Phe-tRNA (Ac-Phe-tRNA), which is specific for the P-site (Wilson *et al*., 2000b). Twenty-fold excess of uncharged tRNA reduced iTLS binding by 61% (Fig. 3.4B), whereas the same amount of excess iTLS reduced binding of acetylated Phe-tRNA by 52% (Fig. 3.4C). Thus, the ability to specifically compete with Ac-Phe-tRNA suggests that the iTLS at

Figure 3.4. TCV iTLS Binds 80S Yeast Ribosomes. (A) iTLS binding to 80S ribosomes. 2-100 pmol of [^{32}P] 5'-end labeled wt TCV iTLS (positions 3901 to 4017) were combined with 25 pmol of yeast 80S ribosomes and bound RNA was detected following filter binding. The fraction of ribosomes active in iTLS binding is comparable with yeast Phe-tRNA binding with similarly prepared yeast ribosomes (Petrov *et al*., 2004).**(**B**)** Effect of uncharged tRNA on iTLS binding. Ribosomes (30 pmol) were pre-incubated with 0-600 pmol of $tRNA_{Phe}$ followed by addition of 30 pmol of labeled iTLS. **(**C**)** Effect of iTLS on Phe-tRNA and Ac-Phe-tRNA binding. For P-site specificity, ribosomes (30 pmol) were incubated with 0-600 pmol of iTLS followed by addition of 30 pmol of labeled Ac-Phe-tRNA. For A-site competition, ribosomes were pre-incubated with 0-600 pmol of iTLS, followed by addition of labeled Phe-tRNA. Data are expressed as percentage of initial binding (without competing RNA) at given competing RNA/ribosomes molar ratios.

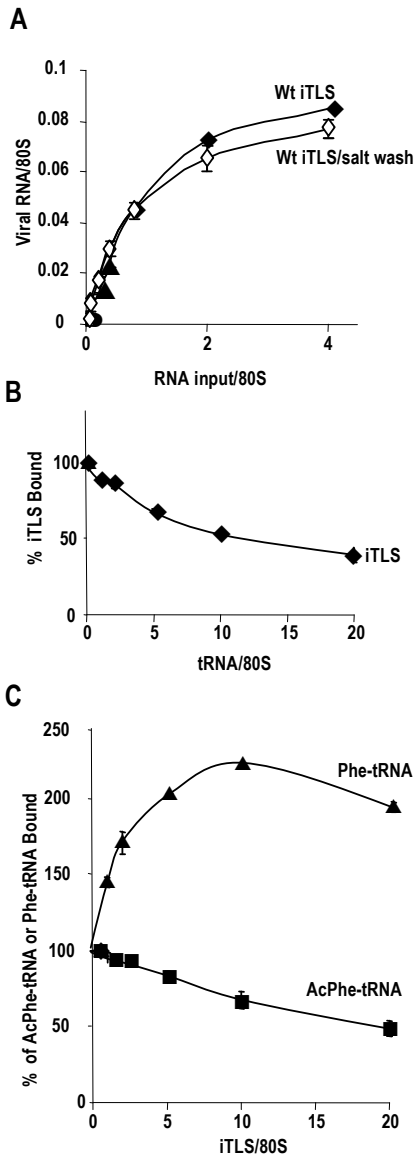

Performed by Arturas Meskauskas

least partially occupies the ribosomal P-site. Binding of iTLS to 80S ribosomes significantly stimulated binding of Phe-tRNA to the A-site in the absence (Fig. 3.4C) or presence (not shown) of pre-incubation with tRNA to saturate the P-site. Similar stimulation of A-site binding for aminoacylated tRNAs when the P-site is occupied by deacylated tRNA has been previously demonstrated (van Noort *et al*., 1985). Altogether, these data indicate that the TCV iTLS binds the 80S P-site in a translation factor-independent fashion, however, additional interaction with the E-site cannot be ruled out.

The Terminal Loop of H4b May Form Parallel Basepairing with a Downstream Linker In Vivo

Molecular modeling using RNA2D3D predicted the existence of parallel basepairing ($\Psi_{2'}$) between the H4b terminal loop and downstream flanking sequences in the TCV iTLS (Fig. 3.3A). To test for this tertiary interaction, compensatory mutational analysis was performed. Single-site mutations that were predicted to disrupt this interaction were introduced into H4b (A3951U) or the linker between H4b and H5 (U3963A) (Fig. 3.5A). In vitro ribosome binding assays showed that A3951U and U3963A bound 80S ribosomes to an affinity that was equivalent to (K_d=0.51 μM) or about 2-fold less (K_d=1.03 μM) than wt iTLS, respectively. iTLS containing both mutations (A3951U/U3963A), which were predicted to reform the pseudoknot, bound ribosomes slightly better than wt (K_d=0.39 μM), giving support for the existence of $\Psi_{2'}$ (Fig. 3.5B). A3951U accumulated in protoplasts to 73% of wt TCV levels and U3963A

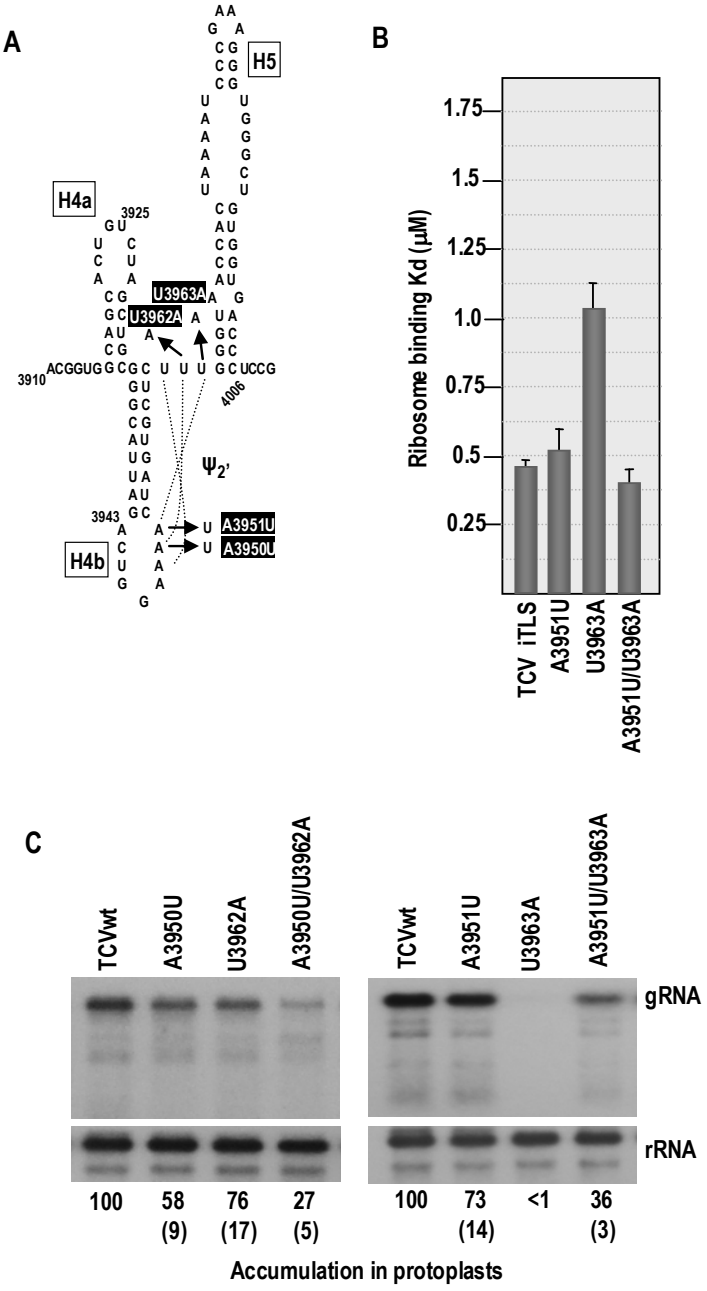

Figure 3.5. Evidence for the Existence of $\Psi_{2'}$ in TCV iTLS. (A) Depiction of the iTLS region with predicted $\Psi_{2'}$ parallel basepairing shown by dotted lines. Names of constructs are indicated by black boxes. (B) In vitro ribosome binding using 80S ribosomes and selected TCV mutants. Names of mutants are designated using TCV base positions and substitution types. Bars represent the average of three experiments and standard error is shown by error bars. (C) Compensatory mutational analysis for 2 series of mutants. Numbers below blots show the average accumulation of 3 trials at 40 hpi and standard deviation is indicated in parentheses. gRNA=genomic TCV RNA; rRNA= ribosomal RNA. Ribosome binding performed by Arturas Meskauskas.

to levels that were below detection. The double mutant exhibited levels of accumulation that were 36% of wt TCV, suggesting that the lethal effects of U3963A could be partially restored in the presence of A3951U (Fig. 3.5C). A second series of alterations were constructed to test the predicted middle basepair of the $\Psi_{2'}$. A3950U in H4b loop and U3962A in the downstream flanking sequence accumulated to levels that were 58% and 76% in comparison to TCV wt, respectively. However, A3950U/U3962A accumulated to 27% of TCV wt levels, indicating that the double mutation was not compensatory (Fig. 3.5C). These results suggest that basepairs comprising $\Psi_{2'}$ may form differently than predicted with RNA2D3D analysis.

Mutations Disrupting Ψ_3 and in Upstream Hairpin H4 Reduce TCV Accumulation In Vivo and 80S Ribosome Binding In Vitro

Ψ_3 mutations G3913C or C3922G, which decreased TCV accumulation to 1-2% of wt (Fig. 3.2B), caused a 5-fold reduction in ribosome binding (K_d=2.38 μM and 2.44 μM, respectively) (Fig. 3.6B). Compensatory mutant G3913C/C3922G, which restored Ψ_3 and TCV accumulation to 55% of wt (Fig. 3.2B), enhanced ribosome binding to near wt levels (K_d=0.56 μM; Fig. 3.6B). Modeling the effect of G3913C on iTLS structure revealed complete disruption of Ψ_3 and substantial disruption of the iTLS (Fig. 3.3E).

Mutation m10, located in the asymmetrical loop of upstream hairpin H4 (Fig. 3.6A), was previously found to substantially reduce TCV levels in a manner that was unconnected to the hairpin's ability to bind the RdRp (Sun and Simon, 2006). The lengthened fragment iTLS+H4 (Fig. 3.6A) reduced ribosome binding 3-fold compared

Figure 3.6. Alterations in the iTLS and Flanking Upstream and Downstream Regions. (A) Location of fragments and alterations. Mutation designations are boxed in black. (B) Ribosome binding to iTLS fragment with mutations in Ψ_3. K_d were calculated from three independent experiments. Standard error bars are shown. (C) Ribosome binding to the iTLS+H4 fragment with and without sequence alterations. (D) Ribosome binding to the iTLS + 3' and iTLS + H4 + 3'. Mutated fragments contain an alteration of the 3' terminal cytidylates to adenylates. (E) Binding of ribosomal subunits to the iTLS fragment in the presence and absence of poly(U).

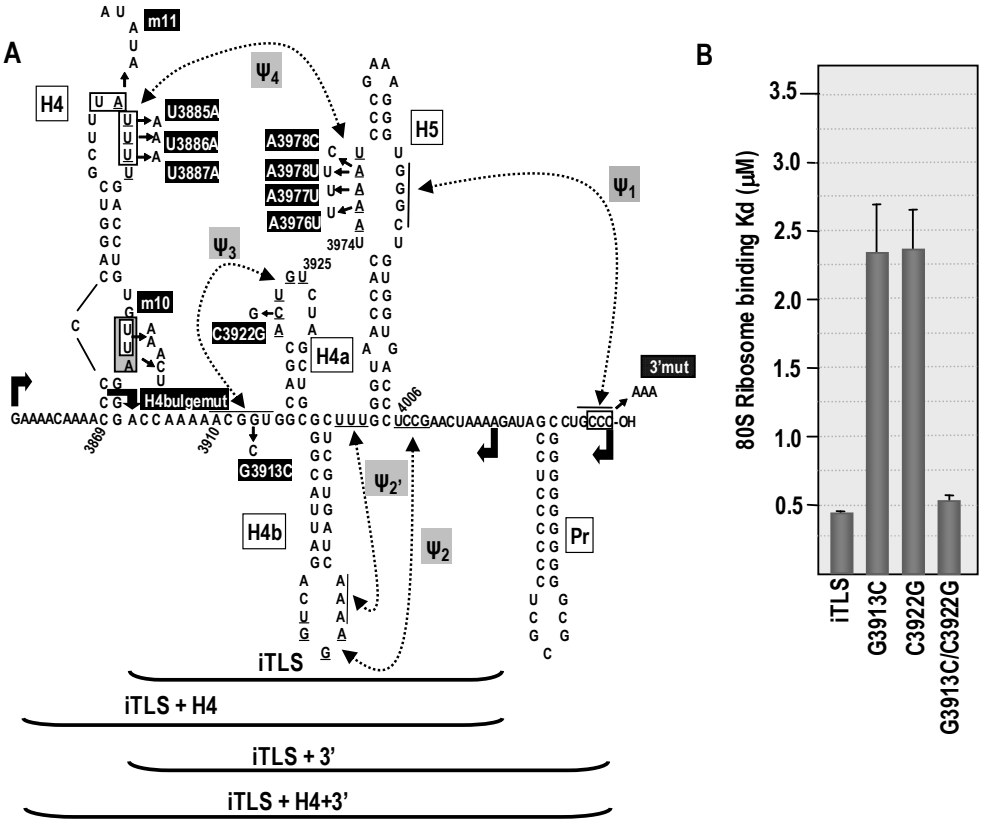
A
B
m11
H4
U3885A
U3886A
U3887A
Ψ4
H5
A3978C
A3978U
A3977U
A3976U
Ψ1
Ψ3
m10
C3922G
H4a
3'mut
AAA
H4bulgemut
GAAAACAAAACG A CCAAAAACGGUGGCGCUUUGCUCCGAACUAAAAGAUAGCCUGCCC-OH
3869
3910
4006
G3913C
Ψ2'
H4b
Ψ2
Pr
iTLS
iTLS + H4
iTLS + 3'
iTLS + H4+3'
80S Ribosome binding Kd (μM)
3.5
3.0
2.5
2.0
1.5
1.0
0.5
iTLS
G3913C
C3922G
G3913C/C3922G

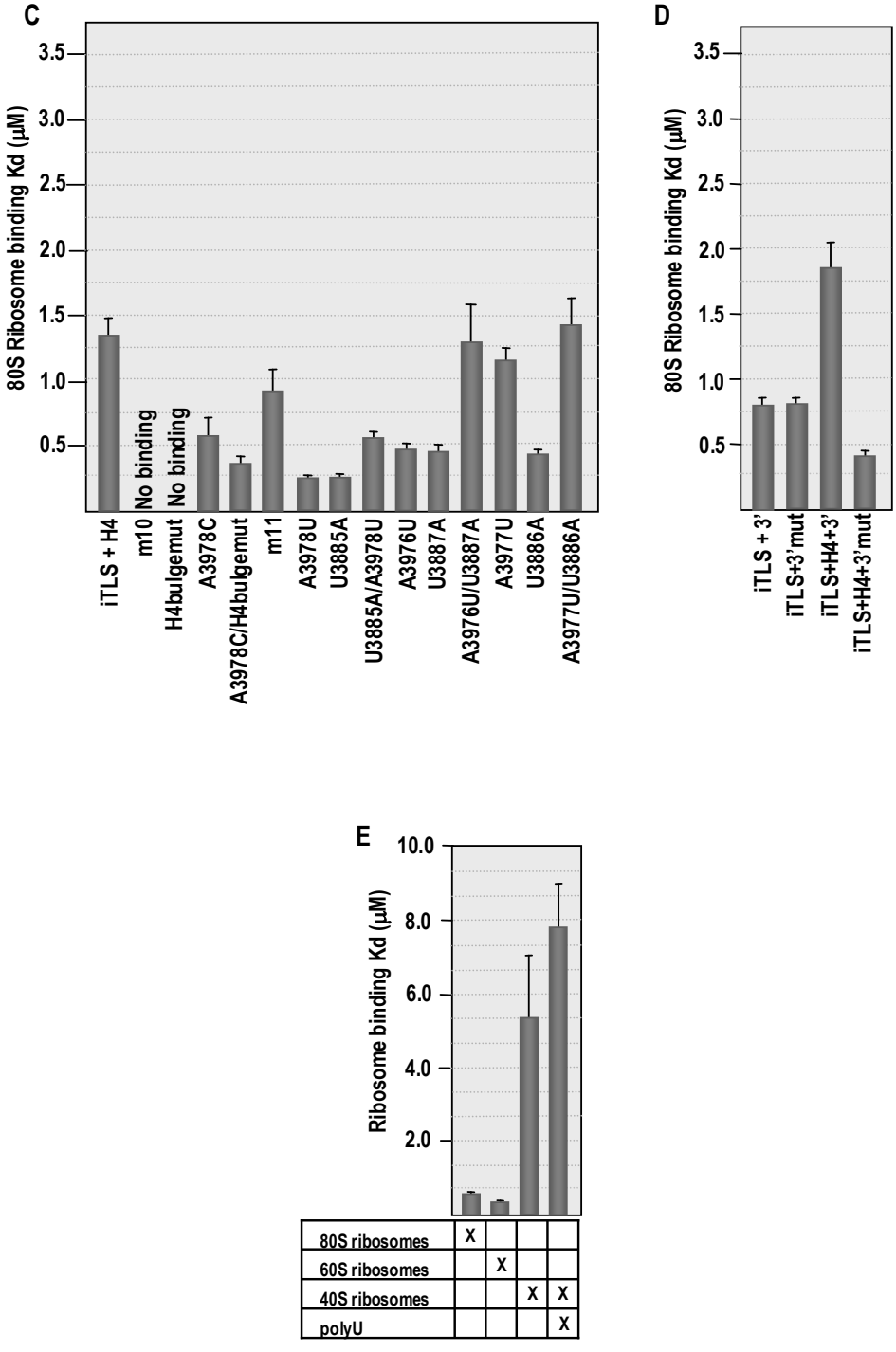

Ribosome binding performed by Arturas Meskauskas

with binding to the iTLS alone and inclusion of the m10 mutation abolished binding (Fig. 3.6C). A second three base alteration in the H4 asymmetric loop (H4bulgemut) also reduced binding to undetectable levels. Altogether, these results indicate that mutations that substantially reduce TCV levels *in vivo* also reduce ribosome binding *in vitro*.

To determine if H4 affects iTLS ribosome binding through possible pairing between the H4 terminal loop (5'-AUUUU) and the 5' side of the H5 LSL (3'-UAAAA) (denoted as Ψ_4 in Fig. 3.6A), the iTLS+H4 fragment containing single and compensatory alterations were assayed for 80S ribosome binding. m11 in the H4 terminal loop reversed the effect of adding H4 to the the iTLS (K_d=0.91 μM) and A3978C in the H5 LSL counteracted both the inclusion of H4 with the iTLS and H4bulgemut mutation (K_d=0.61 μM and 0.36 μM, respectively; Fig. 3.6C). A3978U (in H5) and putative partner U3885A (in H4), enhanced ribosome binding to the iTLS+H4 fragment (K_d=0.27 μM). The alterations together (U3885A/A3978U), which should restore Ψ_4, reduced ribosome binding by 2.2-fold, suggesting that an interaction inhibitory to ribosome binding was re-established. A3976U (in H5) and U3887A (in H4) assayed in the iTLS+H4 fragment similarly enhanced ribosome binding to levels found for the iTLS alone, whereas combining the mutations (A3976U/U3887A) reduced ribosome binding to iTLS+H4 levels (Fig. 3.6C). A3977U (K_d=1.14 μM) in H5 did not exhibit an enhancement for ribosome binding in comparison to the iTLS+H4 fragment; however, A3977U was able to reverse the effect of U3886A (K_d=0.41 μM) in H4 when both were present in A3977U/U3886 (K_d=1.46 μM; Fig. 3.6C). These results support the Ψ_4 interaction between H4 and H5 *in vitro*, which reduces ribosome binding to the iTLS.

Ψ_1 Formation Reduces Ribosome Binding in the Presence of the iTLS and Upstream H4 Region In Vitro

The effects of the TCV 3' terminal region when present with the iTLS (iTLS + 3') and the iTLS with upstream H4 region (iTLS + H4 + 3') were assayed for their ability to bind ribosomes (Fig. 3.6D). iTLS + 3' and iTLS + H4 + 3' were reduced for ribosome binding in comparison to the iTLS fragment (K_d=0.77 μM and 1.83 μM, respectively), suggesting that sequence in the 3' terminal region was repressing ribosome binding (Fig. 3.6D). One possibility was that formation of Ψ_1 between the H5 LSL and 3' terminus altered iTLS structure leading to reduced ribosome binding. To test for this possibility, Ψ_1 was disrupted by converting the 3' terminal cytidylates to adenylates in the iTLS +3' (iTLS + 3'mut) and iTLS + H4 + 3' (iTLS + H4 + 3'mut) RNA fragments. While the iTLS + 3'mut bound ribosomes as well as the iTLS + 3' fragment, the iTLS + H4 + 3'mut had a 4.6-fold enhancement in comparison to its corresponding wt fragment, suggesting that Ψ_1 formation in iTLS + H4 + 3' causes a reduction in ribosome binding *in vitro* (Fig. 3.6D).

The iTLS Binds 60S Ribosomal Subunits

Although 80S ribosomes can be found at high concentrations in stressed cells, the iTLS likely interacts with 40S or 60S ribosomal subunits. 80S ribosomes were dissociated and gradient fractionated 40S and 60S subunits were assayed for iTLS binding (Fig. 3.6E). The iTLS bound to 60S subunits slightly better than to 80S ribosomes (K_d=0.34 μM and 0.45 μM, respectively) while the affinity of the iTLS for 40S subunits was nearly 16-fold lower. In the presence of poly(U), which blocks non-

specific interactions in the mRNA channel, binding to 40S subunits was 23-fold lower than binding to 60S subunits, suggesting that the low levels of 40S binding were partly non-specific (Fig. 3.6E). These results suggest that the iTLS interaction with 80S ribosomes is through binding to the 60S subunit.

H4 Asymmetrical Loop and a Downstream Linker May Be Functionally Antagonistic

Mutagenesis of the H4 asymmetrical loop (mutant m10) showed that this region was important for binding of ribosomes *in vitro* (Fig. 3.6C). Sequence analysis of the H4 and downstream flanking nucleotides revealed a potential interaction between the uridylates at positions 3897 and 3898 in the asymmetrical loop and adenylates spanning positions 3906 to 3910 (Fig. 3.7A). Since no predictions could be made on which adenylates were involved in basepairing, all positions were changed to uridylates to disrupt the proposed pseudoknot (H4Linkmut) or in combination with m10 to restore the interaction (m10/H4Linkmut; Fig. 3.7A). H4Linkmut bound ribosomes at a K_d of 0.82 μM, whereas m10/H4Linkmut appeared compensatory for the deleterious effects of m10 (K_d=0.28 μM; Fig. 3.7B). Due to the ability of H4Linkmut to bind ribosomes at an affinity greater than wt (TCV iTLS + H4), these results are not consistent with pseudoknot formation; however, the compensatory effect of m10/H4Linkmut suggests a relationship between H4 and the downstream linker. One possibility is that H4 asymmetrical loop and downstream linker are functionally antagonistic, with H4Linkmut stabilizing an RNA conformation that recruits ribosomes and m10 favoring a structure that binds RdRp. The effects of H4Linkmut may be dominant to m10 in the mutant

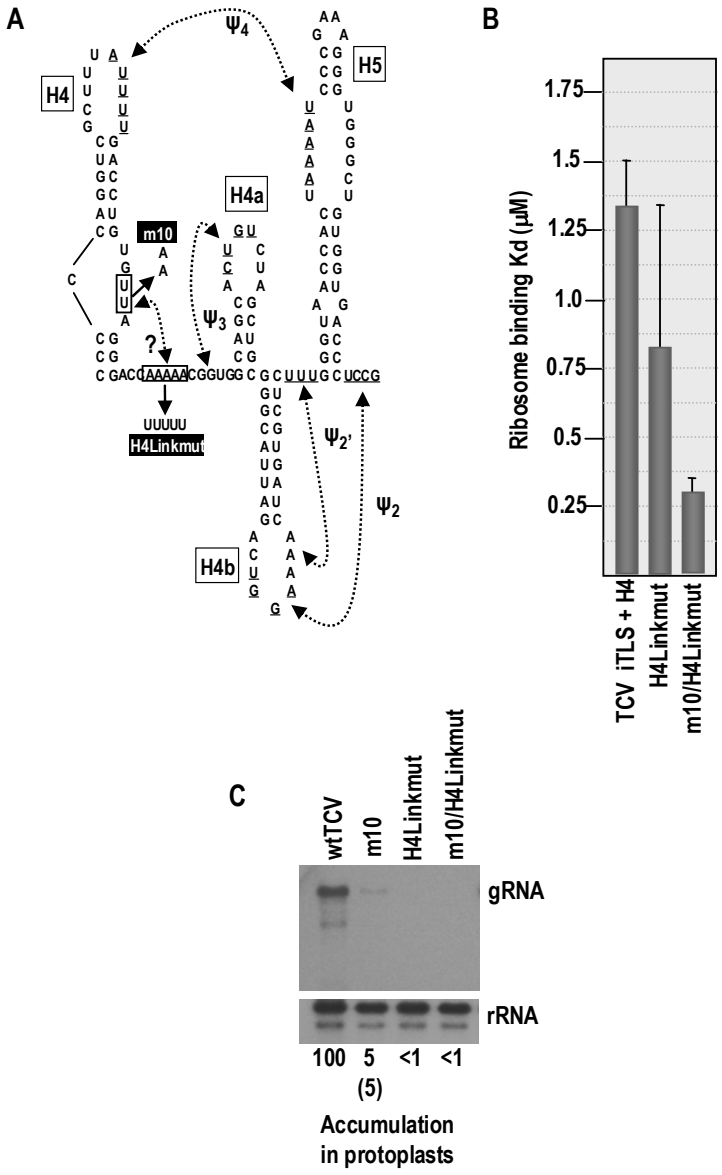

Figure 3.7. Importance of the H4 Asymmetrical Loop and Downstream Flanking Sequences. (A) Putative structure of the iTLS and upstream H4 region. Predicted tertiary interactions are shown by dotted lines. The possible interaction between H4 asymmetrical loop and downstream linker is designated with a question mark. Names of mutants are given in black boxes. (B) 80S ribosome binding of TCV mutants. Bars represent three trials and error bars indicate standard error. (C) Viral accumulations of TCV mutants in protoplasts at 40 hpi. Numbers with and without parentheses represent standard deviations and relative viral accumulations for three trials, respectively. Ribosome binding performed by Arturas Meskauskas.

m10/H4Linkmut, resulting in a high affinity for ribosomes. Testing in protoplasts showed that m10 had a 95% reduction in viral accumulation in comparison to wt TCV and both H4Linkmut and M10/H4Linkmut were at levels below detection, confirming that these regions were important *in vivo* (Fig. 3.7C).

The TCV 5' UTR Does Not Basepair with the 3' UTR to Promote Accumulation in Protoplasts

Recruitment of 60S ribosomal subunits to the TCV 3'UTR suggests that transfer of translational proteins to the 5' end may occur for assembly of 80S ribosomes and translation initiation at the 5' end. One possibility is that RNA-RNA basepairing between the 3' UTR and 5' UTR of TCV may bring the two termini together to facilitate 60S ribosomal subunit transfer. Sequence analysis of the TCV 5' UTR identified sequence at TCV positions 30 to 34 (5'-AAAAU) that can potentially interact with bases in the H4 terminal loop (3'-UUUUA). Single-site changes were made in either the 5' UTR (A33U) or H4 (U3885A), which were predicted to disrupt the interaction between the UTRs (Fig. 3.8A). Accumulation in protoplasts showed that A33U and U3885A were at 53% and 41% of wt TCV levels, respectively (Fig. 3.8B). However, combining the alterations (A33U/U3885A), which should restore the long-distance basepairing, failed to rescue accumulation (30% in comparison to wt TCV levels). A possibility is that weakening Ψ_4 by mutant U3885A may mask the compensatory effect of restoring the predicted 5' UTR-3' UTR interaction. Another series of constructs were generated to address this issue. A3978U in H5, mutant U3885A/A3978U, and mutant A33U/U3885A/A3978U were constructed to disrupt Ψ_4, restore Ψ_4, and restore the

Figure 3.8. Proposed Interaction Between the 3' UTR and 5' UTR of TCV. (A) Illustration of the potential interaction (indicated by underlined nucleotides) between the H4 terminal loop and sequence in the 5' UTR. Names of mutants are shown in black boxes. (B) Viral accumulation levels of TCV mutants at 40 hpi. Names of constructs are given above the blot and numbers below show average accumulation levels of 3 trials and standard deviations (in parentheses). gRNA=genomic TCV RNA; rRNA= ribosomal RNA.

5’ UTR-3’ UTR basepairing and Ψ_4, respectively. A3978U and U3885A/A3978U had accumulation levels of 31% and 12% in comparison to wt TCV, respectively. However, A33U/U3885A/A3978U did not appear to be compensatory with 4% of wt TCV levels, suggesting that RNA-RNA basepairing with the H4 terminal loop and the identified 5’ UTR sequence does not occur (Fig. 3.8B).

To determine if there is sequence specificity of the TCV 5’ UTR (63 b) *in vivo*, the region was precisely replaced with the 5’ UTRs of the closely-related carmoviruses, JINRV (J5UTR) and CCFV (C5UTR). The 5’ UTR of JINRV is 31 b long and contains no stretches of nucleotides shared by its counterpart in TCV (Fig. 3.9A). Accumulation of J5UTR in protoplasts revealed levels that were equivalent to wt TCV, suggesting that differences in length and nucleotide composition between the TCV and JINRV 5’ UTRs were not detrimental *in vivo* (Fig. 3.9B). Interestingly, the J5UTR construct did have increased levels of subgenomic RNA synthesis in comparison to wt TCV. The ratio between genomic and subgenomic RNAs for wt TCV was 10.1:1, whereas J5UTR had a ratio of 3.4:1, suggesting that the TCV 5’ UTR regulates subgenomic RNA synthesis by an unknown mechanism (Fig. 3.9B). The CCFV 5’ UTR is 36 b long and contains a stretch of polypyrimidines in close proximity to the AUG initiation codon, which is also found in TCV (Fig. 3.9A). C5UTR was found to accumulate to 19% of wt TCV levels, showing that no correlation exists between nucleotide conservation and ability to accumulate in protoplasts (Fig. 3.9B). These results are not consistent with an RNA-RNA basepairing between the 5’ UTR and 3’ UTR of TCV using this assay.

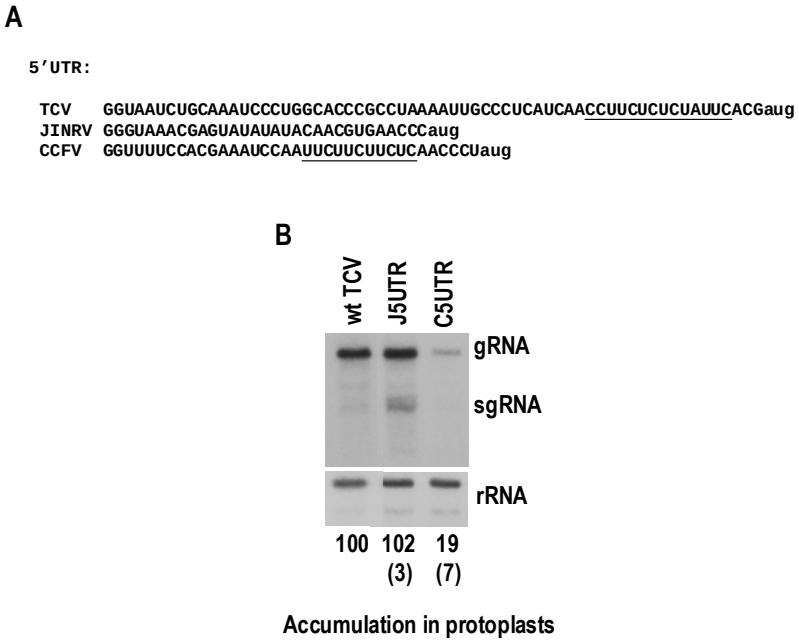

Figure 3.9. Replacement of the TCV 5' UTR with Analogous Sequences from JINRV and CCFV 5' UTRs. (A) Nucleotide composition of the TCV, JINRV, and CCFV 5' UTR regions. Lowercase letters indicate the AUG initiation codon for translation. Underlined bases are the polypyrimidine-rich sequences in TCV and CCFV 5' UTRs. (B) Viral accumulation levels in protoplasts at 40 hpi. Construct names are given above blot and numbers below indicate average accumulation levels of gRNAs and standard deviations (in parentheses) for three trials. gRNA=genomic TCV RNA; sgRNA=subgenomic TCV RNAs; rRNA=ribosomal RNA.

Discussion

In this chapter, a translational enhancer in the 3' region of a viral RNA has been determined to structurally mimic a tRNA. While aminoacylated tRNA-like structures at the 3' termini of some non-viral RNAs and capped viral RNAs have been well-characterized (Fechter *et al*., 2001; Saguy *et al*., 2005), 3' proximal internal tRNAs have not been previously reported. The TCV iTLS binds the P-site of 80S ribosomes in the absence of translation factors, similar to dicistrovirus IRESs (Wilson *et al*., 2000b). However, whereas dicistrovirus IRESs and the IRES associated with HCV are located 5' of the initiation site and bind directly to 40S ribosomal subunits in a factor-independent manner (Fraser and Doudna, 2007), cap-independent translation in TCV involves 3' proximal iTLS binding to 60S subunits.

Mutations in two regions of the TCV 5' UTR that were found to be important for translation *in vivo* reduced binding to 40S ribosomal subunits *in vitro*. These regions are complementary to two sequences in 18S rRNA that are topologically adjacent in the mRNA entrance tunnel of the small subunit (V.A. Stupina and A.E. Simon, unpublished results). These 18S rRNA sequences are in regions previously determined to either interact directly with IRES sequences (Hu *et al*., 1999) or were complementary to sequences having IRES activity (Akbergenov *et al*., 2004). While the HCV and dicistrovirus IRESes forego a requirement for scanning by positioning the ribosome P site at the initiating AUG (Fraser and Doudna, 2007), out-of-frame AUGs constructed in the 5' UTR of TCV suggested that ribosome entry at or near the 5' end of TCV requires

subsequent scanning to the initiation codon (V.A. Stupina and A.E. Simon, unpublished results).

Two possibilities are envisioned for how 60S subunit binding to the iTLS and 40S binding to the 5' UTR are involved in cap-independent translation in TCV (Fig. 3.10A): The small subunit binds to the 5’ UTR, is joined by the large subunit/iTLS complex (resulting in circularization of the RNA template), followed by scanning to the initiation codon (Fig. 3.10B); or the small subunit binds elsewhere, possibly near the iTLS, followed by local assembly of the ribosome. The ribosome then transfers to the 5’ end through 40S subunit interaction in a process known as "shunting" (Fig. 3.10C). Ribosomes can be directed to shunt to a location harboring sequences complementary to the 18S rRNA, indicating involvement of the small subunit in the process (Chappell *et al*., 2006a). Recent findings that additional sequences upstream of the iTLS are also important for translation and contain at least two additional sites that bind 40S subunits (A. Meskauskas, V. Stupina, J. C. McCormack, and A. E. Simon, unpublished results) currently favors the second model. Both models suggest that sequestering ribosomal subunits following termination allows for more rapid re-initiation of translation for efficient synthesis of viral products.

Recently, Li and Wong (2007) reported that nearly all TCV 3’ mutants tested accumulated at or near wt levels in Arabidopsis protoplasts (in contrast with Hibiscus protoplasts), including ones containing extensive deletions that removed nearly all of the 3' UTR or substantially altered the structure of the Pr. These results contradict current results, as well as two previous reports not cited by Li and Wong (Carpenter *et al*., 1995;

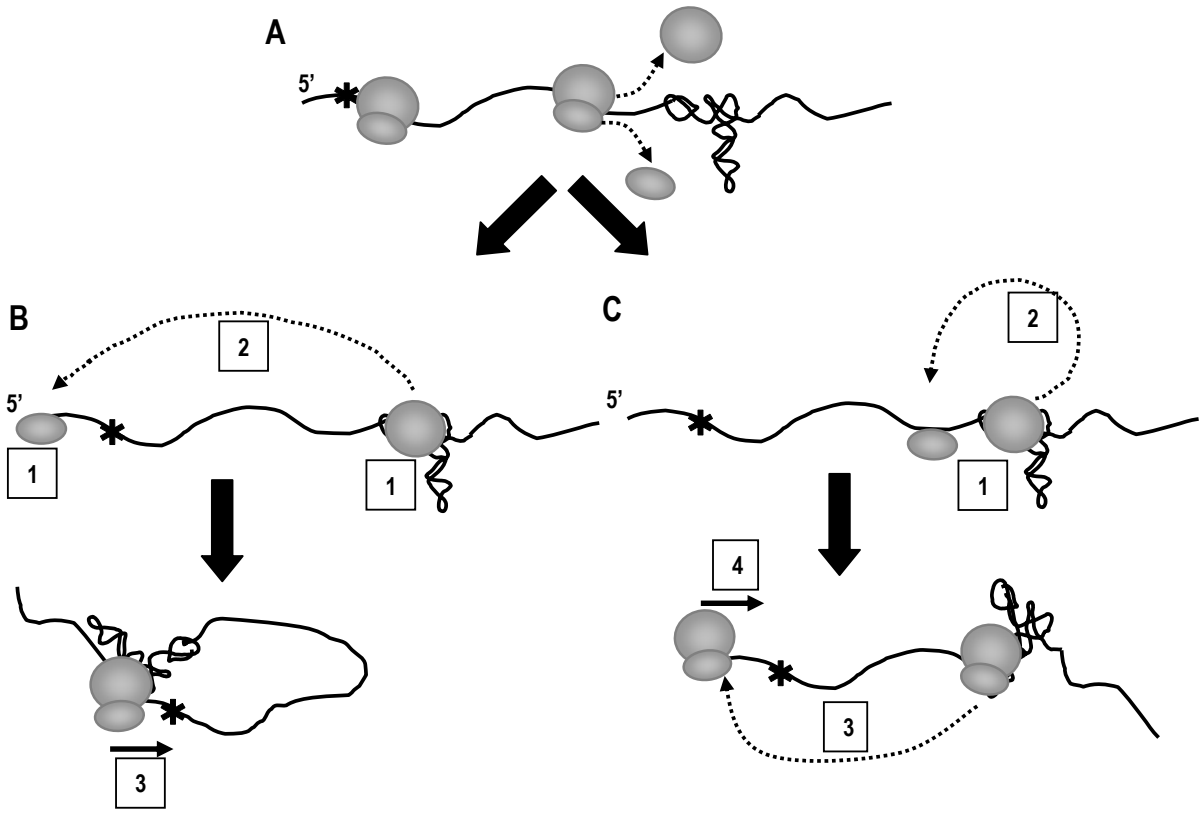

Figure 3.10. Model for Cap-Independent Translation of TCV. (A) Translating ribosomes arrest at termination codon followed by release of 60S and 40S subunits. (B) [1] 60S subunit binds iTLS and 40S subunit binds 5' UTR; [2] joining of subunits circularizes the RNA template; [3] the iTLS is released and ribosome scans to initiation codon. (C) Alternative model. [1] 60S subunit is reutilized by binding to iTLS and 40S subunit binds to an unidentified upstream element; [2] joining of subunits leads to assembly of 80S ribosome**;** [3] transfer of 80S ribosome to 5' end, possibly through sequences complementary to 18S rRNA; [4] ribosome scans to initiation codon.

Zhang *et al*., 2006c) and reports on related viruses (e.g., Panaviene *et al*., 2005). Therefore, no explanation can be given for the uniquely variant results reported by Li and Wong (2007).

CHAPTER IV

MEMBERS OF THE GENUS CARMOVIRUS UTILIZE DIFFERENT TRANSLATIONAL STRATEGIES FOR EXPRESSION OF THEIR SINGLE-STRANDED RNA GENOMES

Introduction

Cap-dependent translation of cellular mRNAs commences with binding of eIF4F to the 5' cap structure and association of the poly(A) binding protein with the 3' poly(A) tail. Protein-protein interactions between the termini have been proposed to circularize the template RNA (Wells *et al*., 1998), which allows for recruitment of the 43S ribosomal complex containing the small ribosomal subunit, aminoacylated initiator tRNA (Met-$tRNA_i$), eIF1A, eIF2, and eIF3. The ribosome subunit complex then scans from the 5' terminus using an ATP-dependent mechanism until an AUG in a favorable context is identified. eIF5B promotes release of eIF2 by GTP hydrolysis, displacement of the remaining translation initiation factors, and recruitment of the 60S ribosomal subunit to form an 80S ribosome that can initiate the elongation phase of translation once eIF5B dissociates (Merrick, 2004; Preiss and Hentze, 2003).

While many uncapped animal viral RNAs contain highly-structured internal ribosomal entry sequences (IRESes) in their 5' untranslated regions (UTRs) that can

recruit the cellular translational machinery (Fraser and Doudna, 2007), viruses that infect plants do not contain similar 5' structured elements. Instead, some contain sequences in their 3' UTRs that are able to enhance translation from the 5' terminus (Fabian and White, 2004; Karetnikov *et al*., 2006; Shen and Miller, 2004). Nearly all genera in the Families *Tombusviridae* and *Luteoviridae* harbor 3' UTR enhancers that are associated with sequences that have been shown to or are predicted to pair with bases at their 5' ends to circularize the RNA genomes. *Barley yellow dwarf luteovirus* (BYDV) and satellite Tobacco necrosis virus (sTNV) enhancers are able to bind eIF4F and eIF4E, respectively. However, how these 3' UTR enhancers recruit ribosomes to the template is unknown (Miller and White, 2006, Kneller *et al*., 2006; Dreher and Miller, 2006).

As described in earlier chapters, *Turnip crinkle virus* (TCV) is a member of the genus Carmovirus in the Family *Tombusviridae*. The uncapped 4054 nt viral genomic RNA terminates in a 3' hydroxyl group and contains 5 open reading frames (ORFs) that encode proteins involved in replication (p28 and p88), movement (p8 and p9), and encapsidation and RNA silencing suppression (p38; Fig. 1.3; Qu and Morris, 2000; Hacker *et al*., 1992; Qu *et al*., 2003). TCV, along with 12 of 13 carmoviruses, contains a 3' proximal hairpin that has been tentatively identified as the core promoter for minus-strand synthesis (Pr) based on analysis of the comparable hairpin in the TCV-associated satellite RNA, satC (Fig. 4.1A; Sun and Simon, 2006; Zhang *et al*., 2004a; Song and Simon, 1995) The hairpin upstream of the TCV Pr (H5) has been proposed to function as an RNA-dependent RNA-polymerase (RdRp) chaperone and as a regulator of minus-strand synthesis through tertiary interaction (Ψ_1) between its large symmetrical loop (LSL) and 3' terminal bases (Fig. 4.1A; Fig. 2.3B; Fig. 2.6). Next to H5 is hairpin 4b

(H4b), which forms Ψ_2 between its terminal loop and sequence adjacent to the base of H5 (Fig. 4.1A). Ψ_2 is also present in satC and is part of a structural switch regulating minus-strand synthesis (Zhang *et al*., 2006a). A hairpin juxtaposed (H4a) with H4b participates in an H-type pseudoknot (Ψ_3) with upstream flanking sequences (Fig. 4.1A). The region encompassing sequence from Ψ_3 to Ψ_2 forms a novel internal tRNA-like structure (iTLS) that binds 60S ribosomal subunits and enhances translation from the 5' end (Fig. 3.3B; Fig. 3.6E; V.A. Stupina and A.E. Simon, unpublished results). Two sequences in the 5'UTR, which exhibit IRES activity and 40S ribosomal subunit binding, may be directly involved in ribosome assembly or shunting from the 3'end (V.A. Stupina and A.E. Simon, unpublished results).

In this chapter, phylogenetic comparisons were performed using *mfold*-predicted 3'UTR structures to identify possible iTLSes in other carmoviruses (Zuker, 2003). Out of the 13 additional confirmed or tentative members, only *Cardamine chlorotic fleck virus* (CCFV; Fig. 4.1B) and *Japanese iris necrotic ring virus* (JINRV; Fig. 4.1C) have the capacity to form the 5 elements (H4a, H4b, H5, Ψ_2, and Ψ_3) important for iTLS formation. The CCFV, but not JINRV, iTLS region was able to bind 80S ribosomes *in vitro* and functionally replace the TCV iTLS *in vivo*. The size and symmetry of the H5 small symmetrical loop (SSL) was found to be an important feature in TCV iTLS *in vivo*, and predicted to be a major difference between the CCFV and JINRV iTLS regions. However, analysis of the CCFV and JINRV H5 elements in full-length TCV RNA *in vivo*, did not account for the marked differences in ribosome binding between the carmoviral iTLSes. Instead, the stem size and presence of non-Watson-Crick basepairs in the H4b stem may be critical factors for iTLS activity. These results indicate that

Figure 4.1. 3' Ends of TCV, CCFV, and JINRV. (A) Predicted structure of a partial region of TCV 3'UTR using phylogenetic comparisons, *mfold* structural prediction analysis, and in vivo and in vitro compensatory mutational analysis. Primary (Tail, Link1, Link2, and UPΨ_3) and secondary (Pr, H5, H4b, H4a, and H4) structural *cis*-acting elements are indicated by white boxes and tertiary interactions (Ψ_1, Ψ_2, Ψ_3, and Ψ_4) are boxed in grey. Bases comprising iTLS and iTLS + H4 fragments shown in Fig. 4.4 are indicated by black arrows and lines below the structure. (B) Structure of CCFV, Blue lake stain, 3' end. Predictions were made using phylogenetic comparisons and *mfold* structural prediction analysis. *Cis*-acting elements were designated according to analogous sequences and structures in TCV. (C) Structure of the JINRV 3' end. "+2G" above the black arrow represents the addition of two non-templated guanylates to the 5' end of the JiTLS RNA fragment, which was required for in vitro transcription.

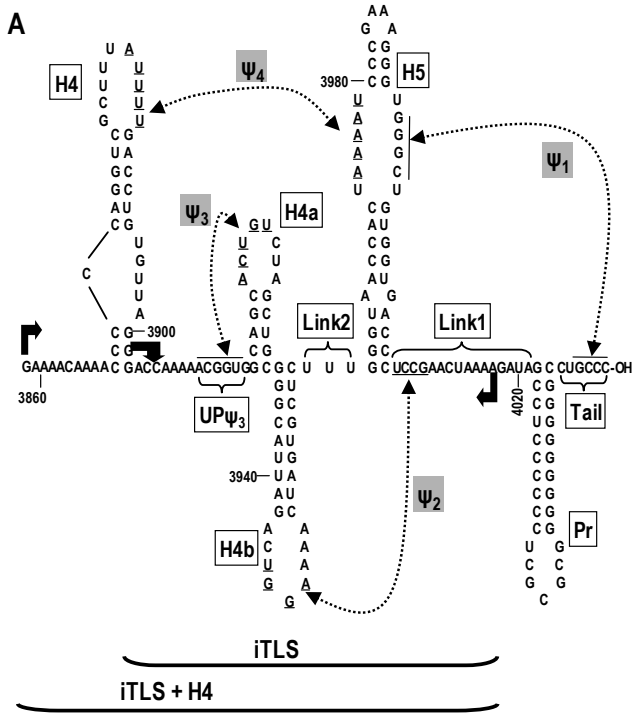
A
H4
H5
H4a
H4b
Link2
Link1
Tail
Pr
Ψ4
Ψ3
Ψ1
Ψ2
UPΨ3
3900
3940
3980
4020
3860
iTLS
iTLS + H4

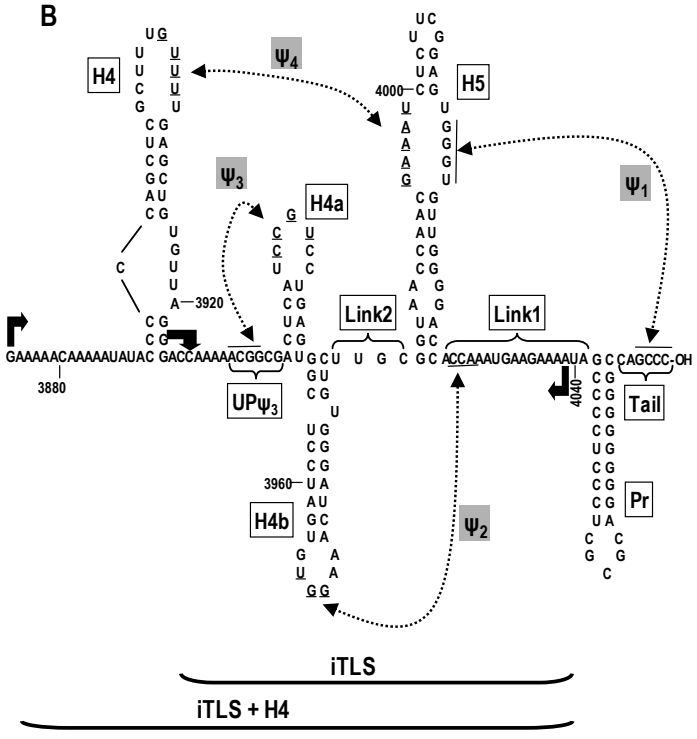
B
H4
H5
H4a
H4b
Link2
Link1
Tail
Pr
Ψ4
Ψ3
Ψ1
Ψ2
UPΨ3
3920
3960
4000
4040
3880
iTLS
iTLS + H4

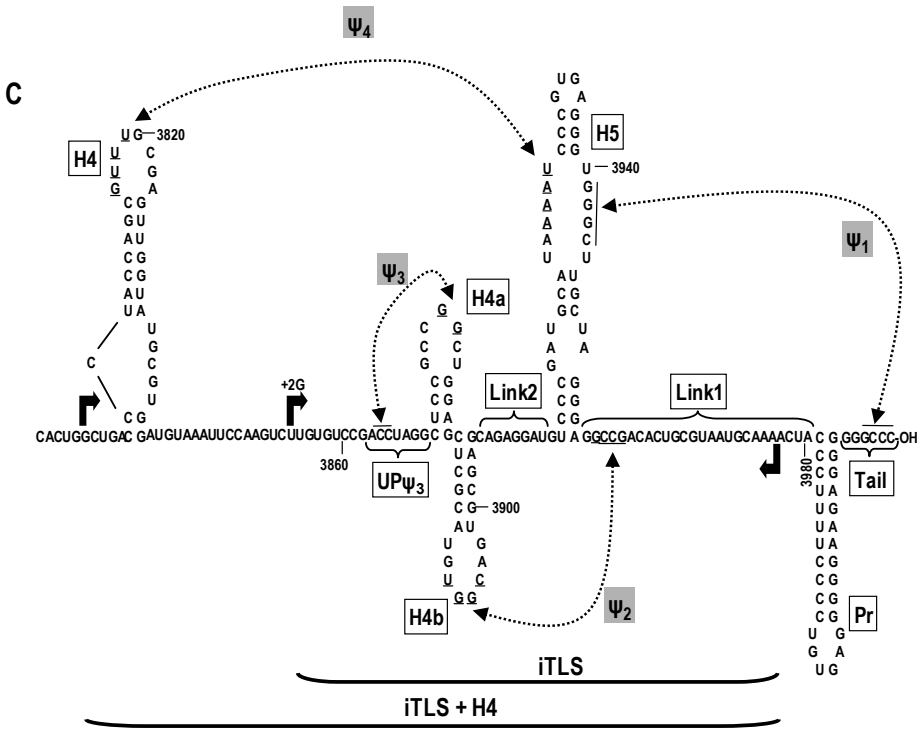
C
Ψ4
H4
H5
Ψ1
Ψ3
H4a
Link2
Link1
+2G
3860
UPΨ3
Tail
H4b
Ψ2
Pr
iTLS
iTLS + H4

closely-related viruses assigned to the same genus can use different strategies for protein expression of their genomes.

Materials and Methods

Construction of TCV Mutants

JH5 (Table 4.1) was made by annealing 20 ng of oligonucleotides JINVSL5(+) and JINVSL5(-) in 20 μl of water (Table 4.2). Oligonucleotides were denatured at 100˚C for 2 minutes, subjected to pulse centrifugation, placed in near boiling water, and allowed to cool to room temperature. Hybridized oligonucleotides were then digested with SpeI and SnaBI and ligated into similarly digested pTSNL5 (Table 4.1). CH5 (Table 4.1) was constructed exactly as JH5, except oligonucleotides CCFVSL5(+) and CCFVSL5(-) were used (Table 4.2). JPr, JH5Pr, CPr, and CH5Pr (Table 4.1) were made by annealing either oligonucleotides JINVPr(+) and JINVPr(-) or oligonucleotides CCFVPr(+) and CCFVPr(-) using an identical procedure used for the H5 constructs (Table 4.2). However, hybridized oligonucleotides were treated with T4 PNK, digested with SnaBI, and either inserted into pTSNL5 digested with SnaBI and SmaI for JPr and CPr or ligated into JH5 or CH5 digested with SnaBI and SmaI for JH5Pr and CH5Pr (Table 4.1).

CH4a and JH4a (Table 4.1) were constructed by PCR using template pTSNL5, oligonucleotide 3331, and either oligonucleotides CCFVH4A or JINVH4A, respectively (Table 4.2). Products were digested with MscI and SpeI and ligated into pTSNL5 digested with the same enzymes (Table 4.1). To create constructs CH4aH5 and JH4aH5, the above digested H4a PCR products were ligated, respectively, into constructs CH5 and

JH5 digested with MscI and SpeI (Table 4.1). CH4bLink2 and CH4bLink2H5 were generated by PCR using oligonucleotide 3164, and either template pTSNL5 and mutant oligonucleotide CCFVH4B or template CH5 and CCFVH4BH5, respectively (Table 4.1; Table 4.2). Inserts were digested with BsmI and SnaBI and ligated into similarly digested pTSNL5 (Table 4.1). JH4bLink2 and JH4bLink2H5 were constructed identically to CH4bLink2 and CH4bLink2H5, except that template pTSNL5 and oligonucleotide JINVH4B were used for JH4bLink2 and template JH5 and oligonucleotide JINVH4BH5 were used for JH4bLink2H5 (Table 4.1; Table 4.2). CH4aH4bLink2H5 was created by PCR using template CH4aH5, oligonucleotide 3164, and oligonucleotide CCFVH4AH4BH5 (Table 4.1; Table 4.2). Product was digested with BsmI and SnaBI and ligated into pTSNL5 digested with the same enzymes (Table 4.1). JH4aH4bLink2H5 was made identically to CH4aH4bLink2H5, except template JH4aH5 and oligonucleotide JINVH4AH4BH5 were used (Table 4.1; Table 4.2). JH4b, JH4aH4b, JH4aH4bUPΨ_3, CH4b, CH4aH4b, CH4aH4bUPΨ_3, were generated by PCR using template pTSNL5, oligonucleotide 3164, and a mutant oligonucleotide (JINVH4BONLY, JINVH4AH4B, JINVH4AH4BDR, CCFVH4BONLY, CCFVH4AH4B, CCFVH4AH4BDR), respectively (Table 4.1; Table 4.2). PCR products were digested with BsmI and SnaBI and ligated into similarly digested pTSNL5 (Table 4.1).

JLinker and Clinker were made by PCR using pTSNL5 template, oligonucleotide 3164, and either JINV Linker or CCFV Linker oligonucleotide, respectively (Table 4.1; Table 4.2). Inserts were treated with T4 PNK and Klenow, digested with BsmI, and ligated into pTCV66 cleaved with BsmI and SmaI (Table 4.1). JH5Linker1 and

CH5Linker1 were made by PCR using either JH5 or CH5, oligonucleotide 3164, and either oligonucleotide JINVH5Linker or CCFVH5Linker, respectively (Table 4.1; Table 4.2). Products were treated with T4 PNK and Klenow, digested with BsmI, and inserted into pTCV66 digested with BsmI and SmaI (Table 4.1). CLinker1Pr and JLinker1Pr were generated by PCR using either JPr or CPr template, oligonucleotide 3164, and either JINVLinker Pr or CCFVLinkerPr oligonucleotide, respectively (Table 4.1; Table 4.2). Products were kinased with T4 PNK, blunt-ended with Klenow, digested with BsmI, and introduced into BsmI and SmaI-digested pTCV66 (Table 4.1). JH5Link1PrTail and CH5Link1PrTail were constructed by PCR using pTCV66 template, oligonucleotide 3164, and either oligonucleotide JINVH5LinkerPrTail or CCFVH5LinkerPrTail, respectively (Table 4.1; Table 4.2). Products were digested with SpeI and SmaI and ligated into similarly digested pTSNL5 (Table 4.1). JiTLS and CiTLS were constructed by PCR using either JH4aH4bDR or CH4aH4bDR template, oligonucleotide 3164, and either JINRViTLSTCV or CCFViTLSTCV oligonucleotide, respectively (Table 4.1; Table 4.2). Inserts were digested with BsmI and SnaBI and ligated into pTSNL5 digested with the same enzymes (Table 4.1).

Constructs CU, GU, CΔ, and GΔ were made by PCR using pTSNL5 template, oligonucleotide 3661, and oligonucleotide TCVH5SIL (Table 4.1; Table 4.2). Products were digested with SpeI and SnaBI and ligated into similarly digested pTSNL5 (Table 4.1). CΔ-A4002G and GΔ-C4003A were constructed by PCR using template pTSNL5, oligonucleotide 3661, and either oligonucleotide CΔA2 or GΔB1, respectively (Table 4.1; Table 4.2). Products were digested with SpeI and SnaBI and ligated into pTSNL5 digested with the same enzymes (Table 4.1). UNCG, LSLterm, LSLΔ, and H5Δ, were

made by PCR using pTCV66 template, oligonucleotide 3164, and either oligonucleotide TCVH5UNCG, TCVLSLterm, TCVLSLdel, or TCVH5del, respectively (Table 4.1; Table 4.2). PCR inserts were treated with Klenow, digested with BsmI, and ligated into pTCV66 cleaved with BsmI and SmaI (Table 4.1).

U110C and JH5/U110C were made by PCR using JH5 template, oligonucleotide SspIpUC19, and oligonucleotide T110C (Table 4.1; Table 4.2). Products were digested with SspI and Bsu36I and ligated into either pTCV66 or JH5 digested with the same enzymes, respectively (Table 4.1). A3420G and JH5/A3420G were constructed by PCR using pTCV66 template, A3420G oligonucleotide, and KK57 oligonucleotide (Table 4.1; Table 4.2). PCR products were digested with MscI and SpeI and ligated either into similarly digested pTCV66 or JH5, respectively (Table 4.1; Table 4.2). To create A3420G/A3524G and JH5/A3420G/A3524G, a clone containing these alterations was digested using MscI and SpeI and the fragment ligated into either pTCV66 or JH5 digested with the same enzymes, respectively (Table 4.1). A3524G and JH5/A3524G were constructed using template A3420G/A3524G, oligonucleotide G3420A, and oligonucleotide KK57 (Table 4.1; Table 4.2). Products were digested with MscI and SpeI and ligated into either pTCV66 or JH5, respectively (Table 4.1). U3927C and CH5/U3927C were created by PCR using pTCV66 template, oligonucleotide 3331, and oligonucleotide T3927C (Table 4.1; Table 4.2). Products were digested with MscI and SpeI and ligated either into similarly digested pTCV66 or CH5, respectively (Table 4.1).

Construction of TCV iTLS RNA Fragments

TSNL5-iTLS, CH4a, CH4b, CH4aH4b, and CH4aH4bUPΨ_3 (Table 4.3) fragments were made by PCR using either template pTSNL5 for wt or the respectively named template, oligonucleotide T7-H4M1H, which contains a T7 RNA promoter, and oligonucleotide pTSNL5-Linker (Table 4.1; Table 4.2). UNCG, LSLterm, and LSLΔ (Table 4.3), were made by PCR using template pTCV66 for wt or the respectively named template, oligonucleotide T7-H4M1H, and oligonucleotide TCV-Linker (Table 4.1; Table 4.2). H5Δ (Table 4.3) was made identically to the other H5 deletion fragments, except H5ΔTCV-Linker oligonucleotide was used in place of TCV-Linker (Table 4.2). JiTLS, CiTLS, JiTLS+H4, and CiTLS+H4 (Table 4.3) fragments were constructed by 2 rounds of PCR. The first round used 250 pmol of either T7-JINRViTLS(+) and JINRViTLS(-) for JiTLS, T7-CCFViTLS(+) and CCFViTLS(-) for CiTLS, T7-JINRVH4iTLS(+) and JINRVH4iTLS(-) for JiTLS+H4, or T7-CCFVH4iTLS(+) and CCFVH4iTLS(-) for CiTLS+H4, in a 50 μl reaction volume (Table 4.2). Oligonucleotides were designed to allow for 20 bases of complementarity between the (+) and (-) primers and PCR was performed to fill in the overhangs. The first round PCR was diluted by 10-fold and 0.5 μl employed as a template for the second round. The second round used oligonucleotide T7 and either oligonucleotide JINRV-Linker for JiTLS and JiTLS+H4 or CCFV-Linker for CiTLS and CiTLS+H4 (Table 4.2; Table 4.3). All PCR products were in vitro transcribed using T7 RNA polymerase followed by treatment with RQ1 RNase-free DNase (Promega) to digest the template DNA.

Determining TCV Accumulation Levels in Protoplasts

TABLE 4.1. Summary of Full-Length TCV Mutants Used in Chapter IV

Name	Description
pTCV66	Wt TCV
pTSNL5	Wt TCV with a SnaBI site created by insertion of a cytidylate, guanylate, and uridylate, downstream of position 4014
CH5	pTSNL5 with H5 of CCFV
CH4a	pTSNL5 with H4a of CCFV
CH4b	pTSNL5 with H4b of CCFV
CH4aH4b	pTSNL5 with H4a and H4b of CCFV
CH4aH4bUPΨ$_3$	pTSNL5 with H4a/H4b/UP ψ$_3$ of CCFV
CH4bLink2	pTSNL5 with H4b and downstream linker of CCFV
CH4bLink2H5	pTSNL5 with H4b/downstream linker/H5 of CCFV
CH4aH4b Link2H5	pTSNL5 with H4a/H4b/downstream linker/H5 of CCFV
CH4aH5	pTSNL5 with H4a and H5 of CCFV
CLink1	pTSNL5 with linker between H5 and Pr of CCFV
CPr	pTSNL5 with Pr of CCFV
CH5Link1	pTSNL5 with H5 and downstream linker of CCFV
CLink1Pr	pTSNL5 with Pr and upstream linker of CCFV
CH5Pr	pTSNL5 with H5 and Pr of CCFV
CH5Link1PrTail	pTSNL5 with sequence from H5 to 3' terminus of CCFV
CiTLS	pTSNL5 with complete predicted iTLS of CCFV
JH5	pTSNL5 with H5 of JINRV
JH4a	pTSNL5 with H4a of JINRV
JH4b	pTSNL5 with H4b of JINRV
JH4aH4b	pTSNL5 with H4a and H4b of JINRV
JH4aH4bUPΨ$_3$	pTSNL5 with H4a/H4b/UPψ$_3$ of JINRV
JH4bLink2	pTSNL5 with H4b and downstream linker of JINRV

Name	Description
JH4bLink2H5	pTSNL5 with H4b/downstream linker/H5 of JINRV
JH4aH4b Link2H5	pTSNL5 with H4a/H4b/downstream linker/H5 of JINRV
JH4aH5	pTSNL5 with H4a and H5 of JINRV
JLink1	pTSNL5 with linker between H5 and Pr of JINRV
JPr	pTSNL5 with Pr of JINRV
JH5Link1	pTSNL5 with H5 and downstream linker of JINRV
JLink1Pr	pTSNL5 with Pr and upstream linker of JINRV
JH5Pr	pTSNL5 with H5 and Pr of JINRV
JH5Link1PrTail	pTSNL5 with sequence from H5 to 3' terminus of JINRV
JiTLS	pTSNL5 with complete predicted iTLS of JINRV
CU	pTSNL5 with an adenylate to cytidylate mutation at position 3968 and guanylate to uridylate mutation at position 4001
GU	pTSNL5 with an adenylate to guanylate mutation at position 3968 and guanylate to uridylate mutation at position 4001
CΔ	pTSNL5 with an adenylate to cytidylate mutation at position 3968 and a deletion of a guanylate at position 4001
GΔ	pTSNL5 with an adenylate to guanylate mutation at position 3968 and a deletion of a guanylate at position 4001
CΔ-A4002G	pTSNL5 with an adenylate to cytidylate mutation at position 3968, a deletion of a guanylate at position 4001, and an adenylate to guanylate mutation at position 4002
GΔ-C4003A	pTSNL5 with an adenylate to guanylate mutation at position 3968, a deletion of a guanylate at position 4001, and a cytidylate to adenylate mutation at position 4003
UNCG	pTCV66 with replacement of the H5 GAAA tetraloop with a UUCG tetraloop
LSLterm	pTCV66 with deletion of the H5 upper stem and tetraloop and fusion of the 5' and 3' sides of the LSL to form a large terminal LSL
LSLΔ	pTCV66 containing only the H5 lower stem capped by a GAAA tetraloop
H5Δ	pTCV66 with deletion of the entire H5 and fusion of the upstream and downstream flanking sequences

Name	Description
U110C	pTCV66 with a uridylate to cytidylate mutation at position 110
JH5/U110C	pTSNL5 with a uridylate to cytidylate mutation at position 110 and H5 of JINRV
A3420G	pTCV66 with an adenylate to guanylate mutation at position 3420
JH5/A3420G	pTSNL5 with an adenylate to guanylate mutation at position 3420 and H5 of JINRV
A3524G	pTCV66 with an adenylate to guanylate mutation at position 3524
JH5/A3524G	pTSNL5 with an adenylate to guanylate mutation at position 3524 and H5 of JINRV
A3420G/A3524G	pTCV66 with an adenylate to guanylate mutation at position 3420 and 3524
JH5/A3420G/ A3524G	pTSNL5 with an adenylate to guanylate mutation at position 3420 and 3524 and H5 of JINRV
U3927C	pTCV66 with a uridylate to cytidylate mutation at position 3927
CH5/U3927C	pTSNL5 with a uridylate to cytidylate mutation at position 3927 and H5 of CCFV

TABLE 4.2. Summary of Oligonucleotides Used in Chapter IV

Application	Name	Position	Sequence[b]	Polarity[c]
TCV mutagenesis	CCFVSL5 (+)	3949-4019[a]	5'-AAACTAGTGCTCTTTGGTAACCAACGAAATCTC TTCGGAGTGGGTGTTGGGGACCTCCGAACTAcgtA AAGA	+
	CCFVSL5 (-)	3949-4019[a]	5'-TCTTTacgTAGTTCGGAGGTCCCCAACACCCACTC CGAAGAGATTTCGTTGGTTACCAAAGAGCACTAG TTT	-
	JINVSL5 (+)	3949-4019[a]	5'-AAACTAGTGCTCTTTTCCCGATGCATAAAATCC CGTGAGGGTGGGCTTGCTAGGGATCCGAACTAcg tAAAGA	+
	JINVSL5 (-)	3949-4019[a]	5'-TCTTTacgTAGTTCGGATCCCTAGCAAGCCCACC CTCACGGGATTTTATGCATCGGGAAAAGAGCAC TAGTTT	-
	CCFVPr(+)	4015-4054[a]	5'-gtAAAGATAGCCCCTCCCTCGCGCAGGGGGGGG CCTGCCC	+
	CCFVPr(-)	4015-4054[a]	5'-GGGCAGGCCCCCCCCTGCGCGAGGGAGGGGC TATCTTTac	-
	JINVPr(+)	4015-4054[a]	5'-gtAAAGATACCCTTTTCCCCTGTGAGGGGGAA GAGGGCTGCCC	+
	JINVPr(-)	4015-4054[a]	5'-GGGCAGCCCTCTTCCCCCTCACAGGGGAAAAG GGTATCTTTac	-
	3331	3331-3348[a]	5'-TGTGGCGGATGGTATCAG	+
	CCFVH4A	3895-3960[a]	5'-GAGCACTAGTTTTCCAGTCTAATGCCCACTCAG GACGGATGAGTCACCGTTTTTGGTCCCTAACA	-
	JINVH4A	3895-3960[a]	5'-GAGCACTAGTTTTCCAGTCTAATGCCCCTCCAG CCGGCGGAGCACCGTTTTTGGTCCCTAACA	-
	3164	3164-3181[a]	5'-ATGAGCCCTTCAACCACC	+
	CCFVH4B	3916-4019[a]	5'-TCTTTacgTAGTTCGGAGGGTCACCACAGCCCA CCCTTTCGGGATTTTAGTGGTTACCCGCAAGAC ACCCTAGTTTCCACACTAGGAGCCGCAGCTAGA CAGTGCTGC	-

Application	Name	Position	Sequence[b]	Polarity[c]
	JINVH4B	3916-4019[a]	5'-TCTTTacgTAGTTCGGAGGGTCACCACAGCCCA CCCTTTCGGGATTTTAGTGGTTACCCCATCCTC TGCTCGCACTGCCACATGCGAGGCAGCTAGAC AGTGCTGC	-
	CCFVH4B H5	3916-4019[a]	5'-TCTTTacgTAGTTCGGAGGTCCCCAACACCCAC TCCGAAGAGATTTCGTTGGTTACCGCAAGACACC CTAGTTTCCACACTAGGAGCCGCAGCTAGACAG TGCTGC	-
	JINVH4B H5	3916-4019[a]	5'-TCTTTacgTAGTTCGGATCCCTAGCAAGCCCAC CCTCACGGGATTTTATGCATCGGGACATCCTCT GCTCGCACTGCCACATGCGAGGCAGCTAGACA GTGCTGC	-
	CCFVH4A H4BH5	3916-4019[ad]	5'-TCTTTacgTAGTTCGGAGGTCCCCAACACCCAC TCCGAAGAGATTTCGTTGGTTACCGCAAGACAC CCTAGTTTCCACACTAGGAGCCACTCAGGACGG ATGAGT	-
	JINVH4A H4BH5	3916-4019[ad]	5'-TCTTTacgTAGTTCGGATCCCTAGCAAGCCCAC CCTCACGGGATTTTATGCATCGGGACATCCTCT GCTCGCACTGCCACATGCGAGCTCCAGCCGGC GGAG	-
	CCFVH4B ONLY	3916-4019[a]	5'-TCTTTacgTAGTTCGGAGGGTCACCACAGCCCA CCCTTTCGGGATTTTAGTGGTTACCCAAAGACA CCCTAGTTTCCACACTAGGAGCCGCAGCTAGAC AGTGCTGC	-
	JINVH4B ONLY	3916-4019[a]	5'-TCTTTacgTAGTTCGGAGGGTCACCACAGCCCA CCCTTTCGGGATTTTAGTGGTTACCCAAACTCG CACTGCCACATGCGAGGCAGCTAGACAGTGC TGC	-
	CCFVH4A H4B	3901-4019[a]	5'-TCTTTacgTAGTTCGGAGGGTCACCACAGCCCA CCCTTTCGGGATTTTAGTGGTTACCCAAAGACA CCCTAGTTTCCACACTAGGAGCCACTCAGGAC GGATGAGTCACCGTTTTTGGTCC	-
	JINVH4A H4B	3901-4019[a]	5'-TCTTTacgTAGTTCGGAGGGTCACCACAGCCCA CCCTTTCGGGATTTTAGTGGTTACCCAAACTCG CACTGCCACATGCGAGCTCCAGCCGGCGGAG CACCGTTTTTGGTCC	-
	CCFVH4A H4BDR	3901-4019[a]	5'-TCTTTacgTAGTTCGGAGGGTCACCACAGCCCA CCCTTTCGGGATTTTAGTGGTTACCCAAAGACA CCCTAGTTTCCACACTAGGAGCCACTCAGGAC GGATGAGTCGCCGTTTTTGGTCC	-

Application	Name	Position	Sequence[b]	Polarity[c]
	JINVH4AH4BDR	3901-4019[a]	5'-TCTTTacgTAGTTCGGAGGGTCACCACAGCCCACCCTTTCGGGATTTTAGTGGTTACCCAAACTCGCACTGCCACATGCGAGCTCCAGCCGGCGGAGCCTAGGTTTTGGTCC	-
	CCFV Linker	3986-4054[a]	5'-GGGCAGGCCCCCCCCCCGCGCGAGGGGGGAGGCTATTTTCTTCATTTGGTGGGTCACCACAGCCCACCCT	-
	JINV Linker	3986-4054[a]	5'-GGGCAGGCCCCCCCCCCGCGCGAGGGGGGAGGCTAGTTTTGCATTACGCAGTGTCGGCCGGGTCACCACAGCCCACCCT	-
	CCFVH5 Linker	3985-4054[ad]	5'-GGGCAGGCCCCCCCCCCGCGCGAGGGGGGAGGCTATTTTCTTCATTTGGTGGTCCCCAACACCCACTCCG	-
	JINVH5 Linker	3985-4054[ad]	5'-GGGCAGGCCCCCCCCCCGCGCGAGGGGGGAGGCTAGTTTTGCATTACGCAGTGTCGGCCTCCCTAGCAAGCCCACCCTC	-
	CCFV LinkerPr	3984-4054[a]	5'-GGGCAGGCCCCCCCCTGCGCGAGGGAGGGGCTATTTTCTTCATTTGGTGGGTCACCACAGCCCACCCTTT	-
	JINV LinkerPr	3986-4054[a]	5'-GGGCAGCCCTCTTCCCCCTCACAGGGGAAAAGGGTAGTTTTGCATTACGCAGTGTCGGCCGGGTCACCACAGCCCACCCT	-
	CCFVH5 LinkerPr Tail	3982-4054[ad]+ 15b vector	5'-**CTCTAGAGGATCCCC**GGGCTGGCCCCCCCCTGCGCGAGGGAGGGGCTATTTTCTTCATTTGGTGGTCCCCAACACCCACTCCGAAG	-
	JINVH5 LinkerPr Tail	3985-4054[ad] + 15b vector	5'-**CTCTAGAGGATCCCC**GGGCCCCCCTCTTCCCCCTCACAGGGGAAAAGGGTAGTTTTGCATTACGCAGTGTCGGCCTCCCTAGCAAGCCCACCCTC	-
	CCFViTLSTCV	3941-4022[ad]	5'-CTATCTTTacgTAGTTTGGTGGTCCCCAACACCCACTCCGAAGAGATTTCGTTGGTTACCGCAAGACACCCTAGTTTCCACACT	-
	JINRViTLSTCV	3934-4022[ad]	5'-CTATCTTTacgTAGTCGGCCTCCCTAGCAAGCCCACCCTCACGGGATTTTATGCATCGGGACATCCTCTGCTCGCACTGCCACATGCGAG	-
	TCVH5SIL	3964-4021[a]	5'-TATCTTTacgTAGTTCGGAGGGTN*ACCACAGCCCACCCTTTCGGGATTTTAGTGGTN**ACCC	-
	CΔA2	3961-4019[a]	5'-TCTTTacgTAGTTCGGAGGGCΔACCACAGCCCACCCTTTCGGGATTTTAGTGGTGACCCAAA	-

Application	Name	Position	Sequence[b]	Polarity[c]
	GΔB1	3961-4019[a]	5'-TCTTTacgTAGTTCGGAGGTTΔACCACAGCCC ACCCTTTCGGGATTTTAGTGGTCACCCAAA	-
	TCVH5 UNCG	3963-4054[a]	5'-GGGCAGGCCCCCCCCCCGCGCGAGGGGGG AGGCTATCTTTTAGTTCGGAGGGTCACCAC AGCCCACCCCGAAGGGATTTTAGTGGTTAC CCA	-
	TCVLSL term	3960-4054[a]	5'-GGGCAGGCCCCCCCCCCGCGCGAGGGGGG AGGCTATCTTTTAGTTCGGAGGGTCACCACA GCCCAΔATTTTAGTGGTTACCCAAAG	-
	TCVLSL del	3954-4054[a]	5'-GGGCAGGCCCCCCCCCCGCGCGAGGGGGG AGGCTATCTTTTAGTTCGGAGGGTCACCACΔT TTCΔGTGGTTACCCAAAGAGCACT	-
	TCVH5 del	3943-4054[a]	5'-GGGCAGGCCCCCCCCCCGCGCGAGGGGGG AGGCTATCTTTTAGTTCGGAΔAAAGAGCACTA GTTTTCCAGT	-
	SspIpUC19	n/a[f]	5'-**TTTCAATATTATTGAAGCAT**	n/a[f]
	T110C	91-137[a]	5'-TGAACCTCAGGGTAGTACCTGGCTCCTGGG AGTCCCACTGCGAGCGC	-
	A3420G	3380-3436[a]	5'-ATCATGGCCACCTACGGCCAAGGAGCCAAT GATGCCGCCCGACTCGGTGAAGTGCGA	+
	G3420A	3380-3451[a]	5'-ATCATGGCCACCTACGGCCAAGGAGCCAAT GATGCCGCCCAACTCGGTGAAGTGCGAGTC GAGTACACCGTG	+
	T3927C	3909-3961[a]	5'-AGAGCACTAGTTTTCCAGTCTAATGCCCGCA GCTGGACAGTGCTGCCACCGTT	-
Generation of iTLS fragments	T7-H4M1H	3901-3912[a]	5'-*TAATACGACTCACTATAG*GGACCAAAAACG	+
	pTSNL5-Linker	4005-4017[a]	5'-TTTacgTAGTTCGGAG	-
	T7-CCFV iTLS(+)	3922-3980[e]	5'-*TAATACGACTCACTATAG*GGACCAAAAACG GCGACTCATCCGTCCTGAGTGGCTCCTAGT GTGGAAACTAGGGTGTC	+
	CCFV iTLS(-)	3961-4039[e]	5'-TTTTCTTCATTTGGTGGTCCCCAACACCCAC TCCGAAGAGATTTCGTTGGTTACCGCAAGAC ACCCTAGTTTCCACACT	-

Application	Name	Position	Sequence[b]	Polarity[c]
	CCFV H4iTLS(+)	3874-3948[e]	5'-*TAATACGACTCACTATAG*GAAAAACAAAAAT ATACCCCCAGCTCGCTTTGTTTTGAGCTGTG TTAGGGACCAAAAACGGCGACTCATCCGTCC	+
	CCFV H4iTLS(-)	3929-4039[e]	5'-TTTTCTTCATTTGGTGGTCCCCAACACCCAC TCCGAAGAGATTTCGTTGGTTACCGCAAGA CACCCTAGTTTCCACACTAGGAGCCACTCAGG ACGGATGAGTCGCCGTTT	-
	T7	n/a[f]	5'-*TAATACGACTCACTATAG*	+
	CCFV-Linker	4022-4039[e]	5'-TTTTCTTCATTTGGTGGT	-
	T7-JINRV iTLS(+)	3854-3925[e]	5'-*TAATACGACTCACTATAG***gg**TTGTGTCCGAC CTAGGCTCCGCCGGCTGGAGCTCGCATGTG GCAGTGCGAGCAGAGGATGTCCCGATGCATA	+
	JINRV iTLS(-)	3906-3977[e]	5'-TTTTGCATTACGCAGTGTCGGCCTCCCTAGC AAGCCCACCCTCACGGGATTTTATGCATCGG GACATCCTCT	-
	JINRV H4iTLS(+)	3801-3893[e]	5'-*TAATACGACTCACTATAG*GCTGACCCTACC AGCGTTTGCGAGTTGGTATGCGTGGATGTA AATTCCAAGTCTTGTGTCCGACCTAGGCTCCG CCGGCTGGAGCTCGCATGT	+
	JINRV H4iTLS(-)	3873-3977[e]	5'-TTTTGCATTACGCAGTGTCGGCCTCCCTAGC AAGCCCACCCTCACGGGATTTTATGCATCGG GACATCCTCTGCTCGCACTGCCACATGCGAG CTCCAGCCGGCG	-
	JINRV-Linker	3959-3977[e]	5'-TTTTGCATTACGCAGTGT	-
	3661	3661-3677[a]	5'-TGACTTCTCGGTCCTGG	+
	KK57	4035-4054[a]	5'-GGGCAGGCCCCCCCCCCGCG	-
	TCV-Linker	3998-4017[a]	5'-TTTTAGTTCGGAGGGTCACC	-

Application	Name	Position	Sequence[b]	Polarity[c]
	H5ΔTCV-Linker	3956-4017[a]	5'-TTTTAGTTCGGAAAAGAGCA	-
Northern blotting	3181	3181-3199[a]	5'-CCAGAGCCACCTTGCCTCCG	-
	Oligo 13	3944-3963[a]	5'-AAAGAGCACTAGTTTTCCAG	-
	3892	3893-3913[a]	5'-CCGTTTTTGGTCCCTAACACA	-

[a] Positions correspond to the base number in genomic TCV of the pTCV66 vector

[b] Underlined letters indicate mutated bases in comparison to pTCV66 plasmid sequence. Lowercase letters represent bases present in pTSNL5 vector only. Uppercase bold letters illustrate sequence derived from the vector region of pTCV66. Bold italicized letters show T7 RNA promoter sequence. Lowercase bold letters indicate bases added for in vitro RNA transcription. N*= 40% C, 20% A, 20% G, and 20% T; N**=40% T, 20% A, 20% G, and 20% C; Δ=deletion of base(s)

[c] "+" and "-" indicate homology and complementarity, respectively, to TCV, CCFV (Blue lake), or JINRV plus strands

[d] Base positions at the 3' borders of the oligonucleotides were determined using analogous nucleotide positions to TCV for either CCFV (Blue lake) or JINRV sequence

[e] Base positions were determined from CCFV (Blue lake) or JINRV sequence

[f] n/a= not applicable

TABLE 4.3. Summary of iTLS RNA Fragments Used in Chapter IV

Name	Description
iTLS	TCV wt fragment (position 3901-4017)
UNCG	TCV fragment (position 3901-4017) with replacement of the H5 GAAA tetraloop with a UUCG tetraloop
LSLterm	TCV fragment (position 3901-4017) with deletion of the H5 upper stem and tetraloop and fusion of the 5' and 3' sides of the LSL to form a large terminal LSL
LSLΔ	TCV fragment (position 3901-4017) containing only the H5 lower stem capped by a GAAA tetraloop
H5Δ	TCV fragment (position 3901-4017) with deletion of the entire H5 and fusion of the upstream and downstream flanking sequences
TSNL5-iTLS	TCV wt fragment (position 3901-4017) with an insertion of a cytidylate, guanylate, and uridylate, downstream of position 4014
CH4a	TSNL5 (position 3901-4017) with H4a of CCFV
CH4b	TSNL5 (position 3901-4017) with H4b of CCFV
CH4aH4b	TSNL5 (position 3901-4017) with H4a and H4b of CCFV
CH4aH4bUPΨ$_3$	TSNL5 (position 3901-4017) with H4a/H4b/UPψ$_3$ of CCFV
JiTLS	iTLS of JINRV
JiTLS+H4	H4 and iTLS of JINRV
CiTLS	iTLS of CCFV
CiTLS+H4	H4 and iTLS of CCFV

Preparation and inoculation of protoplasts and Northern blotting of TCV RNA were previously described in Chapter II.

Results

Symmetry and Position of H5 Small Symmetrical Loop (SSL) Is Important for TCV Accumulation

Correct assembly of the replicase containing the RdRp (Fig. 2.6), regulation of minus-strand synthesis through Ψ_1 (Fig. 2.3B), and repression of 80S ribosome binding to the iTLS (Fig. 3.6C), are regulated by sequences in both sides of the large symmetrical loop (LSL) of H5. Also present in H5 in a position more proximal to the base of the hairpin is the small symmetrical loop (SSL), an element comprising an A-G loop of unknown function (Fig. 4.2A). To determine its importance, mutations were engineered in the SSL and viral accumulation levels compared to wt TSNL5 *in vivo*. Wt TSNL5 was transcribed from pTSNL5, a TCV construct containing a SnaBI site created by insertion of a cytidylate, guanylate, and uridylate, downstream of position 4014. Replacement of the A-G with either a C-U or G-U resulted in a small reduction (17% and 31%, respectively) in accumulation in comparison to wt TSNL5, suggesting that the SSL does not have a high level of sequence specificity (Fig. 4.2A,B). Creation of C-Δ and G-Δ by deletion of the SSL 3' side in the C-U and G-U mutants were predicted to contain H5 structures with a one-base bulge instead of a symmetrical loop (Fig. 4.2A). Viral accumulation levels for these mutants were below the level of detection, indicating that SSL symmetry was critical for viral accumulation *in vivo* (Fig. 4.2B).

SSL mutants were then inoculated onto turnip seedlings and the viral RNA progeny extracted at 20 days, cloned, and sequenced, to identify second-site mutations in the iTLS associated with SSL alterations. Sequencing of the H5 lower stem showed that the mutated SSL was maintained in progeny derived from the C-U and G-U constructs, whereas second-site mutations in the SSL were identified in C-Δ and G-Δ progeny. Four of 16 clones for C-Δ progeny contained an insertion of a uridylate in the H5 lower stem, which is predicted to re-establish the SSL containing a C-U mismatch and be compensatory for the original alteration (Fig. 4.2A, compare C-Δ and C-U in Fig 4.2B). Another C-Δ clone had an adenylate to guanylate substitution at position 4002 (C-Δ/A4002G) that was predicted to form a U-C mismatch shifted one nucleotide closer to the base of H5 (Fig. 4.2A). A G-A loop at the same position as the wt SSL may form with a cytidylate to adenylate second-site change found in 5 out of 16 clones derived from the G-Δ mutant (G-Δ/C4003A; Fig. 4.2A). To assess the compensatory effect of these changes on viral accumulation, TCV constructs containing the original alterations with respective second-site mutations were generated and tested in protoplasts. Both C-Δ/A4002G and G-Δ/C4003A accumulated to detectable levels, showing that they were partially alleviating the detrimental effects of the original changes made. G-Δ/C4003A exhibited a greater compensatory effect than C-Δ/A4002G, suggesting that positioning of the loop five nucleotides from the base of H5 is an important feature of the SSL (Fig. 4.2B).

Additional second-site changes that were predicted to re-create the SSL included an insertion of an adenylate at the deleted position of three G-Δ clones and a uridylate to

Figure 4.2. Importance of TCV H5 Small Symmetrical Loop (SSL). (A) Illustrations of wt and mutant H5 denoting the large symmetrical loop (LSL) and SSL in brackets. Boxed nucleotides show bases comprising the SSL with names of constructs (C-U, G-U, C-Δ, and G-Δ) given below each structure. The "Δ" symbol represents a base deletion. Black arrows for C-Δ and G-Δ mutants indicate second-site alterations found at 20 dpi in progeny RNA from turnip plants inoculated with these constructs. Adjacent parentheses show number of clones out of 16 sequenced from two plants containing the specified second-site mutation. Predicted H5 structures of CΔ and GΔ containing either an adenylate to guanylate (C-Δ/A4002G) or cytidylate to adenylate (G-Δ/C4003A) alteration, respectively, are shown next to the parental constructs. (B) Relative accumulation levels of SSL mutations in protoplasts at 40 hpi. Wt TSNL5 was transcribed from pTSNL5, a TCV construct with a SnaBI site created by insertion of a cytidylate, guanylate, and uridylate, downstream of position 4014. Standard deviations are represented by error bars. (C) Location of additional 3' UTR second-site alterations found in progeny viral RNA derived from SSL mutants inoculated on turnip plants. Black arrows illustrate types of substitutions and adjacent parentheses indicate parental constructs and number of clones out of 16 sequenced from two plants containing the second-site alterations.

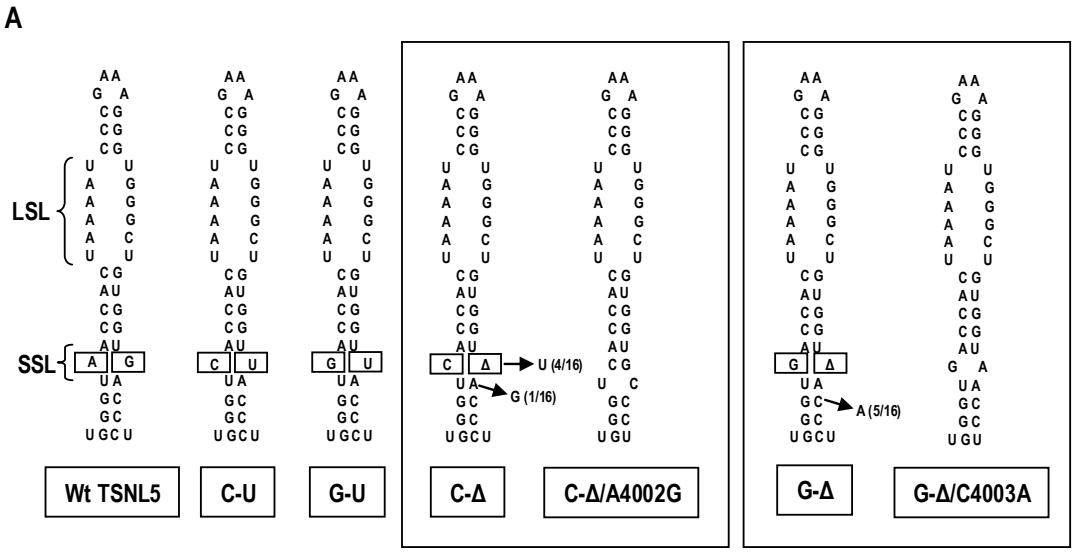
A
LSL
SSL
Wt TSNL5
C-U
G-U
C-Δ
C-Δ/A4002G
G-Δ
G-Δ/C4003A
U (4/16)
G (1/16)
A (5/16)

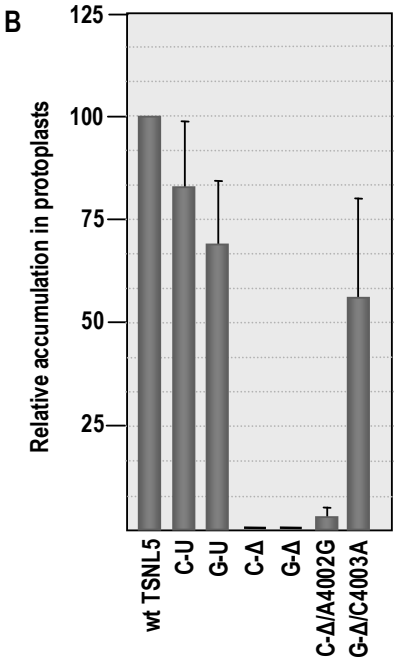
B
Relative accumulation in protoplasts
125
100
75
50
25
wt TSNL5
C-U
G-U
C-Δ
G-Δ
C-Δ/A4002G
G-Δ/C4003A

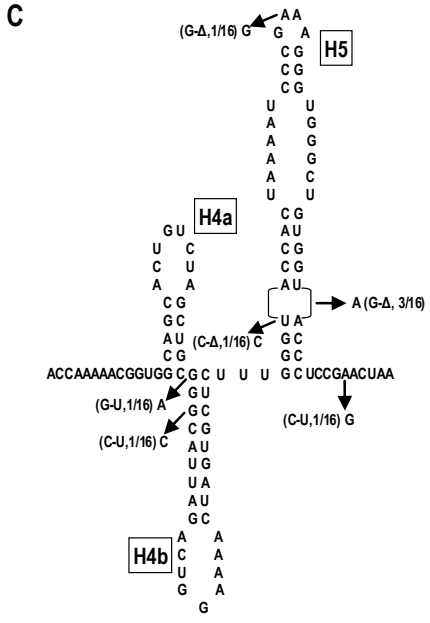
C
H5
H4a
H4b
(G-Δ,1/16) G
A (G-Δ, 3/16)
(C-Δ,1/16) C
ACCAAAAACGGUGGCGCUUUGCUCCGAACUAA
(G-U,1/16) A
(C-U,1/16) C
(C-U,1/16) G

cytidylate change in a clone derived from C-Δ, which was predicted to form a loop containing two cytidylates on its 5' side and an adenylate on its 3' side (Fig. 4.2C). Changes were also observed in regions outside of the H5 lower stem. A clone from G-Δ contained a change in the H5 terminal loop that maintained the GNRA tetraloop motif, whereas two changes in clones derived from G-U and C-U destabilized H4b by shortening or increasing flexibility in the stem (Fig. 4.2C). One change was found downstream of H5 in a partner sequence of Ψ_2 and appeared to strengthen the pseudoknot by increasing the number of potential basepairs from 4 to 5 (Fig. 4.2C).

H5 Is Not Essential for 80S Ribosome Binding In Vitro

Some stemloops containing GNRA tetraloop motifs form tertiary interactions with the minor groove of A-form RNA (Pley, 1994). To determine if the GAAA terminal loop of H5 participates in tertiary structure, these bases were replaced with a tetraloop of equivalent stability (UUCG) and tested in protoplasts and for 80S ribosome binding using an iTLS RNA fragment (Fig. 4.3A; Fig. 4.1A). Results showed that the UNCG construct accumulated to near wild-type levels *in vivo* and ribosome binding was reduced only by about 2-fold (K_d=0.84 μM) *in vitro*, suggesting that the tetraloop is not involved in any important tertiary RNA interactions (Fig. 4.3B,C).

H5 was next analyzed by generating a series of truncations. LSLterm was constructed by deletion of the upper stem and tetraloop and fusion of the 5' and 3' sides of the LSL to form a large terminal loop (Fig. 4.3A). Viral accumulation and ribosome binding were both reduced by 3-fold in comparison to wt (Fig. 4.3B,C), showing that the

upper stemloop was not a critical element. Eliminating the LSL and upper stem and capping the lower stem with a GNRA tetraloop resulted in undetectable levels of viral accumulation in protoplasts and binding by 80S ribosomes (LSLΔ; Fig. 4.3A,B,C). However, an iTLS fragment containing a deletion of the entire H5 (H5Δ) bound 80S ribosomes at a K_d of 0.98 μM (Fig. 4.3C), indicating that H5 is not critical for ribosome binding *in vitro* (Fig. 4.3A,C).

CCFV iTLS Functions Similarly To the TCV iTLS, in Contrast with the Putative iTLS of JINRV

Cis-acting elements involved in translation are known for only a few members of the genus Carmovirus. In *Melon necrotic spot virus* (MNSV), a 3' UTR 100 b region containing a predicted hairpin is implicated in eIF4E binding, suggesting that this region may be involved in recruitment of translational proteins in a manner similar to the translational enhancers of satellite Tobacco necrosis virus (STNV) and Barley yellow dwarf luteovirus (BYDV) (Nieto *et al*., 2006; Gazo *et al*., 2004; Kneller *et al*., 2006). Translation of the CP ORF of *Hibiscus chlorotic ringspot virus* (HCRSV) is driven by an upstream 100 b IRES, which cooperates with a region containing a 6 b sequence (5'-GGGCAG) in the 3' UTR *in vitro* (Koh *et al*., 2003; Koh *et al*., 2002). While the 3' UTRs of TCV, MNSV, and HCRSV, are important for translation, the *cis*-acting elements involved are quite different, suggesting that carmoviruses use disparate strategies for protein expression.

CCFV is the most closely related carmovirus to TCV, with 69% sequence similarity across the genome (Robertson *et al*., 2007). Using a combination of *mfold* and

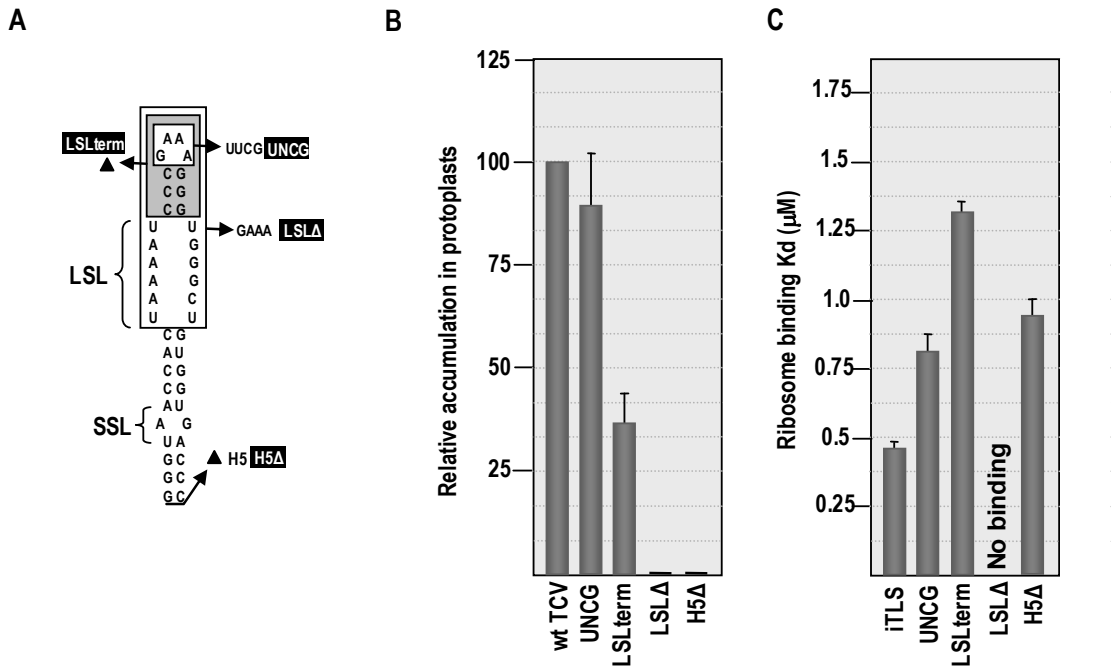

Figure 4.3. Deletional Analysis of H5. (A) Depiction of H5 deletion mutants. The UNCG mutant contains a replacement of the GAAA tetraloop with UUCG. LSLterm contains a deletion of the tetraloop and upper stem and fusion of the 5' and 3' sides of the LSL to form a large terminal loop. LSLΔ contains a deletion of the LSL and upper stem with capping of the lower stem with a GAAA tetraloop. H5Δ contains deletion of the entire H5 with fusion of the upstream and downstream flanking sequences. (B) Relative accumulations in comparison to wt TCV of deletion constructs in protoplasts at 40 hpi. Standard deviations are represented by error bars. (C) In vitro ribosome binding of iTLS RNA fragments containing H5 deletions using 80S yeast ribosomes. Standard errors are given by error bars.

Ribosome binding performed by Arturas Meskauskas

phylogenetic comparisons of carmoviral 3' UTRs, a possible conformation for the CCFV 3' region (Blue lake) is proposed (Fig. 4.1B; Zuker, 2003). As with other carmoviruses, the CCFV 3' end contains a stable Pr hairpin and upstream H5 with sequence in the LSL that can basepair with the terminal 3' bases (Ψ_1, Fig. 2.3B). The existence of H4b is strongly suggested as multiple differences in a second CCFV isolate (Clear lake) maintain the stem structure. CCFV H4b contains a 5 nt identity in the terminal loop with TCV H4b (5'-UGGAA), whereas the CCFV H4b stem is proposed to contain a unique bulge loop. The putative CCFV Ψ_2 differs from the known TCV Ψ_2 by having just 3 Watson-Crick basepairs beginning one nucleotide downstream of H5. Base pairing between the loop of H4a and upstream sequences (Ψ_3) also appears less stable than the comparable pseudoknot in TCV, with 4 Watson-Crick pairs (Fig. 4.1B).

JINRV is more distantly related to TCV with a whole genome sequence identity of 54% (Robertson *et al.*, 2007). H4a and UP Ψ_3 have a predicted 2 b complementarity five bases upstream of H4a, which may be too unstable for Ψ_3 formation. While Ψ_2 is of comparable stability to its TCV analog, the JINRV H4b stem is 3 bp shorter and lacks two non-Watson-Crick basepairs. In comparison to TCV, the Link2 spacer is 6 b longer, which increases the distance between H4b and H5, and the lower stem of H5 is weaker due to the presence of a 3 b asymmetrical loop (Fig. 4.1C).

To determine if the CCFV and JINRV iTLSes function like their TCV counterpart, RNA fragments containing the CCFV and JINRV iTLSes were generated and tested for their ability to bind 80S ribosomes *in vitro* (Fig. 4.1B,C). Results for CCFV showed a 3-fold decrease (K_d=1.62 μM) in ribosome binding in comparison to

TCV iTLS, whereas JINRV was unable to bind ribosomes at detectable levels (Fig. 4.4A). RNA2D3D structural prediction analysis of the CCFV iTLS region confirmed that it was able to form a structure resembling a tRNA, but with a kinked "anticodon" stemloop (H5) (Fig. 4.4B). The region spanning from Ψ_3 to Ψ_2 in TCV was next replaced in full-length TCV to make constructs containing analogous sequences from CCFV (CiTLS) and JINRV (JiTLS). Viral accumulation levels in protoplasts revealed that CiTLS was at 65% of wt levels, whereas JiTLS failed to accumulate to detectable levels (Fig. 4.5B). These results strongly indicate that the CCFV iTLS, but not the comparable JINRV region, is functioning similarly as the TCV element.

TCV H4 represses iTLS binding to 80S ribosomes through Ψ_4 (Fig. 3.6C), a tertiary interaction between the terminal loop of H4 and the 5' side of the H5 LSL that occurs *in vitro* (Fig. 3.6A). CCFV contains an equivalent H4 at an identical position as TCV's hairpin and with 3 base variations that are predicted to maintain the stem and the 5 bp Ψ_4 with its cognate H5 (Fig. 4.1B). A possible JINRV H4 may be present 33 b upstream of H4a. This structure has a terminal loop that can potentially form a 4 bp Ψ_4, and contains an asymmetrical loop with three out of six bases conserved in TCV H4. The lower stem is only 2 G:C basepairs, which may be too unstable to form, and the upper stem is extended by 1 bp in comparison to TCV. To determine if the analogous H4 regions of CCFV and JINRV (Fig. 4.1B,C) alter the ability of their cognate iTLSes to bind 80S ribosomes *in vitro*, both H4 and iTLS were engineered in the same RNA fragments (CiTLS+H4 and JiTLS+H4). Ribosome binding of JiTLS+H4 remained at undetectable levels and CiTLS+H4 had binding reduced to levels below detection in

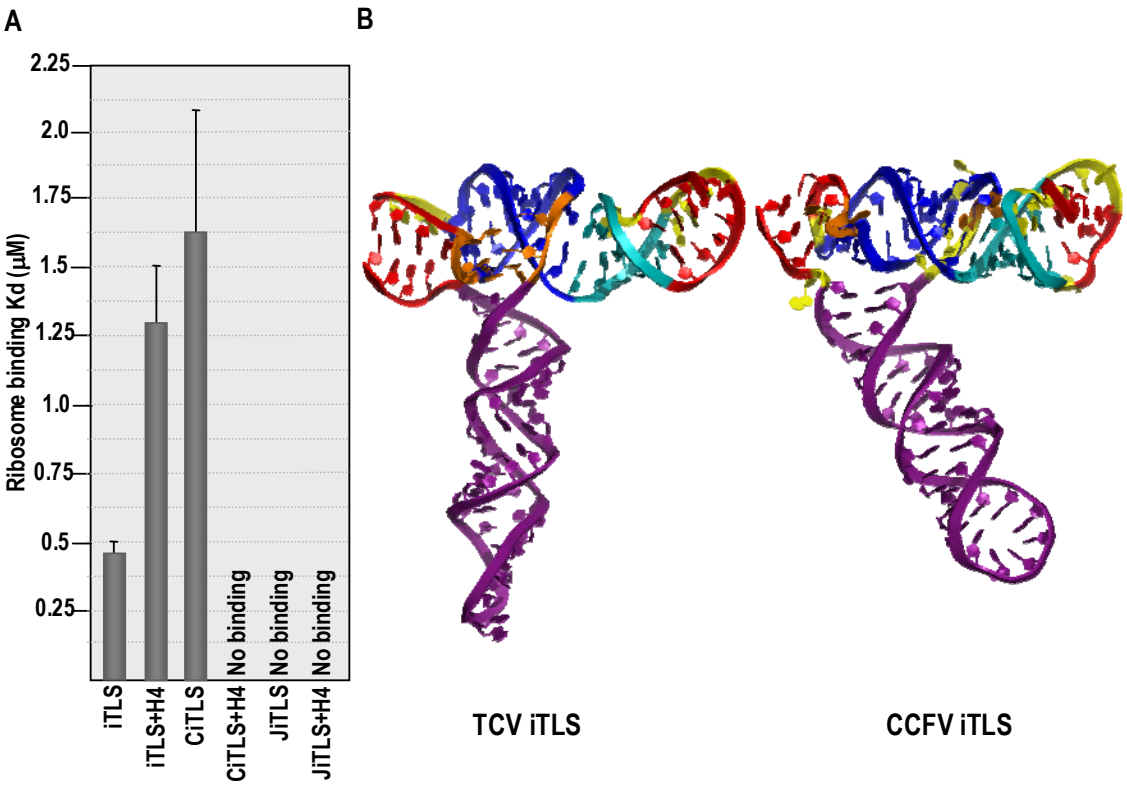

Figure 4.4. Functional Analysis of the Analogous CCFV and JINRV iTLS Regions. (A) In vitro ribosome binding of RNA fragments containing the iTLS using 80S yeast ribosomes. Standard errors are given by error bars. (B) Computer structural prediction analysis of the CCFV, Blue lake strain, using the RNA2D3D program.

Ribosome binding performed by Arturas Meskauskas
Molecular modeling performed by Yaroslava G. Yingling

comparison to CiTLS, suggesting that H4 of CCFV may be repressing 80S ribosome binding using basepairing that is equivalent to Ψ_4 in TCV (Fig. 4.1B,C; Fig. 4.4A).

H4a, H4b, and UP Ψ_3 Comprise a Subdomain within the iTLS

Individual hairpin elements in TCV iTLS were replaced with equivalent structures from CCFV and JINRV in full-length virus and tested for their ability to accumulate in protoplasts. The predicted CCFV H4b contains a bulged uridylate and two G:U basepairs in its stem, whereas H4b of JINRV has a stem 3 bp shorter than the TCV structure and no intervening single-stranded regions (Fig. 4.5A). CCFV and JINRV H4b both contain sequences in their terminal loops that are predicted to form a 4 and 3 bp Ψ_2 with TCV partner sequences, respectively (Fig. 4.5A). The CCFV H4b (CH4b) replacement showed a high level of tolerance (62% in comparison to wt); however, the JINRV H4b exchange (JH4b) accumulated to levels below detection, suggesting that length, sequence, and/or flexibility of the H4b stem are critical features of a functional iTLS *in vivo* (Fig. 4.5B). JINRV H5 contains an identical LSL as TCV and a 3 b SSL that destabilizes the lower stem. In comparison to TCV, the CCFV SSL is one base larger and the LSL is one base smaller, but is predicted to form Ψ_1 and Ψ_4 with TCV partner sequences using the same number of bases as wt TCV (Fig. 4.5A) The H5 replacements (CH5 and JH5) showed an equal reduction in accumulation of about 90%, suggesting that a common feature of CH5 and JH5, such as a weaker lower stem, was responsible for low tolerance of these exchanges (Fig. 4.5B). CCFV H4a is the same length as the TCV analog, but contains 3 base variations in the loop that weaken Ψ_3

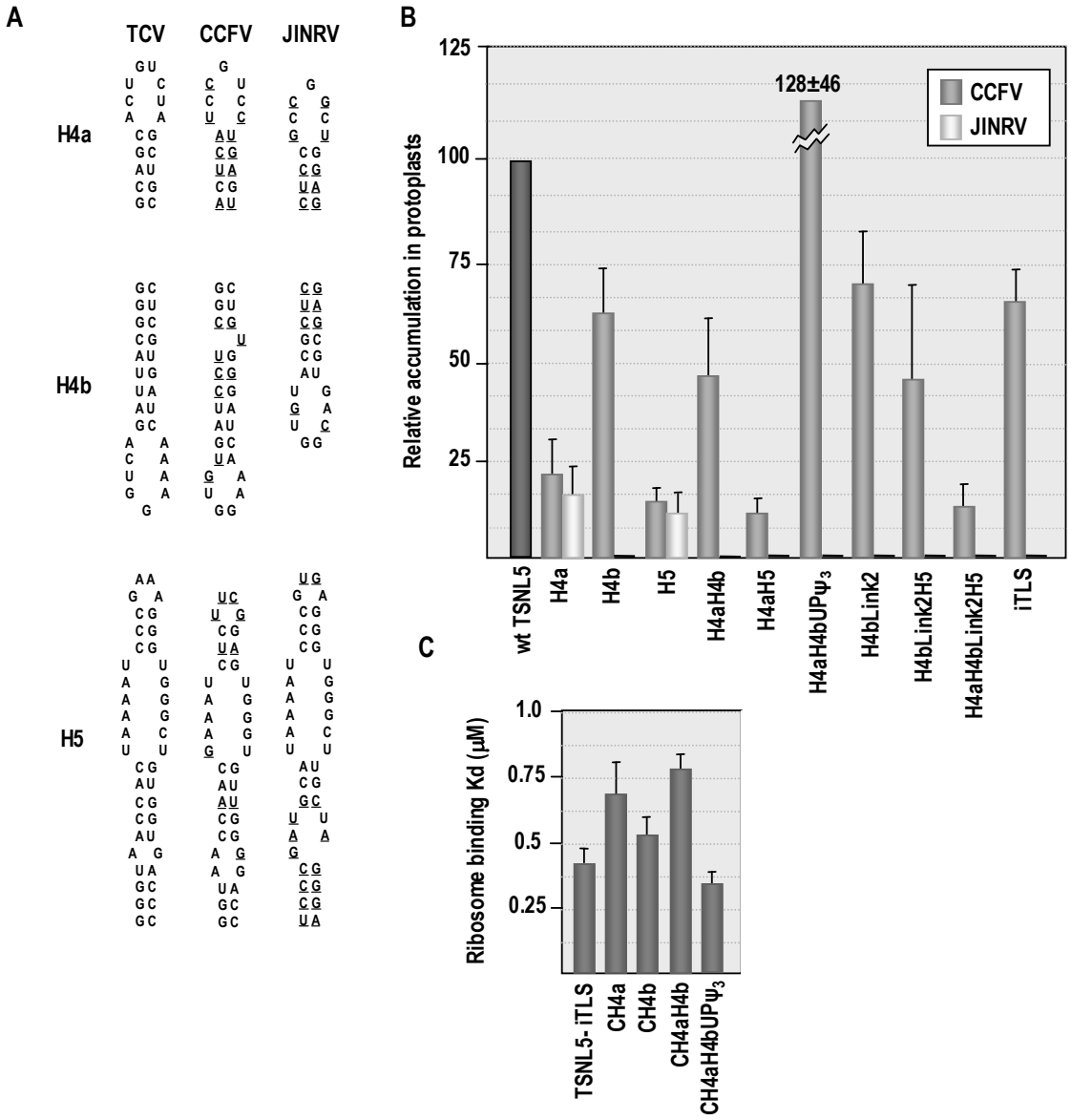

Figure 4.5. Stepwise Replacements of the TCV iTLS with Heterologous Sequences from CCFV, Blue Lake Strain, and JINRV. (A) Sequences and structures of H4a, H4b, and H5 of TCV, CCFV, and JINRV. Underlined bases in the CCFV and JINRV hairpins indicate base differences with TCV. (B) Relative accumulation of TCV mutant constructs in comparison to wt TSNL5 (black bar) at 40 hpi in protoplasts. Accumulation levels of CCFV replacement constructs are shown by bars in grey and JINRV mutants are represented by bars in white. Standard deviations are shown with error bars. (C) In vitro ribosome binding of TCV RNA fragments containing the specified elements of CCFV using 80S yeast ribosomes. Construct names begin with C to denote CCFV sequence followed by the names of the sequences being replaced. Standard errors are given by error bars. Ribosome binding performed by Arturas Meskauskas.

by 1 bp and eliminate a centrally-located G:U pair with TCV partner sequence. JINRV H4a also weakens Ψ_3 by 1 bp and contains a stem that is 1 bp shorter than TCV's hairpin (Fig. 4.5A). Replacements of TCV H4a with CCFV (CH4a) and JINRV (JH4a) sequences were not well-tolerated with accumulation levels of 21% and 16% of wt TCV levels respectively, suggesting that the sequence and structure of Ψ_3 exhibit specificity (Fig. 4.5B).

TCV replacement mutants containing multiple elements comprising the analogous CCFV and JINRV iTLS regions were constructed to address whether cooperativity existed between iTLS sequences and structures. H4a's association with H5 and H4b was examined with construction of H4aH5 and H4aH4b double replacements. Both JINRV hairpin constructs accumulated to levels below detection (Fig. 4.5B), confirming the lethal effect of JINRV H4b and the low tolerances of JINRV H4a and H5, respectively. CCFV H4aH5 accumulated to levels that were slightly lower than the single exchanges, but the H4aH4b substitution from CCFV exhibited levels of accumulation that appeared to be partially compensatory in comparison to CH4a and CH4b (Fig. 4.5B). The cognate Ψ_3 was next tested alongside the replaced H4a and H4b (H4aH4bUP Ψ_3). While the JINRV triple replacement remained at levels below detection, the corresponding CCFV construct accumulated to levels that were about 3-fold higher than the H4aH4b mutant, which supports the existence of an iTLS subdomain comprising H4a, H4b, and the upstream flanking region (Fig. 4.5B). To determine if the H4aH4bUPΨ_3 subdomain was involved in translation, a series of mutant iTLS RNA fragments were made. iTLSes containing the CCFV H4a (CH4a) or H4b (CH4b) bound 80S yeast ribosomes with a K_d of 0.68 μM and 0.53 μM, respectively (Fig. 4.5C). Double replacement with H4a and

H4b (CH4aH4b) did not improve ribosome binding (K_d=0.77 μM); however, addition of Ψ_3 (CH4aH4bΨ_3) restored ribosome binding to levels that were 1.3-fold higher (K_d= 0.35 μM) than wt iTLS (Fig. 4.5C). These results confirm the existence of a subdomain in the 5' portion of the iTLS involved in ribosome binding.

The 3' portion of the iTLS was analyzed by replacing H4b and downstream flanking sequence (Link2) or H4b, Link2, and H5. Results showed that there was no significant difference between H4b and H4bLink2 accumulation for either the CCFV or JINRV replacements (Fig. 4.5B). Addition of CCFV H5 to its cognate H4b and Link2 (CH4bLink2H5) resulted in accumulation levels that were lower than the H4b replacement, yet 3-fold higher than the replacement of H5 by itself, suggesting a partial restoration in viral accumulation (Fig 4.5B). However, adding CCFV H4a (H4aH4bLink2H5) did not further improve accumulation levels (Fig. 4.5B).

Second-Site Changes Associated with JH5 and CH5 Are Found in Coding Sequences That Affect Viral Accumulation

JH5 and CH5 were inoculated onto turnip seedlings, incubated for 55 days, and then the viral progeny extracted and cloned. Partial sequencing (TCV positions 20-935 and 2815-4020) of progeny from JH5 identified three second-site alterations: a uridylate to cytidylate alteration (U110C) in the RdRp ORF and two adenylate to guanylate changes (A3420G and A3524G) in the CP ORF of the same clone. Intriguingly, all three mutations were found in similar elements comprising CC(C/U)A (Fig. 4.6A), but encoding a different amino acid. These results suggest that these second-site alterations are important at the RNA level.

Figure 4.6. Identification and Accumulation of TCV Containing Second-Site Mutations Found in Progeny Derived from JH5 and CH5. (A) Partial sequencing analysis (TCV positions 20-935 and 2815-4020) of viral progeny derived from JH5. Names of identified second-site mutations are designated. One clone contained both A3420G and A3524G. Underlined bases indicate the CC(C/U)A sequences. Location of second-site mutations in TCV and the resulting codon change are given. Letters in red show potential complementarity of plant 18S rRNA at around position 1110 with TCV RNA. (B) Accumulation in protoplasts of constructs containing the second-site mutations identified in JH5 progeny. Total RNA was extracted from protoplasts at 40 hpi and probed with an oligonucleotide complementary to TCV**.** (C) Partial sequencing analysis (TCV positions 20-935 and 2815-4020) of viral progeny derived from CH5. Name and location of identified second-site mutation is given. Location of the second-site mutation in TCV is given. (D) Accumulation in protoplasts of constructs containing the second-site mutation identified in CH5 progeny. Total RNA was extracted from protoplasts at 40 hpi and probed with an oligonucleotide complementary to TCV.

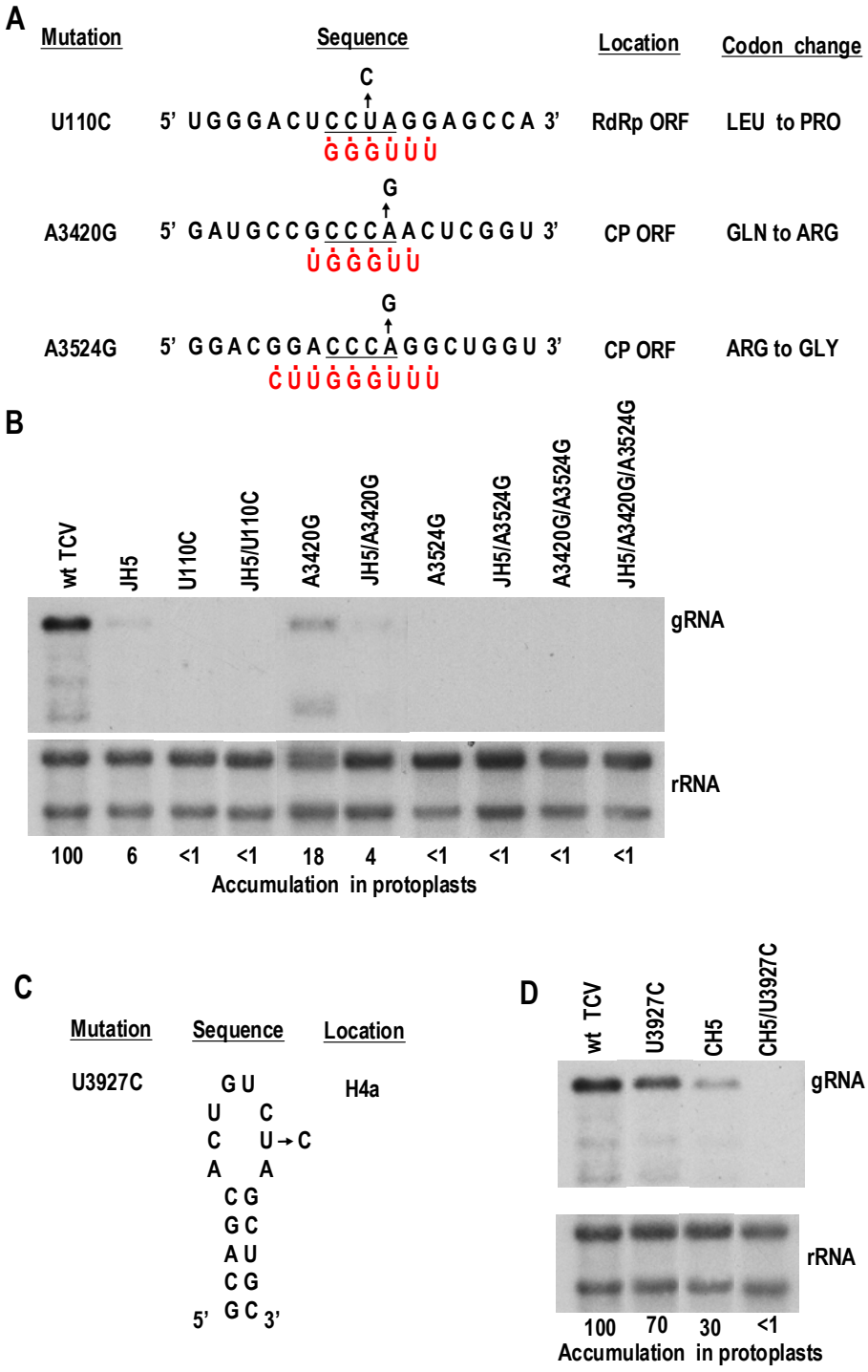
A
Mutation
Sequence
Location
Codon change
C
U110C
5' U G G G A C U C C U A G G A G C C A 3'
RdRp ORF
LEU to PRO
G G G U U U
G
A3420G
5' G A U G C C G C C C A A C U C G G U 3'
CP ORF
GLN to ARG
U G G G U U
G
A3524G
5' G G A C G G A C C C A G G C U G G U 3'
CP ORF
ARG to GLY
C U U G G G U U U
B
wt TCV
JH5
U110C
JH5/U110C
A3420G
JH5/A3420G
A3524G
JH5/A3524G
A3420G/A3524G
JH5/A3420G/A3524G
gRNA
rRNA
100 6 <1 <1 18 4 <1 <1 <1 <1
Accumulation in protoplasts
C
Mutation
Sequence
Location
U3927C
G U
U C
C U→C
A A
C G
G C
A U
C G
5' G C 3'
H4a
D
wt TCV
U3927C
CH5
CH5/U3927C
gRNA
rRNA
100 70 30 <1
Accumulation in protoplasts

To determine if the second-site changes were compensating for the JINRV H5 replacement, each mutation was introduced into either wt TCV or JH5 constructs and inoculated into protoplasts. U110C by itself or with JINRV H5 (JH5/U110C) accumulated to levels below detection (Fig. 4.6B). A3420G and A3524G accumulated to 18% and to undetectable levels respectively, whereas these mutations with JINRV H5 (JH5/A3420G and JH5/A3524G) accumulated to 4% and to levels below detectability in comparison to wt (Fig. 4.6B). Since A3420G and A3524G were found together in the same clone, additional TCV constructs containing both alterations in the absence (A3420G/A3524G) or presence of JINRV H5 (JH5/A3420G/A3524G) were tested and found to accumulate to levels below detection in protoplasts (Fig. 4.6B). These results do not support the second-site alterations compensating for the original JINRV H5 replacement *in vivo*; however, they may be beneficial at specific steps in the viral life cycle or compensatory when combined with other unidentified second-site changes. One possibility is that replacement of H5, which is adjacent to and may alter the structure of the H4aH4bΨ_3 subdomain that binds 60S ribosomal subunits, leads to second-site alterations that are involved in recruitment of translational proteins involved in assembly of 80S ribosomes. Analysis of the TCV regions where the second-site mutations were found revealed a nucleotide composition that could potentially form 6 (110 and 3420 regions) or 9 basepairs (3524 region) with solvent-accessible nucleotides at around position 1110 of plant 18S rRNA (Akbergenov *et al*., 2004). The JH5 second-site mutations maintained predicted 18S rRNA basepairing, suggesting that these regions may function as 40S ribosomal subunit recruitment elements (Fig. 4.6A).

A uridylate to cytidylate substitution (U3927C) was found in the H4a terminal loop of CH5 progeny sequenced between TCV positions 20-935 and 2815-4020 (Fig. 4.6C). Accumulation in protoplasts of U3927C was reduced by 30% in comparison to wt TCV. In the presence of CCFV H5 (CH5/U3927C), accumulation levels were undetectable, which was unexpectedly deleterious considering that neither CH5 nor U3927C mutants were lethal (Fig. 4.6D). These results suggest that replacement of H5 influences H4a sequence specificity, a finding that is consistent with these hairpins being part of the TCV iTLS domain.

TCV Elements in the 3' Terminal Region Are Not Cooperative in Viral Accumulation

In the carmovirus HCRSV, replacement of its H5 or Pr with analogous TCV elements was lethal to viral accumulation, but simultaneously replacing both rescued genomic RNA accumulation to near wild- type levels (Wang and Wong, 2004). To determine if HCRSV results are applicable to TCV, a similar replacement strategy was employed using CCFV and JINRV analogs. CCFV Pr contains an identical stem length and a terminal loop that is 2 b smaller in comparison to TCV, whereas JINRV Pr has a stem that is 1 bp longer and a terminal loop that is 1 b larger (Fig. 4.7A). Previous results showed that replacement of TCV Pr with the CCFV structure was better tolerated than substitution with the JINRV hairpin *in vivo* (Zhang *et al*, 2006b). To confirm these data, protoplast inoculations for the Pr replacements were re-performed and viral accumulation levels determined to be 94% for the CCFV sequence and undetectable for the JINRV Pr, in comparison to wt (Fig. 4.7A,B). Replacement of CCFV H5 and Pr together accumulated to levels that were significantly lower than the Pr substitution by itself (Fig.

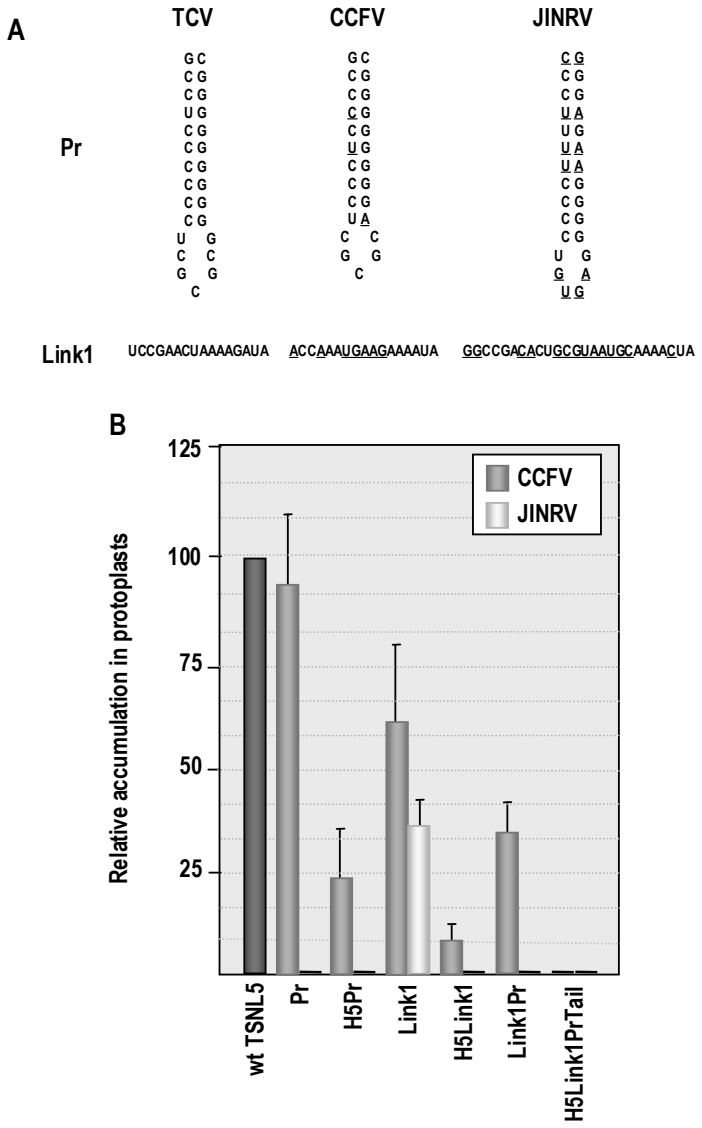

Figure 4.7. Stepwise Replacements of the TCV 3' Terminal Region with Analogous Elements from CCFV (Blue Lake), and JINRV. (A) Sequences and structures of the Pr and Link1 regions of TCV, CCFV, and JINRV. Underlined bases of the CCFV and JINRV elements indicate variations with TCV sequences. (B) Relative accumulation of TCV mutants in comparison to wt TSNL5 (black bar) at 40 hpi in protoplasts. Wt TSNL5 was transcribed from the pTSNL5 construct. Accumulation levels of CCFV replacement constructs are shown by bars in grey and JINRV mutants are represented by bars in white. Standard deviations are shown with error bars.

4.7B) and at similar levels as the H5 exchange (Fig. 4.5B), whereas JINRV H5Pr remained at levels that were below detection (Fig. 4.7B). These results do not support a cooperative relationship between H5 and Pr of CCFV and JINRV in a TCV background.

Simultaneous TCV replacements were performed to investigate the importance and relationship of elements in the 3' terminal region. Link1, an intervening sequence between H5 and Pr, was substituted for equivalent CCFV and JINRV sequences (Fig. 4.7A). In comparison to TCV, CCFV Link1 is one base longer and contains base variations at 7 positions, whereas the JINRV analog is a 26 b region that varies at 14 positions. Both CCFV and JINRV Link1 contain a stretch of 4 adenylates near their 3' borders and are predicted to form a 3 bp Ψ_2 with TCV partner sequences (Fig. 4.7A). In protoplasts, the CCFV Link1 (CLink1) mutant was reduced in accumulation by 39% and JINRV (JLink1) by 64%, in comparison to wt (Fig. 4.7B). Modest reductions in accumulation for the Link1 replacements suggest that there is relatively low sequence specificity for this region in comparison to the iTLS and Pr. Link1's association with H5 or Pr was tested by engineering constructs containing these regions in combination. Both H5Link1 and Link1Pr for CCFV accumulated to levels that were lower than their respective single replacements and the identical JINRV mutants were at undetectable levels (Fig. 4.7B). Substitution of sequences from H5 to the Tail (H5Link1PrTail) exhibited accumulation levels below detection for both CCFV and JINRV constructs (Fig. 4.7B). In all, these results are inconsistent with cooperativity between the 3' terminal elements.

Discussion

TCV contains a novel 3' UTR translational enhancer that functions by recruiting 60S ribosomal subunits to the viral template for assembly into 80S ribosomes. The TCV iTLS, which folds into a structure mimicking a canonical tRNA, contains an acceptor stem region comprising H4a, H4b, Ψ_2, and Ψ_3, and an analogous anticodon stemloop formed by H5. Phylogenetic comparisons between TCV and the 13 other carmoviruses revealed that only CCFV and JINRV contained the 5 equivalent structural features found in the iTLS of TCV. (Fig. 4.1A,B,C). Using 80S ribosome binding experiments, the CCFV iTLS region was found to have an affinity 3-fold lower than TCV, but no specific binding was detected with JINRV (Fig. 4.4B). Replacement of the TCV iTLS in full-length viral RNA with the CCFV region resulted in accumulation levels that were 65% of wt, whereas the JINRV replacement was lethal *in vivo* (Fig. 4.5B). These results give evidence for the existence of an iTLS in CCFV, but not in JINRV.

To assess why the analogous JINRV iTLS region could not function as a 60S ribosomal subunit binding element, stepwise replacements of the TCV iTLS were performed. Both H4a and H5 from either CCFV or JINRV were equally detrimental for viral accumulation, suggesting that these elements were not responsible for the marked differences observed in ribosome binding of the analogous carmoviral iTLSes (Fig. 4.5B). However, testing of the H4b from JINRV revealed that it was severely defective relative to the CCFV analog, showing that H4b may be a major determinant for JINRV's inability to function like the TCV or CCFV iTLSes (Fig. 4.5B). While both CCFV and JINRV H4b replacements preserve basepairing with their TCV Ψ_2 partner sequences (4 and 3 bp, respectively), the stem of JINRV H4b is 3 bp shorter and less flexible due to the

lack of G:U basepairing, in comparison to TCV iTLS (Fig. 4.5A). Due to the structured elements flanking H4b, a short inflexible H4b stem may not be able to facilitate Ψ_2 formation. Alternatively, JINRV H4b may form a distorted Ψ_2 that causes the remainder of the iTLS structure to fold incorrectly and lose its ability to bind ribosomes.

The H5 element of the iTLS is known to be a multifunctional element that is involved in repressing ribosome binding and minus-strand synthesis by sequences presented in its LSL (Fig. 3.6C; Fig. 2.3B). Deletion of the entire H5 revealed that this element was not required for 80S ribosome binding *in vitro* (Fig 4.3C), showing that H4a, H4b, Ψ_2, and Ψ_3, contain the primary determinants for 60S ribosomal subunit binding. To test for this possibility, replacement of this region in TCV iTLS with equivalent CCFV sequences showed that ribosome binding was reduced with the H4a and/or H4b substitutions, but rescued with the triple replacement of H4a, H4b, and UPΨ_3, suggesting that the iTLS contains a H4aH4bUPΨ_3 subdomain (Fig. 4.5C).

While HCRSV has a similar whole genome nucleotide sequence identity (57%) to TCV than JINRV (Robertson *et al*., 2007), it lacks all of the elements comprising the 60S ribosomal subunit binding subdomain. HCRSV does contain H5 with an LSL identical to TCV's, but only a 2 bp upper stem and a lower stem lacking an SSL (Wang and Wong, 2004). Deletion of the HCRSV tetraloop or disruption of the upper stem to generate a large terminal loop resulted in detectable levels of viral accumulation in protoplasts (Wang and Wong, 2004), similar to results found for TCV (LSLterm; Fig. 4.3B). However, mutagenesis indicated that the sequence, but not the structure, of the lower stem was a vital feature of HCRSV H5 (Wang and Wong, 2004), a finding that differs from results in TCV where the critical importance is the LSL (LSLΔ; Fig. 4.3B). H5 in

HCRSV also appears to function synergistically with its cognate Pr, showing that H5 and downstream sequences are cooperative (Wang and Wong, 2004). In contrast, this association between the 3' terminal hairpins was not evident in TCV (Fig. 4.7B). These results suggest that TCV H5 functions differently than its analog in HCRSV.

Analysis of the three most closely related carmoviruses (CCFV, JINRV, and HCRSV) based on whole genome sequence nucleotide identity (Robertson *et al*., 2007) shows that CCFV exhibits reduced ability to function like the TCV iTLS, whereas the analogous JINRV region exhibits no iTLS activity *in vitro* and in *vivo* . For HCRSV and the remainder of the carmoviruses, which lack one or more of the elements comprising an iTLS, the possibility that their regions immediately upstream of their analogous H5 structures contain 60S ribosomal subunit binding elements appears unlikely based on structural features found to be important for TCV and CCFV iTLSes. Despite previous work speculating that a common translational strategy may exist for an entire viral family (Fabian and White, 2004), this study shows that even closely-related viruses of the same genus may use different strategies for promoting translation.

CONCLUSIONS

This dissertation describes an internal tRNA-like structure (iTLS) located in the 3'UTR of *Turnip crinkle virus* (TCV), a small uncapped non-polyadenylated plus-stranded RNA virus belonging to the genus Carmovirus in the Family *Tombusviridae*. The iTLS comprises three hairpins (H4a, H4b, and H5) and two pseudoknots (Ψ_2 and Ψ_3) that adopt a canonical tRNA conformation according to the RNA structural prediction program RNA2D3D (Fig. 3.2B; Fig. 3.3B). Disruption and restoration of Ψ_3 was detrimental and compensatory respectively, in viral accumulation and ribosome binding, providing evidence for the functional importance of iTLS *in vivo* (Fig. 3.2B; Fig. 3.6B). The iTLS specifically bound 60S ribosomal subunits and 80S ribosomes at the P-site in a factor-independent manner, but not 40S subunits (Fig. 3.6E; Fig. 3.4A,B,C). These results identify the first known example of an RNA element that specifically binds the large ribosomal subunit.

The TCV 5'UTR contains two regions important for small ribosomal subunit binding, which were predicted to be complementary to a solvent-accessible region of plant 18S rRNA near the mRNA entrance tunnel of ribosomes (V.A. Stupina and A.E. Simon, unpublished results). One proposed model for translation of TCV involves protein-protein interactions between 60S ribosomal subunits bound to the iTLS and 40S ribosomal subunits associated with the 5' UTR, which would promote translation by assembling 80S ribosomes and circularizing the viral RNA (Fig. 3.10B). Another possibility is that 40S ribosomal subunits are recruited to *cis*-acting elements near the 3'

end and interact with 60S ribosomal subunits bound to the iTLS to assemble 80S ribosomes that are then shunted to the 5' end to initiate translation (Fig. 3.10C).

Since plus-strands of RNA viruses function as both mRNAs for translation and as templates for minus-strand synthesis, viruses must tightly regulate these mutually exclusive steps in their life cycles. Inclusion of upstream or downstream regions flanking the TCV iTLS reduced ribosome binding *in vitro* (Fig. 3.6C, D). Mutations introduced into pseudoknots predicted to form between the H5 LSL and 3' terminus (Ψ_1) or H4 terminal loop and H5 LSL (Ψ_4) showed that formation of Ψ_1 or Ψ_4 may induce a switch between translation and replication by repressing iTLS activity (Fig. 3.6C, D).

The structure of a repressed iTLS for RdRp recruitment and initiation of minus-strand synthesis from the 3' end is unknown. Do Ψ_2 and Ψ_3 exist in a TCV RNA conformation that is able to initiate replication? Results using satC, an untranslated subviral RNA containing a nearly identical 3' end with TCV, show that its Ψ_2 may be part of a pre-active RNA conformation involved in minus-strand synthesis (Zhang *et al.*, 2006a). RdRp binding assays using the iTLS + H4 + 3' RNA fragment (Fig. 3.6A) revealed that mutagenesis of the UPΨ_3 region, but not disruption of Ψ_3, abolished binding (M. Young and A.E. Simon, unpublished results). These results suggest that RdRp recruitment is facilitated by contact with UPΨ_3, which is available for binding through Ψ_3 disruption. Another potential RdRp binding site is the stretch of adenylates in the 5' side of the TCV H5 LSL (M. Young and A.E. Simon, unpublished results), which corroborates findings showing that this region is critical in viral accumulation and may be involved in properly folding the RdRp *in vivo* (Fig. 2.5B, Fig. 2.6).

A ~170 b internal deletion spanning sequence from the 3' border of the CP ORF to upstream of H4 resulted in 20% translational activity in comparison to wt using an in vivo luciferase assay, suggesting that 3' UTR elements outside of the iTLS are also important for translation (V.A. Stupina and A. E. Simon, unpublished results). An element in this region known as motif 3 hairpin (M3H) was previously reported as being a recombination hotspot and important for accumulation in plants and protoplasts (Carpenter *et al.*, 1995). A luciferase construct containing a deletion of M3H exhibited reduced activity *in vivo*, indicating the importance of this element in translation (V.A Stupina and A.E. Simon, unpublished results). Ribosome binding assays of an RNA fragment containing only M3H revealed that it was able to bind 40S ribosomal subunits, showing that M3H may be involved in ribosome assembly (J.C. McCormack, A. Meskauskas, and A.E. Simon, unpublished results).

What is the importance of regions in the RdRp and CP ORFs found to contain second-site mutations associated with JINRV H5 replacement? Since CP expression is not required for accumulation in protoplasts (Hacker *et al.*, 1992), the lethal effect of some mutations (A3524G) is presumably at the RNA level *in vivo*, suggesting the existence of a critical internally-located *cis*-acting element in TCV (Fig. 4.6B). Sequence analysis revealed that all second-site mutations were located in CC(C/U)A sequences, which may potentially pair with a solvent-accessible portion of plant 18S rRNA located near the mRNA entrance tunnel (Fig. 4.6A). If these regions are determined to function as 40S ribosomal subunit recruitment elements using in vitro ribosome binding assays, what is the biological significance of having multiple binding sites located throughout the TCV genome? One possibility is that TCV may initiate

translation by dynamic ribosomal clustering. 40S ribosomal subunits may associate and disassociate with RNA elements, which increases the probability of binding near an AUG codon (Chappell *et al*., 2006b).

Mfold structural prediction analysis and 3' UTR phylogenetic comparisons of all carmoviruses indicated that only CCFV and JINRV had the potential to form all the structural features found in the TCV iTLS (Fig. 4.1B,C; Zuker, 2003). However, 80S ribosome binding studies and replacement of the TCV iTLS with the other carmoviral iTLS candidates suggest that only the CCFV iTLS was able to function like TCV's (Fig. 4.4A, Fig. 4.5B). These results show that members in the same viral genus utilize different translational strategies, a finding that is counter to previous reports suggesting the existence of a common mechanism in Family *Tombusviridae* (Fabian and White, 2004). Stepwise replacements of TCV iTLS with CCFV elements showed that H4a, H4b, and UPΨ_3 may form an iTLS domain (Fig. 4.5B), a result that is consistent with in vivo translation data showing 80% activity when sequence encompassing the middle of H4b to the 3' terminus was deleted (V.A. Stupina and A.E. Simon, unpublished results). H5 appears to be a second iTLS subdomain that is dispensable for ribosome binding, suggesting that it functions primarily in replication (Fig. 4.3C).

One question that needs to be further addressed is: What regions of the TCV iTLS are bound by 60S ribosomal subunits? Cryo-electron microscopy (CryoEM) of iTLS RNA complexed with 60S ribosomal subunits would elucidate the contact points of the large subunit. iTLS bound by 80S ribosomes could also be analyzed to determine if conformational changes occur upon association of the small and large ribosomal subunits. Another question that needs to be answered is: How do other carmoviruses translate their

genomes? CCFV bound 80S ribosomes at a reduced level in comparison to TCV, suggesting that additional elements in CCFV may be required for translation *in vivo*. While the JINRV iTLS region did not appear to function as a ribosomal subunit recruitment element, it may still enhance translation downstream of binding. Mutagenesis of CCFV and JINRV iTLS regions in cognate full-length virus and luciferase constructs would clarify the similarities and differences with the TCV iTLS.

What is the biological significance of the iTLS? Since cap-dependent host protein synthesis occurs during infection with TCV, viral RNAs must compete with cellular mRNAs for recruitment of ribosomes. The iTLS may provide a translational advantage for TCV by facilitating more efficient recycling of 60S ribosomal subunits upon ribosome disassembly. Characterization of the TCV iTLS may be relevant to 3-5% of cellular mRNAs that exhibit cap-independent translation under physiological stress (Merrick, 2004). Preliminary data show that the mRNAs of Ornithine decarboxylase (ODC) and Vascular endothelial growth factor (VEGF) contain sequences in their 3' UTRs that are able to bind 80S yeast ribosomes and are predicted to have a similar structural arrangement as elements comprising the TCV iTLS (J.C. McCormack, V.A. Stupina, A. Meskauskas, and A.E. Simon, unpublished results). Downregulation of the ODC and VEGF iTLSes by mutagenesis of analogous base positions known to be important for TCV iTLS activity may be a potential therapeutic strategy for patients afflicted by tumors caused by overexpression of ODC and VEGF.

REFERENCES

Adkins, S., Stawicki, S.S., Faurote, G., Siegel, R.W., and Kao, C.C. 1998. Mechanistic analysis of RNA synthesis by RNA-dependent RNA polymerase from two promoters reveals similarities to DNA-dependent RNA polymerase. *RNA.* **4:** 455-470.

Akbergenov, R.Zh., Zhanybekova, S.Sh., Kryldakov, R.V., Zhigailov, A., Polimbetova, N.S., Hohn, T., and Iskakov, B.K. 2004. ARC-1, a sequence element complementary to an internal 18S rRNA segment, enhances translation efficiency in plants when present in the leader or intercistronic region of mRNAs. *Nucleic Acids Res.* **32:** 239-247.

Alvarez, D.E., Lodeiro, M.F., Ludueña, S.J., Pietrasanta, L.I., and Gamarnik, A.V. 2005. Long-range RNA-RNA interactions circularize the dengue virus genome. *J Virol.* **79:** 6631-6643.

Baird, S.D., Turcotte, M., Korneluk, R.G., and Holcik, M. 2006. Searching for IRES. *RNA.* **12:** 1755-1785.

Barends, S., Bink, H.H., van den Worm, S.H., Pleij, C.W., and Kraal, B. 2003. Entrapping ribosomes for viral translation: tRNA mimicry as a molecular Trojan horse. *Cell.* **112:** 123-129.

Barrera, I., Schuppli, D., Sogo, J.M., and Weber, H. 1993. Different mechanisms of recognition of bacteriophage Qbeta plus and minus strand RNAs by Qbeta replicase. *J Mol Biol.* **232:** 512-521.

Bass, B.L. 2002. RNA editing by adenosine deaminases that act on RNA. *Annu Rev Biochem.* **71:** 817-846.

Bass, B.L., Weintraub, H., Cattaneo, R., and Billeter, M.A. 1989. Biased hypermutation of viral RNA genomes could be due to unwinding/modification of double-stranded RNA. *Cell.* **56:** 331.

Boehringer, D., Thermann, R., Ostareck-Lederer, A., Lewis, J.D., and Stark, H. 2005. Structure of the hepatitis C Virus IRES bound to the human 80S ribosome: remodeling of the HCV IRES. *Structure.* **13:** 1695-1706.

Bradrick, S.S., Walters, R.W., and Gromeier, M. 2006. The hepatitis C virus 3'-untranslated region or a poly(A) tract promote efficient translation subsequent to the initiation phase. *Nucleic Acids Res.* **34:** 1293-1303.

Brown, E.A., Zhang, H., Ping, L.H., and Lemon, S.M. 1992. Secondary structure of the 5' nontranslated regions of hepatitis C virus and pestivirus genomic RNAs. *Nucleic Acids Res.* **20:** 5041-5045.

Buck, K.W. 1996. Comparison of the replication of positive-stranded RNA viruses of plants and animals. *Adv Virus Res.* **47:** 159-251.

Carpenter, C.D., and Simon, A.E. 1998. Analysis of sequences and predicted structures required for viral satellite RNA accumulation by in vivo genetic selection. *Nucleic Acids Res.* **26:** 2426-2432.

Carpenter, C.D., Oh, J.-W., Zhang, C., and Simon, A.E. 1995. Involvement of a stem-loop structure in the location of junction sites in viral RNA recombination. *J Mol Biol.* **245:** 608-622.

Carrington, J.C., and Freed, D.D. 1990. Cap-independent enhancement of translation by a plant potyvirus 5' nontranslated region. *J Virol.* **64:** 1590-1597.

Carrington, J.C., Heaton, L.A., Zuidema, D., Hillman, B.I., and Morris, T.J. 1989. The genome structure of turnip crinkle virus. *Virology.* **170:** 219-226.

Cascone, P.J., Haydar, T.F., and Simon, A.E. 1993. Sequences and structures required for recombination between virus-associated RNAs. *Science.* **260:** 801-805.

Cattaneo, R. 1994. Biased (A-->I) hypermutation of animal RNA virus genomes. *Curr Opin Genet Dev.* **4:** 895-900.

Chapman M.R., and Kao C.C. 1999. A minimal RNA promoter for minus-strand RNA synthesis by the brome mosaic virus polymerase complex. *J Mol Biol.* **286:** 709-720.

Chappell, S.A., Dresios, J., Edelman, G.M., and Mauro, V.P. 2006a. Ribosomal shunting mediated by a translational enhancer element that base pairs to 18S rRNA. *Proc Natl Acad Sci U S A.* **103:** 9488-9493.

Chappell, S.A., Edelman, G.M., and Mauro, V.P. 2006b. Ribosomal tethering and clustering as mechanisms for translation initiation. *Proc Natl Acad Sci U S A.* **103:** 18077-18082.

Ciuffreda, P., Rubino, L., and Russo, M. 1998. Molecular cloning and complete nucleotide sequence of galinsoga mosaic virus genomic RNA. *Arch Virol.* **143:** 173-180.

Crotty, S., Cameron, C.E., and Andino, R. 2001. RNA virus error catastrophe: direct molecular test by using ribavirin. *Proc Natl Acad Sci U S A.* **98:** 6895-6900.

de la Torre, J.C., Wimmer, E., and Holland, J.J. 1990. Very high frequency of reversion to guanidine resistance in clonal pools of guanidine-dependent type 1 poliovirus. *J Virol.* **64:** 664-671.

Deiman, B.A., Koenen, A.K., Verlaan, P.W., and Pleij, C.W. 1998. Minimal template requirements for initiation of minus-strand synthesis in vitro by the RNA-dependent RNA polymerase of turnip yellow mosaic virus. *J Virol.* **72:** 3965-3972.

de Smit, M.H., Gultyaev, A.P., Hilge, M., Bink, H.H., Barends, S., Kraal, B., and Pleij, C.W. 2002. Structural variation and functional importance of a D-loop-T-loop interaction in valine-accepting tRNA-like structures of plant viral RNAs. *Nucleic Acids Res.* **30:** 4232-4240.

Dobrikova, E.Y., Grisham, R.N., Kaiser, C., Lin, J., and Gromeier, M. 2006. Competitive translation efficiency at the picornavirus type 1 internal ribosome entry site facilitated by viral cis and trans factors. *J Virol.* **80:** 3310-3321.

Domingo, E., and Holland, J.J. 1997. RNA virus mutations and fitness for survival. *Annu Rev Microbiol.* **51:** 151-178.

Drake, J.W., and Holland, J.J. 1999. Mutation rates among RNA viruses. *Proc Natl Acad Sci U S A.* **96:**13910-13913.

Dreher, T.W. 1999. Functions of the 3'-untranslated regions of positive strand RNA viral genomes. *Annu Rev Phytopathol.* **37:** 151-174.

Dreher, T.W., and Goodwin, J.B. 1998. Transfer RNA mimicry among tymoviral genomic RNAs ranges from highly efficient to vestigial. *Nucleic Acids Res.* **26:** 4356-4364.

Dreher, T.W., and Hall, T.C. 1988a. Mutational analysis of the sequence and structural requirements in brome mosaic virus RNA for minus strand promoter activity. *J Mol Biol.* **201:** 31-40.

Dreher, T.W., and Hall, T.C. 1988b. Mutational analysis of the tRNA mimicry of brome mosaic virus RNA. Sequence and structural requirements for aminoacylation and 3'-adenylation. *J Mol Biol.* **201:** 41-55.

Dreher, T.W., and Miller, W.A. 2006. Translational control in positive strand RNA plant viruses. *Virology.* **344:** 185-197.

Dreher, T.W., Bujarski, J.J., and Hall, T.C. 1984. Mutant viral RNAs synthesized in vitro show altered aminoacylation and replicase template activities. *Nature.* **311:** 171-175.

Dreher, T.W., Tsai, C.H., Florentz, C., and Giegé, R. 1992. Specific valylation of turnip yellow mosaic virus RNA by wheat germ valyl-tRNA synthetase determined by three anticodon loop nucleotides. *Biochemistry.* **31:** 9183-9189.

Duggal., R., Lahser, F.C., and Hall, T.C. 1994. Cis-acting sequences in the replication of plant viruses with plus-sense RNA genomes. *Annu Rev Phytopathol.* **32:** 287-309.

Fabian, M.R., and White, K.A. 2004. 5'-3' RNA-RNA interaction facilitates cap- and poly(A) tail-independent translation of tomato bushy stunt virus mrna: a potential common mechanism for tombusviridae. *J Biol Chem.* **279:** 28862-28872.

Fabian, M.R., and White, K.A. 2006. Analysis of a 3'-translation enhancer in a tombusvirus: a dynamic model for RNA-RNA interactions of mRNA termini. *RNA.* **12:** 1304-1314.

Fabian, M.R., Na, H., Ray, D., and White, K.A. 2003. 3'-Terminal RNA secondary structures are important for accumulation of tomato bushy stunt virus DI RNAs. *Virology.* **313:** 567-580.

Fechter, P., Rudinger-Thirion, J., Florentz, C., and Giegé, R. 2001. Novel features in the tRNA-like world of plant viral RNAs. *Cell Mol Life Sci.* **58:** 1547-1561.

Felden, B., Florentz, C., Giegé, R., and Westhof, E. 1996. A central pseudoknotted three-way junction imposes tRNA-like mimicry and the orientation of three 5' upstream pseudoknots in the 3' terminus of tobacco mosaic virus RNA. *RNA.* **2:** 201-212.

Filomatori, C.V., Lodeiro, M.F., Alvarez, D.E., Samsa, M.M., Pietrasanta, L., and Gamarnik, A.V. 2006. A 5' RNA element promotes dengue virus RNA synthesis on a circular genome. *Genes Dev.* **20:** 2238-2249.

Flint, S.J., Enquist, L.W., Racaniello, V.R., and Skalka, A.M. Principles of Virology: Molecular Biology, Pathogenesis, and Control of Animal Viruses. Washington, D.C.: ASM Press, 2004.

Florentz**,** C., and Giegé, R. tRNA: Structure, Biosynthesis and Function. Washington, D.C.: Am Soc Microbiol., 1995

Fraser, C.S., and Doudna, J.A. 2007. Structural and mechanistic insights into hepatitis C viral translation initiation. *Nat Rev Microbiol.* **5:** 29-38.

French, R., and Ahlquist, P. 1987. Intercistronic as well as terminal sequences are required for efficient amplification of brome mosaic virus RNA3. *J Virol.* **61:** 1457-1465.

Frolov, I., Hardy, R., and Rice, C.M. 2001. Cis-acting RNA elements at the 5' end of Sindbis virus genome RNA regulate minus- and plus-strand RNA synthesis. *RNA.* **7:** 1638-1651.

Gallie, D.R., Tanguay, R.L., and Leathers, V. 1995. The tobacco etch viral 5' leader and poly(A) tail are functionally synergistic regulators of translation. *Gene.* **165:** 233-238.

Gazo, B.M., Murphy, P., Gatchel, J.R., and Browning, K.S. 2004. A novel interaction of Cap-binding protein complexes eukaryotic initiation factor (eIF) 4F and eIF(iso)4F with a region in the 3'-untranslated region of satellite tobacco necrosis virus. *J Biol Chem.* **279:** 13584-13592.

Guan, H., and Simon, A.E. 2000. Polymerization of nontemplate bases before transcription initiation at the 3' ends of templates by an RNA-dependent RNA polymerase: an activity involved in 3' end repair of viral RNAs. *Proc Natl Acad Sci U S A.* **97:** 12451-12456.

Guan, H., Carpenter, C.D., and Simon, A.E. 2000a. Analysis of cis-acting sequences involved in plus-strand synthesis of a turnip crinkle virus-associated satellite RNA identifies a new carmovirus replication element. *Virology.* **268:** 345-354.

Guan, H., Carpenter, C.D., and Simon, A.E. 2000b. Requirement of a 5'-proximal linear sequence on minus-strands for plus-strand synthesis of a satellite RNA associated with turnip crinkle virus. *Virology.* **268:** 355-363.

Guan, H., Song, C., and Simon, A.E. 1997. RNA promoters located on (-)-strands of a subviral RNA associated with turnip crinkle virus. *RNA.* **3:** 1401-1412.

Guilley, H., Carrington, J.C., Balàzs, E., Jonard, G., Richards, K., and Morris, T.J. 1985. Nucleotide sequence and genome organization of carnation mottle virus RNA. *Nucleic Acids Res.* **13:** 6663-6677.

Guo, L., Allen, E.M., and Miller, W.A. 2001. Base-pairing between untranslated regions facilitates translation of uncapped, nonpolyadenylated viral RNA. *Mol Cell.* **7:** 1103-1109.

Hacker, D.L., Petty, I.T., Wei, N., and Morris, T.J. 1992. Turnip crinkle virus genes required for RNA replication and virus movement. *Virology.* **186:** 1-8.

Haenni, A.L., Joshi, S., and Chapeville, F. 1982. tRNA-like structures in the genomes of RNA viruses. *Prog Nucleic Acid Res Mol Biol.* **27:** 85-104.

Hardy, R.W., and Rice, C.M. 2005. Requirements at the 3' end of the sindbis virus genome for efficient synthesis of minus-strand RNA. *J Virol.* **79:** 4630-4639.

Hellen, C.U., and Pestova, T.V. 1999. Translation of hepatitis C virus RNA. *J Viral Hepat.* **6:** 79-87.

Hellen, C.U., and Sarnow, P. 2001. Internal ribosome entry sites in eukaryotic mRNA molecules. *Genes Dev.* **15:** 1593-1612.

Holcik, M., Sonenberg, N., and Korneluk, R.G. 2000. Internal ribosome initiation of translation and the control of cell death. *Trends Genet.* **16:** 469-473.

Holland, J., Spindler, K., Horodyski, F., Grabau, E., Nichol, S., and van de Pol, S. 1982. Rapid evolution of RNA genomes. *Science.* **215:**1577-1585.

Holland, J.J., de la Torre, J.C., and Steinhauer, D.A. 1992. RNA virus populations as quasispecies. *Curr Top Microbiol Immunol.* **176:** 1-20.

Honda, M., Ping, L.H., Rijnbrand, R.C., Amphlett, E., Clarke, B., Rowlands, D., and Lemon, S.M. 1996. Structural requirements for initiation of translation by internal ribosome entry within genome-length hepatitis C virus RNA. *Virology.* **222:** 31-42.

Horst, J., Fraenkel-Conrat, H., and Mandeles, S. 1971. Terminal heterogeneity at both ends of the satellite tobacco necrosis virus ribonucleic acid. *Biochemistry.* **10:** 4748-4752.

Hu, M.C, Tranque, P., Edelman, G. M., and Mauro, V. P. 1999. rRNA-complementarity in the 5' untranslated region of mRNA specifying the Gtx homeodomain protein: evidence that base-pairing to 18S rRNA affects translation efficiency. *Proc Natl Acad Sci U S A.* **96:** 1339-1344.

Huang, M., Koh, D.C., Weng, L.J., Chang, M.L., Yap, Y.K., Zhang, L., and Wong, S.M. 2000. Complete nucleotide sequence and genome organization of hibiscus chlorotic ringspot virus, a new member of the genus Carmovirus: evidence for the presence and expression of two novel open reading frames. *J Virol.* **74:** 3149-3155.

Iwakawa, H.O., Kaido, M., Mise, K., and Okuno, T. 2007. cis-Acting core RNA elements required for negative-strand RNA synthesis and cap-independent translation are separated in the 3'-untranslated region of Red clover necrotic mosaic virus RNA1. *Virology.* **369:** 168-181.

Jackson, R.J., and Kaminski, A. 1995. Internal initiation of translation in eukaryotes: the picornavirus paradigm and beyond. *RNA.* **1:** 985-1000.

Ji, H., Fraser, C.S., Yu, Y., Leary, J., and Doudna JA. 2004. Coordinated assembly of human translation initiation complexes by the hepatitis C virus internal ribosome entry site RNA. *Proc Natl Acad Sci U S A.* **101:** 16990-16995.

Kaminski, A., Howell, M.T., and Jackson, R.J. 1990. Initiation of encephalomyocarditis virus RNA translation: the authentic initiation site is not selected by a scanning mechanism. *EMBO J.* **9:** 3753-3759.

Karetnikov, A., Keränen, M., and Lehto, K. 2006. Role of the RNA2 3' non-translated region of Blackcurrant reversion nepovirus in translational regulation. *Virology.* **354:** 178-191.

Kieft, J.S, Zhou, K., Jubin, R., and Doudna, J.A. 2001. Mechanism of ribosome recruitment by hepatitis C IRES RNA. *RNA.* **7:** 194-206.

Kim, C.H., Kao, C.C., and Tinoco, I. Jr. 2000. RNA motifs that determine specificity between a viral replicase and its promoter. *Nat Struct Biol.* **7:** 415-423.

Kneller, E.L., Rakotondrafara, A.M., and Miller, W.A. 2006. Cap-independent translation of plant viral RNAs. *Virus Res.* **119:** 63-75.

Koh, D.C., Liu, D.X., and Wong, S.M. 2002. A six-nucleotide segment within the 3' untranslated region of hibiscus chlorotic ringspot virus plays an essential role in translational enhancement. *J Virol.* **76:** 1144-1153.

Koh, D.C., Wong, S.M., and Liu, D.X. 2003. Synergism of the 3'-untranslated region and an internal ribosome entry site differentially enhances the translation of a plant virus coat protein. *J Biol Chem.* **278:** 20565-20573.

Kolupaeva, V.G., Lomakin, I.B., Pestova, T.V., and Hellen, C.U. 2003. Eukaryotic initiation factors 4G and 4A mediate conformational changes downstream of the initiation codon of the encephalomyocarditis virus internal ribosomal entry site. *Mol Cell Biol.* **23:** 687-698.

Kolupaeva, V.G., Pestova, T.V., and Hellen, C.U. 2000. An enzymatic footprinting analysis of the interaction of 40S ribosomal subunits with the internal ribosomal entry site of hepatitis C virus. *J Virol.* **74:** 6242-6250.

Kolupaeva, V.G., Pestova, T.V., Hellen, C.U., and Shatsky, I.N. 1998. Translation eukaryotic initiation factor 4G recognizes a specific structural element within the internal ribosome entry site of encephalomyocarditis virus RNA. *J Biol Chem.* **273:** 18599-18604.

Kong, Q., Oh, J.W., Carpenter, C.D., and Simon, A.E. 1997. The coat protein of turnip crinkle virus is involved in subviral RNA-mediated symptom modulation and accumulation. *Virology.* **238:** 478-485.

Kopek, B.G., Perkins, G., Miller, D.J., Ellisman, M.H., and Ahlquist, P. 2007. Three-dimensional analysis of a viral RNA replication complex reveals a virus-induced mini-organelle. *PLoS Biol.* **5:** e220.

Kozak, M. 1999. Initiation of translation in prokaryotes and eukaryotes. *Gene.* **234:** 187-208.

Lai, M.M.C. 1998. Cellular factors in the transcription and replication of viral RNA genomes: a parallel to DNA-dependent RNA transcription. *Virology.* **244:** 1-12.

Levis, R., Schlesinger, S., and Huang, H.V. 1990. Promoter for Sindbis virus RNA-dependent subgenomic RNA transcription. *J Virol.* **64:** 1726-1733.

Levis, R., Weiss, B.G., Tsiang, M., Huang, H., and Schlesinger, S. 1986. Deletion mapping of Sindbis virus DI RNAs derived from cDNAs defines the sequences essential for replication and packaging. *Cell.* **44:** 137-145.

Li, W., and Wong, S.M. 2007. Host-dependent effects of the 3' untranslated region of Turnip crinkle virus RNA on accumulation in Hibiscus and Arabidopsis. *J Gen Virol.* **88:** 680-687.

Lin, Y.J., Liao, C.L., and Lai, M.M. 1994. Identification of the cis-acting signal for minus-strand RNA synthesis of a murine coronavirus: implications for the role of minus-strand RNA in RNA replication and transcription. *J Virol.* **68:** 8131-8140.

Litvak, S., Tarragó, A., Tarragó-Litvak, L., and Allende, J.E. 1973a. Elongation factor-viral genome interaction dependent on the aminoacylation of TYMV and TMV RNAs. *Nat New Biol.* **241:** 88-90.

Litvak, S., Tarrago-Litvak, L., and Chapeville, F. 1973b. Turnip yellow mosaic virus RNA as a substrate of the transfer RNA nucleotidyltransferase II. Incorporation of cytidine 5'-monophosphate and determination of a short nucleotide sequence at the 3' end of the RNA. *J Virol.* **11:** 238-242.

Lomakin, I.B., Hellen, C.U., and Pestova, T.V. 2000. Physical association of eukaryotic initiation factor 4G (eIF4G) with eIF4A strongly enhances binding of eIF4G to the internal ribosomal entry site of encephalomyocarditis virus and is required for internal initiation of translation. *Mol Cell Biol.* **20:** 6019-6029.

Lukavsky, P.J., Otto, G.A., Lancaster, A.M., Sarnow, P., and Puglisi, J.D. 2000. Structures of two RNA domains essential for hepatitis C virus internal ribosome entry site function. *Nat Struct Biol.* **7:** 1105-1110.

Mans, R.M., Pleij, C.W., and Bosch, L. 1991. tRNA-like structures. Structure, function and evolutionary significance. *Eur J Biochem.* **201:** 303-324.

Marcotrigiano, J., Lomakin, I.B., Sonenberg, N., Pestova, T.V., Hellen, C.U., and Burley, S.K. 2001. A conserved HEAT domain within eIF4G directs assembly of the translation initiation machinery. *Mol Cell.* **7:** 193-203.

Mathews, D.H., Sabina, J., Zuker, M., and Turner, D.H. 1999. Expanded sequence dependence of thermodynamic parameters improves prediction of RNA secondary structure. *J Mol Biol.* **288:** 911-940.

Matsuda, D., and Dreher, T.W. 2004. The tRNA-like structure of Turnip yellow mosaic virus RNA is a 3'-translational enhancer. *Virology.* **321:** 36-46.

Matsuda, D., and Dreher, T.W. 2006. Close spacing of AUG initiation codons confers dicistronic character on a eukaryotic mRNA. *RNA.* **12:** 1338-1349.

Matsuda, D., and Dreher, T.W. 2007. Cap- and initiator tRNA-dependent initiation of TYMV polyprotein synthesis by ribosomes: evaluation of the Trojan horse model for TYMV RNA translation. *RNA.* **13:** 129-137.

Matsuda, D., Yoshinari, S., and Dreher, T.W. 2004. eEF1A binding to aminoacylated viral RNA represses minus strand synthesis by TYMV RNA-dependent RNA polymerase. *Virology.* **321:** 47-56.

McKnight, K.L., and Lemon, S.M. 1996. Capsid coding sequence is required for efficient replication of human rhinovirus 14 RNA. *J Virol.* **70:** 1941-1952.

Merrick, W.C. 2004. Cap-dependent and cap-independent translation in eukaryotic systems. *Gene.* **332:** 1-11.

Miller, W.A., and White, K.A. 2006. Long-distance RNA-RNA interactions in plant virus gene expression and replication. *Annu Rev Phytopathol.* **44:** 447-467.

Miller, W.A., Bujarski, J.J., Dreher, T.W., and Hall, T.C. 1986. Minus-strand initiation by brome mosaic virus replicase within the 3' tRNA-like structure of native and modified RNA templates. *J Mol Biol.* **187:** 537-546.

Miller, W.A., Dreher, T.W., and Hall, T.C. 1985. Synthesis of brome mosaic virus subgenomic RNA in vitro by internal initiation on (-)-sense genomic RNA. *Nature.* **313:** 68-70.

Moore, P.B. 1999. Structural motifs in RNA. *Annu Rev Biochem.* **68:** 287-300.

Morrish, B.C., and Rumsby M.G. 2002. The 5' untranslated region of protein kinase Cdelta directs translation by an internal ribosome entry segment that is most active in densely growing cells and during apoptosis. *Mol Cell Biol.* **22:** 6089-6099.

Nagy, P.D., Pogany, J., and Simon, A.E. 1999. RNA elements required for RNA recombination function as replication enhancers in vitro and in vivo in a plus-strand RNA virus. *EMBO J.* **18:** 5653-5665.

Nagy, P.D., Pogany, J., and Simon, A.E. 2001. In vivo and in vitro characterization of an RNA replication enhancer in a satellite RNA associated with turnip crinkle virus. *Virology* **288:** 315-324.

Nagy, P.D., Zhang, C., and Simon, A.E., 1998. Dissecting RNA recombination in vitro: role of RNA sequences and the viral replicase. *EMBO J.* **17:** 2392-2403.

Niesters, H.G., and Strauss, J.H. 1990. Mutagenesis of the conserved 51-nucleotide region of Sindbis virus. *J Virol.* **64:** 1639-1647.

Nieto, C., Morales, M., Orjeda, G., Clepet, C., Monfort, A., Sturbois, B., Puigdomènech, P., Pitrat, M., Caboche, M., Dogimont, C., Garcia-Mas, J., Aranda, M.A., and Bendahmane, A. 2006. An eIF4E allele confers resistance to an uncapped and non-polyadenylated RNA virus in melon. *Plant J.* **48:** 452-462.

Nishiyama, T., Yamamoto, H., Shibuya, N., Hatakeyama, Y., Hachimori, A., Uchiumi, T., and Nakashima, N. 2003. Structural elements in the internal ribosome entry site of Plautia stali intestine virus responsible for binding with ribosomes. *Nucleic Acids Res.* **31:** 2434-2442.

Oh, J.W., Kong, Q., Song, C., Carpenter, C.D., and Simon, A.E. 1995. Open reading frames of turnip crinkle virus involved in satellite symptom expression and incompatibility with Arabidopsis thaliana ecotype Dijon. *Mol Plant Microbe Interact.* **8:** 979-987.

Olsthoorn, R.C., and Bol, J.F. 2002. Role of an essential triloop hairpin and flanking structures in the 3' untranslated region of Alfalfa mosaic virus RNA in in vitro transcription. *J Virol.* **76:** 8747-8756.

Osman, T.A., Hemenway, C.L., and Buck, K.W. 2000. Role of the 3' tRNA-like structure in tobacco mosaic virus minus-strand RNA synthesis by the viral RNA-dependent RNA polymerase in vitro. *J Virol.* **74:** 11671-11680.

Otto, G.A., and Puglisi, J.D. 2004. The pathway of HCV IRES-mediated translation initiation. *Cell.* **119:** 369-380.

Panavas, T., Pogany, J., and Nagy, P.D. 2002. Analysis of minimal promoter sequences for plus-strand synthesis by the Cucumber necrosis virus RNA-dependent RNA polymerase. *Virology.* **296:** 263-274.

Panaviene Z, Panavas T, and Nagy PD. 2005. Role of an internal and two 3'-terminal RNA elements in assembly of tombusvirus replicase. *J Virol.* **79:** 10608-10618.

Panaviene, Z., Panavas, T., Serva, S., and Nagy PD. 2004. Purification of the cucumber necrosis virus replicase from yeast cells: role of coexpressed viral RNA in stimulation of replicase activity. *J Virol.* **78:** 8254-8263.

Pestova, T.V., Hellen, C.U., and Shatsky, I.N. 1996a. Canonical eukaryotic initiation factors determine initiation of translation by internal ribosomal entry. *Mol Cell Biol.* **16:** 6859-6869.

Pestova, T.V., Lomakin, I.B., and Hellen, C.U. 2004. Position of the CrPV IRES on the 40S subunit and factor dependence of IRES/80S ribosome assembly. *EMBO Rep.* **5:** 906-913.

Pestova, T.V., Shatsky, I.N., and Hellen, C.U. 1996b. Functional dissection of eukaryotic initiation factor 4F: the 4A subunit and the central domain of the 4G subunit are sufficient to mediate internal entry of 43S preinitiation complexes. *Mol Cell Biol.* **16:** 6870-6878.

Pestova, T.V., Shatsky, I.N., Fletcher, S.P., Jackson, R.J., and Hellen, C.U. 1998. A prokaryotic-like mode of cytoplasmic eukaryotic ribosome binding to the initiation codon during internal translation initiation of hepatitis C and classical swine fever virus RNAs. *Genes Dev.* **12:** 67-83.

Petrov, A., Meskauskas, A., and Dinman, J.D. 2004. Ribosomal protein L3: Influence on ribosome structure and function. *RNA Biol.* **1:** 59-65.

Pfeffer, M., Kinney, R.M., and Kaaden, O.R. 1998. The alphavirus 3'-nontranslated region: size heterogeneity and arrangement of repeated sequence elements. *Virology.* **240:** 100-108.

Pilipenko, E.V., Pestova, T.V., Kolupaeva, V.G., Khitrina, E.V., Poperechnaya, A.N., Agol, V.I., and Hellen, C.U. 2000. A cell cycle-dependent protein serves as a template-specific translation initiation factor. *Genes Dev.* **14:** 2028-2045.

Pley, H.W., Flaherty, K.M., and McKay D.B. 1994. Model for an RNA tertiary interaction from the structure of an intermolecular complex between a GAAA tetraloop and an RNA helix. *Nature.* **372:** 111-113.

Pogany, J., Fabian, M.R., White, K.A., and Nagy, P.D. 2003. A replication silencer element in a plus-strand RNA virus. *EMBO J.* **22:** 5602-5611.

Pogany, J., White, K.A., and Nagy, P.D. 2005. Specific binding of tombusvirus replication protein p33 to an internal replication element in the viral RNA is essential for replication. *J Virol.* **79:** 4859-4869.

Preiss, T., and Hentze, M.W. 2003. Starting the protein synthesis machine: eukaryotic translation initiation. *BioEssays.* **25:** 1201-1211.

Qin, X., and Sarnow, P. 2004. Preferential translation of internal ribosome entry site-containing mRNAs during the mitotic cycle in mammalian cells. *J Biol Chem.* **279:** 13721-13728.

Qu, F., and Morris, T.J. 2000. Cap-independent translational enhancement of turnip crinkle virus genomic and subgenomic RNAs. *J Virol.* **74:** 1085-1093.

Qu, F., Ren, T., and Morris T.J. 2003. The coat protein of turnip crinkle virus suppresses posttranscriptional gene silencing at an early initiation step. *J Virol.* **77:** 511-522.

Quadt, R., Ishikawa, M., Janda, M., and Ahlquist, P. 1995. Formation of brome mosaic virus RNA-dependent RNA polymerase in yeast requires coexpression of viral proteins and viral RNA. *Proc Natl Acad Sci U S A.* **92:** 4892-4896.

Quigley, G.J. and Rich, A. 1976. Structural domains of transfer RNA molecules. *Science.* **194:** 796-806.

Rajendran, K.S., Pogany, J., and Nagy, P.D. 2002. Comparison of turnip crinkle virus RNA-dependent RNA polymerase preparations expressed in Escherichia coli or derived from infected plants. *J Virol.* **76:** 1707-1717.

Ranjith-Kumar, C.T., Zhang, X., and Kao, C.C. 2003. Enhancer-like activity of a brome mosaic virus RNA promoter. *J Virol.* **77:** 1830-1839.

Ray, D., and White, K.A. 1999. Enhancer-like properties of an RNA element that modulates Tombusvirus RNA accumulation. *Virology.* **256:** 162-171.

Ray, D., and White, K.A. 2003. An internally located RNA hairpin enhances replication of Tomato bushy stunt virus RNAs. *J Virol.* **77:** 245-257.

Ray, S., Yumak, H., Domashevskiy, A., Khan, M.A., Gallie, D.R., and Goss, D.J. 2006. Tobacco etch virus mRNA preferentially binds wheat germ eukaryotic initiation factor (eIF) 4G rather than eIFiso4G. *J Biol Chem.* **281:** 35826-35834.

Rico, P., and Hernández, C. 2004. Complete nucleotide sequence and genome organization of Pelargonium flower break virus. *Arch Virol.* **149:** 641-651.

Rietveld, K., van Poelgeest, R., Pleij, C.W., van Boom, J.H., and Bosch, L. 1982. The tRNA-like structure at the 3' terminus of turnip yellow mosaic virus RNA. Differences and similarities with canonical tRNA. *Nucleic Acids Res.* **10:** 1929-1946.

Rijnbrand, R.C., and Lemon, S.M. 2000. Internal ribosome entry site-mediated translation in hepatitis C virus replication. *Curr Top Microbiol Immunol.* **242:** 85-116.

Riviere, C.J., and Rochon, D.M. 1990. Nucleotide sequence and genomic organization of melon necrotic spot virus. *J Gen Virol.* **71:** 1887-1896.

Robertson, N.L., Côté, F., Paré, C., Leblanc, E., Bergeron, M.G., and Leclerc, D. 2007. Complete nucleotide sequence of Nootka lupine vein-clearing virus. *Virus Genes.* **35:** 807-814.

Saguy, M., Gillet, R., Metzinger, L., and Felden, B. 2005. tmRNA and associated ligands: a puzzling relationship. *Biochimie.* **87:** 897-903.

Schilling-Bartetzko, S., Franceschi, F., Sternbach, H., and Nierhaus, K.H. 1992. Apparent association constants of tRNAs for the ribosomal A, P, and E sites. *J Biol Chem.* **267:** 4693-4702.

Schneider, W.L., and Roossinck, M.J. 2001. Genetic diversity in RNA virus quasispecies is controlled by host-virus interactions. *J Virol.* **75:** 6566-6571.

Schwartz, M., Chen, J., Janda, M., Sullivan, M., den Boon, J., and Ahlquist, P. 2002. A positive-strand RNA virus replication complex parallels form and function of retrovirus capsids. *Mol Cell.* **9:** 505-514.

Shapiro, B.A., Bengali, D., Kasprzak, W., and Wu, J.C. 2001. RNA folding pathway functional intermediates: their prediction and analysis. *J Mol Biol.* **312:** 27-44.

Shen, R., and Miller, W.A. 2004. The 3' untranslated region of tobacco necrosis virus RNA contains a barley yellow dwarf virus-like cap-independent translation element. *J Virol.* **78:** 4655-4664.

Siegel, R.W., Adkins, S., and Kao, C.C. 1997. Sequence-specific recognition of a subgenomic RNA promoter by a viral RNA polymerase. *Proc Natl Acad Sci U S A.* **94:** 11238-11243.

Sierra, S., Dávila, M., Lowenstein, P.R., and Domingo, E. 2000. Response of foot-and-mouth disease virus to increased mutagenesis: influence of viral load and fitness in loss of infectivity. *J Virol.* **74:** 8316-8323.

Simon, A.E., and Howell, S.H. 1986. The virulent satellite RNA of turnip crinkle virus has a major domain homologous to the 3' end of the helper virus genome. *EMBO J.* **5:** 3423-3428.

Sivakumaran, K., and Kao, C.C. 1999. Initiation of genomic plus-strand RNA synthesis from DNA and RNA templates by a viral RNA-dependent RNA polymerase. *J Virol.* **73:** 6415-6423.

Sivakumaran, K., Kim, C.H., Tayon, R. Jr., and Kao, C.C. 1999. RNA sequence and secondary structural determinants in a minimal viral promoter that directs replicase recognition and initiation of genomic plus-strand RNA synthesis. *J Mol Biol.* **294:** 667-682.

Skotnicki, M.L., Mackenzie, A.M., Torronen, M., and Gibbs, A.J. 1993. The genomic sequence of cardamine chlorotic fleck carmovirus. *J Gen Virol.* **74:** 1933-1937.

Sonenberg, N., and Dever, T.E. 2003. Eukaryotic translation initiation factors and regulators. *Curr Opin Struct Biol.* **13:** 56-63.

Song, C., and Simon, A.E. 1994. RNA-dependent RNA polymerase from plants infected with turnip crinkle virus can transcribe (+)- and (-)-strands of virus-associated RNAs. *Proc Natl Acad Sci U S A.* **91:** 8792-8796.

Song, C., and Simon, A.E. 1995. Requirement of a 3'-terminal stem-loop in in vitro transcription by an RNA-dependent RNA polymerase. *J Mol Biol.* **254:** 6-14.

Song, Y., Friebe, P., Tzima, E., Jünemann, C., Bartenschlager, R., and Niepmann, M. 2006. The hepatitis C virus RNA 3'-untranslated region strongly enhances translation directed by the internal ribosome entry site. *J Virol.* **80:** 11579-11588.

Stawicki, S.S., and Kao, C.C. 1999. Spatial perturbations within an RNA promoter specifically recognized by a viral RNA-dependent RNA polymerase (RdRp) reveal that RdRp can adjust its promoter binding sites. *J Virol.* **73:**198-204.

Stoneley, M., Chappell, S.A., Jopling, C.L., Dickens, M., MacFarlane, M., and Willis A.E. 2000. c-Myc protein synthesis is initiated from the internal ribosome entry segment during apoptosis. *Mol Cell Biol.* **20:** 1162-1169.

Strauss, E.G., Rice, C.M., and Strauss, J.H. 1984. Complete nucleotide sequence of the genomic RNA of Sindbis virus. *Virology.* **133:** 92-110.

Stupina, V., and Simon, A.E., 1997. Analysis in vivo of turnip crinkle virus satellite RNA C variants with mutations in the 3'-terminal minus-strand promoter. *Virology.* **238:** 470-477.

Sullivan, M.L., and Ahlquist, P. 1999. A brome mosaic virus intergenic RNA3 replication signal functions with viral replication protein 1a to dramatically stabilize RNA in vivo. *J Virol.* **73:** 2622-2632.

Sun, J.H., and Kao, C.C. 1997a. RNA synthesis by the brome mosaic virus RNA-dependent RNA polymerase: transition from initiation to elongation. *Virology.* **233:** 63-73.

Sun, J.H., and Kao, C.C. 1997b. Characterization of RNA products associated with or aborted by a viral RNA-dependent RNA polymerase. *Virology.* **236:** 348-353.

Sun, X., and Simon, A. E. 2006. A cis-replication element functions in both orientations to enhance replication of Turnip crinkle virus. *Virology.* **352:** 39-51.

Sun, X., and Simon, A.E. 2003. Fitness of a turnip crinkle virus satellite RNA correlates with a sequence-nonspecific hairpin and flanking sequences that enhance replication and repress the accumulation of virions. *J Virol.* **77:** 7880-7889.

Suzuki, S., Hase, S., Takahashi, H., and Ikegami, M. 2002. The genome organization of pea stem necrosis virus and its assignment to the genus Carmovirus. *Intervirology.* **45:** 160-163.

Takamatsu, N., Watanabe, Y., Meshi, T., and Okada, Y. 1990. Mutational analysis of the pseudoknot region in the 3' noncoding region of tobacco mosaic virus RNA. *J Virol.* **64:** 3686-3693.

Takemoto, Y., Kanehira, T., Shinohara, M., Yamashita, S., and Hibi, T. 2000. The nucleotide sequence and genome organization of Japanese iris necrotic ring virus, a new species in the genus Carmovirus. *Arch Virol.* **145:** 651-657.

Timmer, R.T., Benkowski, L.A., Schodin, D., Lax, S.R., Metz, A.M., Ravel, J.M., and Browning, K.S. 1993. The 5' and 3' untranslated regions of satellite tobacco necrosis virus RNA affect translational efficiency and dependence on a 5' cap structure. *J Biol Chem.* **268:** 9504-9510.

Tsukiyama-Kohara, K., Iizuka, N., Kohara, M., and Nomoto, A. 1992. Internal ribosome entry site within hepatitis C virus RNA. *J Virol.* **66:** 1476-1483.

Turner, R.L., and Buck, K.W. 1999. Mutational analysis of cis-acting sequences in the 3'- and 5'-untranslated regions of RNA2 of red clover necrotic mosaic virus. *Virology.* **253:** 115-124.

van Belkum, A., Abrahams, J.P., Pleij, C.W., and Bosch, L. 1985. Five pseudoknots are present at the 204 nucleotides long 3' noncoding region of tobacco mosaic virus RNA. *Nucleic Acids Res.* **13:** 7673-7686.

van Noort, J.M., Kraal, B., and Bosch, L. 1985. A second tRNA binding site on elongation factor Tu is induced while the factor is bound to the ribosome. *Proc Natl Acad Sci U S A.* **82:** 3212-3216.

van Rossum, C.M., Reusken, C.B., Brederode, F.T., and Bol, J.F. 1997. The 3' untranslated region of alfalfa mosaic virus RNA3 contains a core promoter for minus-strand RNA synthesis and an enhancer element. *J Gen Virol.* **78:** 3045-3049.

Vlot, A.C., Neeleman, L., Linthorst, H.J., and Bol, J.F. 2001. Role of the 3'-untranslated regions of alfalfa mosaic virus RNAs in the formation of a transiently expressed replicase in plants and in the assembly of virions. *J Virol.* **75:** 6440-6449.

Wang, C., Sarnow, P., and Siddiqui, A. 1993. Translation of human hepatitis C virus RNA in cultured cells is mediated by an internal ribosome-binding mechanism. *J Virol.* **67:** 3338-3344.

Wang, H.H., and Wong, S.M. 2004. Significance of the 3'-terminal region in minus-strand RNA synthesis of Hibiscus chlorotic ringspot virus. *J Gen Virol.* **85:** 1763-1776.

Wang, J., and Simon, A.E. 1997. Analysis of the two subgenomic RNA promoters for turnip crinkle virus in vivo and in vitro. *Virology.* **232:**174-186.

Wells, S.E., Hillner, P.E., Vale, R.D., and Sachs, A.B. 1998. Circularization of mRNA by eukaryotic translation initiation factors. *Mol Cell.* **2:** 135-140.

Weng, Z., and Xiong, Z. 1997. Genome organization and gene expression of saguaro cactus carmovirus. *J Gen Virol.* **78:** 525-534.

White K.A. 2002. The premature termination model: a possible third mechanism for subgenomic mRNA transcription in (+)-strand RNA viruses. *Virology.* **304:** 147-154.

Wilson, J.E., Pestova, T.V., Hellen, C.U., and Sarnow, P. 2000b. Initiation of protein synthesis from the A site of the ribosome. *Cell.* **102:** 511-520.

Wilson, J.E., Powell, M.J., Hoover, S.E., and Sarnow, P. 2000a. Naturally occurring dicistronic cricket paralysis virus RNA is regulated by two internal ribosome entry sites. *Mol Cell Biol.* **20:** 4990-4999.

Yingling, Y.G., and Shapiro, B.A. 2006. The prediction of the wild-type telomerase RNA pseudoknot structure and the pivotal role of the bulge in its formation. *J Mol Graph Model.* **25:** 261-274.

Yoshii, M., Nishikiori, M., Tomita, K., Yoshioka, N., Kozuka, R., Naito, S., and Ishikawa, M. 2004. The Arabidopsis cucumovirus multiplication 1 and 2 loci encode translation initiation factors 4E and 4G. *J Virol.* **78:** 6102-6111.

You, X.J., Kim, J.W., Stuart, G.W., and Bozarth, R.F. 1995. The nucleotide sequence of cowpea mottle virus and its assignment to the genus Carmovirus. *J Gen Virol.* **76:** 2841-2845.

Ysebaert, M., van Emmelo, J., and Fiers, W. 1980. Total nucleotide sequence of a nearly full-size DNA copy of satellite tobacco necrosis virus RNA. *J Mol Biol.* **143:** 273-287.

Zaccomer, B., Haenni, A.L., and Macaya, G. 1995. The remarkable variety of plant RNA virus genomes. *J Gen Virol.* **76:** 231-247.

Zeenko, V., and Gallie, D.R. 2005. Cap-independent translation of tobacco etch virus is conferred by an RNA pseudoknot in the 5'-leader. *J Biol Chem.* **280:** 26813-26824.

Zhang ,J., Stuntz, R.M., and Simon, A.E. 2004b. Analysis of a viral replication repressor: sequence requirements for a large symmetrical internal loop. *Virology.* **326:** 90-102.

Zhang, F., and Simon, A.E. 2003. Enhanced viral pathogenesis associated with a virulent mutant virus or a virulent satellite RNA correlates with reduced virion accumulation and abundance of free coat protein. *Virology.* **312:** 8-13.

Zhang, G., Zhang, J., and Simon, A.E. 2004a. Repression and derepression of minus-strand synthesis in a plus-strand RNA virus replicon. *J Virol.* **78:** 7619-7633.

Zhang, G., Zhang, J., George, A.T., Baumstark, T., and Simon, A.E. 2006c. Conformational changes involved in initiation of minus-strand synthesis of a virus-associated RNA. *RNA.* **12:** 147-162.

Zhang, J., Zhang, G., Guo, R., Shapiro, B.A., and Simon, A.E. 2006a. A pseudoknot in a preactive form of a viral RNA is part of a structural switch activating minus-strand synthesis. *J Virol.* **80:** 9181-9191.

Zhang, J., Zhang, G., McCormack, J.C., and Simon A.E. 2006b. Evolution of virus-derived sequences for high-level replication of a subviral RNA. *Virology.* **351:** 476-88.

Zuker, M. 2003. Mfold web server for nucleic acid folding and hybridization prediction. *Nucleic Acids Res.* **31:** 3406-3415.